DROPLET MAGNETOFLUIDIC TECHNOLOGY FOR THE DELIVERY OF MOLECULAR DIAGNOSTICS AT THE POINT OF CARE

by
Dong Jin Shin

A dissertation submitted to Johns Hopkins University in conformity with the requirements for the degree of Doctor of Philosophy

Baltimore, Maryland

January, 2016

Abstract

Molecular diagnostic techniques play an increasingly important role in modern medicine. The introduction of highly sensitive and rapid analytical techniques for detection of specific nucleic acid sequences continue to establish new standards of care in areas of emergency care such as pathogen identification. Ongoing research in nucleic acid biomarkers for various types of cancer and neurodegenerative conditions highlight the increasing role that molecular diagnostics will play in the future of medicine. Harnessing these technologies for diagnostic applications at the point of care has the potential to enhance the efficiency of diagnosis and treatment via reduction in both the cost and turnaround time of diagnostic testing at all levels of healthcare delivery. However, the complexity of conventional workflow for sample and reagent handling presents a conceptual hurdle in developing a robust and cost-effective system for point of care diagnostics.

A promising solution may be found in droplet magnetofluidic technology. Past research in this field has demonstrated the potential of unique fluidic control mechanism facilitated solely by magnetic particles. Association, dissociation and transport of sessile droplets on hydrophobic substrates suggest a mode of fluid handling that is quite foreign to conventional approaches involving pneumatics or centrifugation. Indeed, investigators were not ignorant to the ramifications of this technology in medicine. With the advent of 'smart' particles with a magnetizable core whose surfaces could be used to capture and transport specific biomolecules, droplet magnetofluidics is well-poised to bring the pieces together and usher in a new workflow paradigm for biomolecular assays – one which is more portable and simpler to operate.

This thesis investigates the use of droplet magnetofluidics as an enabling technology for point of care diagnostics. Following an introduction to the fundamentals of droplet magnetofluidic kinematics, we conceptualize a novel assay paradigm referred to as 'single-stream assay workflow' describing a linear workflow driven by analyte capture and transport on a movable magnetic particle cluster. Chapters 2 and 3 illustrate examples of single-stream bioassays that are enabled by the droplet magnetofluidic process for genetic and epigenetic biomarker analysis.

Afterwards, we expand our investigation to various components of a complete platform, namely conceptualization and design of a cartridge and an instrument for process automation. Chapter 4 illustrates an example of process integration enabled by a combination of droplet magnetofluidic cartridge and a programmable magnetic actuator. Chapter 5 provides a discussion of design considerations for various aspects of the platform including the cartridge, instrument and the assay, with an emphasis on factors that must be considered in order to bridge the gap between a proof-of-concept and a field-ready platform.

Lastly, we integrate our findings in order to develop a user-friendly diagnostic platform for the evaluation of droplet magnetofluidic workflow in a clinical setting. In Chapter 6, we illustrate a smartphone-based mobile nucleic acid testing station for the evaluation of chlamydia infection in emergency room setting. We will conclude our report with a discussion of future directions for droplet magnetofluidic technology in point of care testing. It is our hope that these findings will inspire the readers to appreciate the wide range of academic and commercial opportunities that droplet magnetofluidics presents to the biomedical field.

Advisor: Jeff Tza-Huei Wang
Committee members: Dr. Charlotte A. Gaydos, Dr. Peter Searson, Dr. Jeff Tza-Huei Wang

Preface

I started my tenure at Johns Hopkins at the age of 23, in the year 2010. Fresh out of college, I had very little knowledge about the world and far less about myself. It is an understatement to say that the doctoral experience at this institution was a wholly transformative one for me. Looking back at the past 5 and a half years, I can say without reservation that this was a golden time spent like no other. Every few months the laws of physics would challenge not only my research direction, but also my understanding of this world and of myself as an extension. There were some encouraging milestones along the way, but perhaps far many more dead ends that ultimately did not survive to tell the tale in this document. If there was anything that helped to keep myself together throughout this journey, it was my good fortune to be able to conduct research at one of the most prestigious and prosperous institutions in the world. The freedom that I had to explore during this time is unlikely to be matched by a whole lot of places, academia and industry alike. Furthermore, I was equally as fortunate to have found the vestiges of a technology that may carry the potential for impact outside the academic environment. Only the dynamic collaborative environment that exists between Johns Hopkins School of Medicine and Whiting School of Engineering could have facilitated the kind of research that I was able to conduct during my tenure here.

This document represents but a fraction of what is involved in a doctoral research experience. Biomedical engineering is unlike any other traditional discipline in that its very essence is in interdisciplinary research. The benefit of hindsight renders many accomplishments in this discipline as simple application of principles from one discipline in the study of another. Much of the research can seem redundant or even trivial in the view of those trained in other disciplines. Now that I have unwittingly trodden down this path

myself, I made two observations about this field. First, making the interdisciplinary connection is rarely a linear process. It requires intuition about the problem being studied, based on a sound understanding of all disciplines involved. The groundwork for understanding the phenomenon may already have been done ahead of you, but connecting the dots is perhaps the more challenging task – not simply to connect, but to connect in such a way that can sustain an entire field to its own merit. While the task can be a source of much headache for many of our colleagues, it seems to be offset by the second observation, which is the sheer enormity of the value that is generated through a single fruitful insight. Incidentally, Johns Hopkins as an institution has a tradition of making these insights in biomedicine, which has served to inspire and guide the efforts of hatchlings such as myself. If it was the intended goal of this program to inculcate the spirit of this tradition in its recruits, they I am very glad to find myself looking favorably upon this journey at its close.

I would like to thank my advisor Prof. Tza-Huei Wang for his continued support and good faith in my vision for future, and the committee members Prof. Gaydos and Searson for their guidance. I also thank the members of the Center for POCT for STDs for their enduring support and encouragement in this long journey. I would like to thank my family for their financial and emotional support, and whose love and generosity helped me to redouble my efforts equally as much as their expectations and traditions. I would like to thank Dr. Kelvin Liu, Yi Zhang and Tushar Rane for serving as exemplary role models during my tenure. This laboratory has been a second family to me, without which I would have surely been lost. I would also like to extend my thanks to all of my colleagues, mentors and mentees who provided support and encouragement throughout this journey.

January 1, 2015

Table of contents

List of Figures

List of Tables

Chapter 1

1. Principles of Droplet Magnetofluidics

1.1 BACKGROUND

Recent advances in bioanalytical techniques have resulted in fast, cost-effective and highly sensitive assays for the analysis of nucleic acid biomarkers. Techniques such as the polymerase chain reaction (PCR) enable us to identify as few as a single fragment of nucleic acid in a matter of hours, setting itself apart from the limited sensitivities of immunoprecipitation techniques or the resource and time-intensive cell culture techniques. However, due to the complex operating procedure associated with sample preparation, amplification and detection, these assays are still performed by technicians or automated instruments in a high-volume centralized facility. If such technology could be made accessible at the sites where patient care is delivered in order to generate immediately actionable test results for the physicians and the patients alike, our capacity to respond to communicable diseases and monitor individual health is likely to be very different from what we have today.

In light of this opportunity, both academic and commercial efforts have been made since the end of 20th century towards developing integrated platforms designed to perform all aspects of molecular diagnostic assays, from sample preparation to detection, on a single device. These micro-total-analysis platforms (μTAS) are designed to perform all aspects of molecular diagnostic assays, from sample preparation to detection, on a single device.

Commercial development of plug-and-play benchtop platforms has already made significant progress in recent years, as demonstrated in products such as Cepheid GeneXpert platform [1] and BioFire FilmArray platform [2] among others. Meanwhile, efforts to further miniaturize assays for mobile medicine have also led to shifting paradigms in academic research towards approaches such as paper-based microfluidic devices [3], capillary pump-driven microfluidic devices [4, 5] and droplet-based platforms [6]. Among these directions, droplet-based fluid handling presents an attractive mode of operation due to their compatibility with conventional assays that are not amenable to lateral-flow technology, such as nucleic acid amplification. Open-surface droplet platforms in particular do not require pneumatic controls for fluid handling and are free from clogging, which is a critical mode of failure in microchannel-based platforms.

Open-surface droplet microfluidic platforms have emerged under various formats. Platforms may be primarily categorized based on the mode of droplet or particle manipulation, some of which include magnetofluidic [6-22], dielectrophoretic (DEP) [23-25], electrowetting-on-dielectric (EWOD) [26-34] and optical [35, 36] approaches. Of particular interest are open-surface droplet magnetofluidic platforms that utilize magnetic forces on particles as a means of both droplet and particle manipulation. This is in contrast to other droplet platforms utilizing EWOD and DEP as the primary mechanism for droplet handling, where the incorporation of magnetic particles requires an auxiliary mode of actuation for magnetic manipulation. Magnetic particles are regularly utilized in biochemical assays as solid phase substrates for analyte capture and purification, which highlights the importance of magnetic manipulation in these platforms.

In this chapter, the theoretical basis for magnetofluidic droplet manipulation will be discussed. Droplet manipulation operations are described as a function of parameters such

as droplet volume and particle size, which are important topics in the context of on-chip process design. Principles outlined in this chapter are essential to understanding the assay designs that are described in subsequent chapters.

1.2 PRINCIPLES OF MAGNETOFLUIDIC DROPLET MANIPULATION

Droplet magnetofluidics in biomedicine has an interdisciplinary origin, as they are the product of recent progress in magnetofluidics, microfabrication and macromolecule purification techniques. From a magnetofluidics perspective, early studies of manipulating liquid containing magnetic particles by using a permanent magnet [7] or an electromagnet [8] paved the way for other investigators to build on the fundamental mechanisms. Additional progress in device fabrication techniques via surface patterning [37] and micro-elevations defined by soft lithography [14] enabled compartmentalization of multiple reagents on one substrate, allowing the entire fluidic workflow of complex bioassays to be recreated on a single device.

Particle transport, fusion and extraction from liquid reagents are essential operations in any biomolecular assay that involves the addition of reagents and aspiration of buffer solutions from magnetic particles. While the specifics of their implementation may vary across platforms, droplet manipulation on an open surface can be generalized as the interaction of three forces. The balance of these components determines the type of droplet handling operation being performed. The first component is the magnetic force, which is a consequence of paramagnetic bead cluster being attracted by an external magnetic field. For magnetic particles clustered in a nonmagnetic medium, the force acting on the particle cluster can be obtained as follows [38]:

$$F_M = \left(\frac{M}{\rho}\right)\chi\frac{B}{\mu_0}\nabla B$$

Here, M and ρ represent the mass and density of magnetic particle cluster, χ is the magnetic susceptibility of the particles, B is the applied magnetic field, and μ_0 is the permeability of free space. In magnet-based droplet manipulation, this component is the only parameter that is actively modulated on the device. As such, all operations are facilitated either by modulating travel velocity or by introducing passive structural components that can modify the other two force components on the droplet. Magnetic force is directly proportional to the mass of the magnetic bead cluster, which highlights an important design parameter for magnetic droplet-based platforms. Because magnetic particles also serve a functional role as the solid substrate on which biochemical analytes are captured, large particle load also increases the functional surface area of the system. However, increase in particle load is accompanied by a concomitant increase in the volume of liquid carried by the magnetic particle cluster, which may result in contamination of subsequent steps in complex bioassays [17].

The second component is the drag or frictional force, which describes the friction imposed on the droplet by physical impediments such as solid surfaces and barriers in contact with the droplet. This force is described by the following equation [20]:

$$F_f \cong K_f R_b \mu U$$

Here K_f is the frictional constant, R_b is the radius of contact area between the droplet and the substrate, μ is the viscosity of surrounding oil medium and U is the velocity of the droplet. From a design perspective, frictional force can become a hindrance to efficient droplet transport, especially when the magnetic force is smaller than frictional force. This is the case with rugged surfaces as well as substrates with high surface energies, which results in an increase in the frictional constant and the contact area. Open-surface droplet microfluidic platforms address this issue by using planar surfaces coated with commercial

fluoropolymers such as amorphous Teflon [9, 10, 14, 17, 18, 28] and Cytop [30, 31] or chemical vapor deposition with chemicals such as organosiloxane (SiOC) [33] and parylene [34]. Coating the substrate with low surface energy chemicals has additional functional roles as a means of preventing contamination via fouling, as well as preventing loss of biological molecules via adsorption to the surface.

A third component is the capillary force, which arises at deformities on the surface of the droplet. This force is particularly relevant for its involvement in droplet fission, which generally takes place after a process of deformation and necking. The maximum capillary force that can be sustained before the droplet of volume V undergoes fission can be followed from derivation by Shikida *et al* [7]:

$$F_{c,max} \cong \gamma(6\pi^2 V)^{\frac{1}{3}}$$

Here γ describes the interfacial tension between droplet and the surrounding oil medium. From a design perspective, reducing this component allows the magnetic particles to dissociate from the parent droplet more easily. This can be facilitated by the addition of surfactants in the oil medium, which may be a necessary condition for fission of magnetic particles from fluids with a high interfacial tension. Optimizing the concentration of surfactants and particle volume can be an important process in developing a robust droplet manipulation platform, especially when the magnetic field gradient is generated by sources substantially weaker than rare-earth permanent magnets. As will be described in Chapter 4, we further characterized the effect of varying bead volume and surfactant concentration on the robustness of their droplet fission operation and observed that an increased surfactant concentration is also accompanied by droplet instability, where reagent priming eventually becomes challenging [17].

Designing a droplet microfluidic platform capable of performing multiple fluidic handling operations requires an intuitive understanding of the interplay between the three forces. These interactions have been investigated by Long *et al* [20] for open-surface droplet manipulation on a planar hydrophobic substrate, in the form of an 'operation diagram' **(Fig. 1.1)** where the relative magnitudes of forces as a function of magnet velocity and particle load result in a particular droplet operation. In this classification scheme, the interaction between the droplet containing magnetic particles and a permanent magnet are categorized under three regimes. The first is particle extraction, which occurs when the magnetic force exceeds the maximum capillary force holding the magnetic plug and the parent droplet together. The second is droplet transport, where the magnetic force is insufficient to overcome the capillary force but is sufficient enough to overcome the friction force acting between the droplet and the device surface. The last regime is droplet disengagement, where the magnetic force is less than both the friction and capillary forces and no further manipulation is achieved by the magnet.

In a later work, Zhang *et al* [18] described an expanded operation diagram **(Fig. 1.2)** to include surface patterns that can dramatically enhance frictional forces in order to facilitate a full range of droplet handling operations. The selective patterning of hydrophobic substrate with hydrophilic surface energy traps (SETs) result in an additional force component attributed to surface tension arising from the wetting of the droplet on the SET. In this arrangement, uniform droplet dispensing in a series of SETs becomes possible for applications including serial dilution and aliquoting [18, 19]. Because surface tension is not a function of velocity but rather the perimeter length of SET, magnet travel velocity can be decoupled from operations such as particle extraction and the operation diagram becomes a function of three static parameters including droplet volume, SET dimension and particle load. This is a significant advantage from a platform design perspective since highly precise

instrumentation is no longer essential to achieve particle extraction and droplet transport in a robust manner. While this example describes a hydrophilic pattern as a means of impeding droplet motion during particle extraction, this concept may be extended to any other methods for immobilizing droplets, such as a physical barrier [7, 14].

1.3 RELEVANCE OF DROPLET MAGNETOFLUIDICS IN POINT OF CARE DIAGNOSTICS

Conventional molecular assay workflow for nucleic acids and proteins involve an iterative process of addition and removal of aqueous buffers for the capture and purification of analytes on a solid substrate, followed by the coupling of the analyte to an enzymatic reaction for detection. While the underlying chemical process is essentially a series of buffer exchanges for the substrate-bound sample, conventional approaches to fluidic handling necessitates complex designs involving fluidic manifolds and control systems that contribute to increased cost and failure rate. This problem highlights the need for a simpler and more scalable fluidic handling strategy to design robust and affordable point of care platforms. To that end, droplet magnetofluidics can be employed in place of conventional fluidic handling process **(Fig. 1.3)**. In this workflow, fluidic manifolds are replaced by a series of discrete, stationary droplet reservoirs interconnected by a smooth hydrophobic surface. Analyte capture and transport is facilitated by surface-modified magnetic beads, which can freely traverse between each reservoir when acted upon by an external magnetic field. By virtue of this approach, a droplet magnetofluidic design bypasses conventional design constraints associated with fluidic routing, valving, measuring and dead volume. As a result, the disposable cartridge retains a simple fabrication workflow and resilience to conventional modes of device failure such as clogging and leakage.

1.4 THESIS ROADMAP

Droplet magnetofluidics offer a unique opportunity to propose an alternative workflow for conventional biochemical assays. Based on the current state of development, our contribution to this topic is organized as follows: 1) conceptualization and demonstration of biochemical assays utilizing the fundamentals of droplet magnetofluidics; 2) development of supporting instrumentation which constitutes an integrated and automated platform for sample processing; and 3) addressing the concerns of scalability and clinical relevance by demonstrating a field-deployable design capable of clinical testing. The following chapters will expand on each of these concepts, organized along specific original contributions that are the products of our research.

First, we illustrate a novel concept for biochemical assay processing, named single-stream assay workflow. This workflow is an invention necessitated by the unique fluidic processing capabilities of droplet magnetofluidics. We demonstrate the utility of this workflow in realizing some of the most pertinent applications in nucleic acid analysis, namely in mutation detection and epigenetic analysis.

Next, we show how this workflow can be integrated into a complete platform with supporting instrumentation. We begin with the development of an automated droplet cartridge processor, capable of integrating all steps between an unprocessed sample and nucleic acid amplification. This is followed by a discussion on the various components of a complete droplet magnetofluidic platform, outlining the steps that are taken in order to transform a laboratory concept into a scalable design capable of field testing.

Lastly, we apply the lessons from the preceding chapters in order to develop a mobile workstation for nucleic acid testing. We demonstrate its application in the detection of chlamydia infection from patients in the emergency care setting, highlighting the importance of design considerations including accessible user interface and packaging.

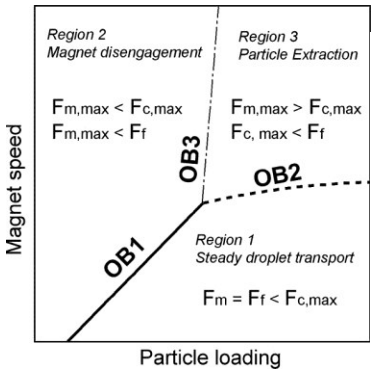
Region 2
Magnet disengagement
Region 3
Particle Extraction
Fm,max < Fc,max
Fm,max < Ff
Fm,max > Fc,max
Fc, max < Ff
OB3
OB2
OB1
Region 1
Steady droplet transport
Fm = Ff < Fc,max
Magnet speed
Particle loading

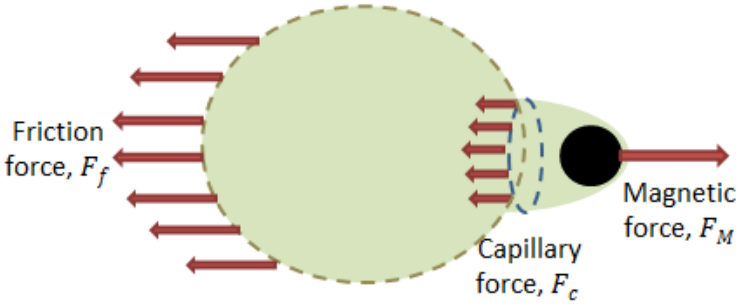
Friction
force, F_f
Capillary
force, F_c
Magnetic
force, F_M

Figure 1.1: Droplet kinematics on a planar hydrophobic substrate.

Left: Operating diagram developed by Long et al as a function of particle loading and magnet velocity. OB1, OB2 and OB3 are the operating boundaries separating each operation regions Right: Top-down schematic of three forces acting on a droplet containing magnetic particles. In general, droplet kinematics involves the relative balance between magnetic force on the particle (F_M), friction force (F_f) and capillary force (F_c). [adopted from ref. 20]

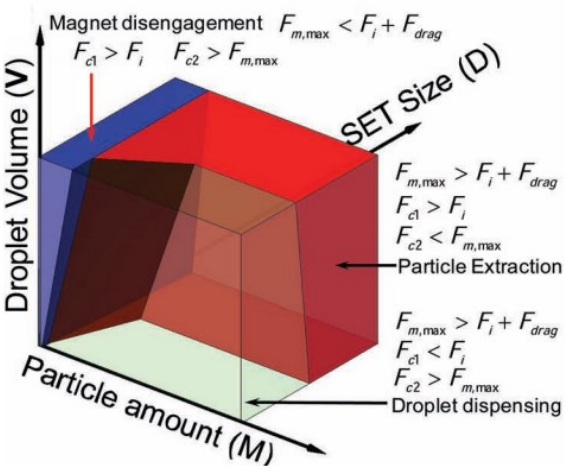
Magnet disengagement $F_{m,max} < F_i + F_{drag}$
$F_{c1} > F_i$ $F_{c2} > F_{m,max}$
Droplet Volume (V)
SET Size (D)
Particle amount (M)
$F_{m,max} > F_i + F_{drag}$
$F_{c1} > F_i$
$F_{c2} < F_{m,max}$
Particle Extraction
$F_{m,max} > F_i + F_{drag}$
$F_{c1} < F_i$
$F_{c2} > F_{m,max}$
Droplet dispensing

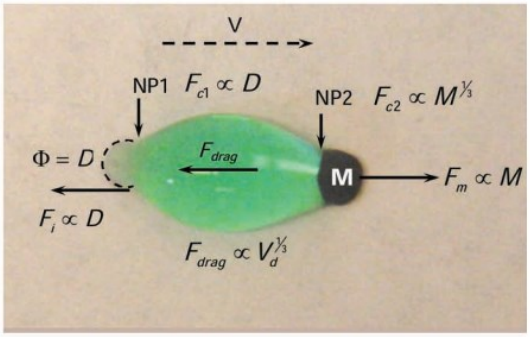
V
NP1 $F_{c1} \propto D$
NP2 $F_{c2} \propto M^{1/3}$
$\Phi = D$
F_{drag}
M
$F_m \propto M$
$F_i \propto D$
$F_{drag} \propto V_d^{1/3}$

Figure 1.2: Droplet kinematics on patterned substrate.

Operating diagram developed by Zhang and Wang as a function of particle loading, droplet volume and SET dimension. With a fixed travel velocity, droplet manipulation operations depend only on the static parameters including droplet volume, particle amount and SET size [from ref. 18].

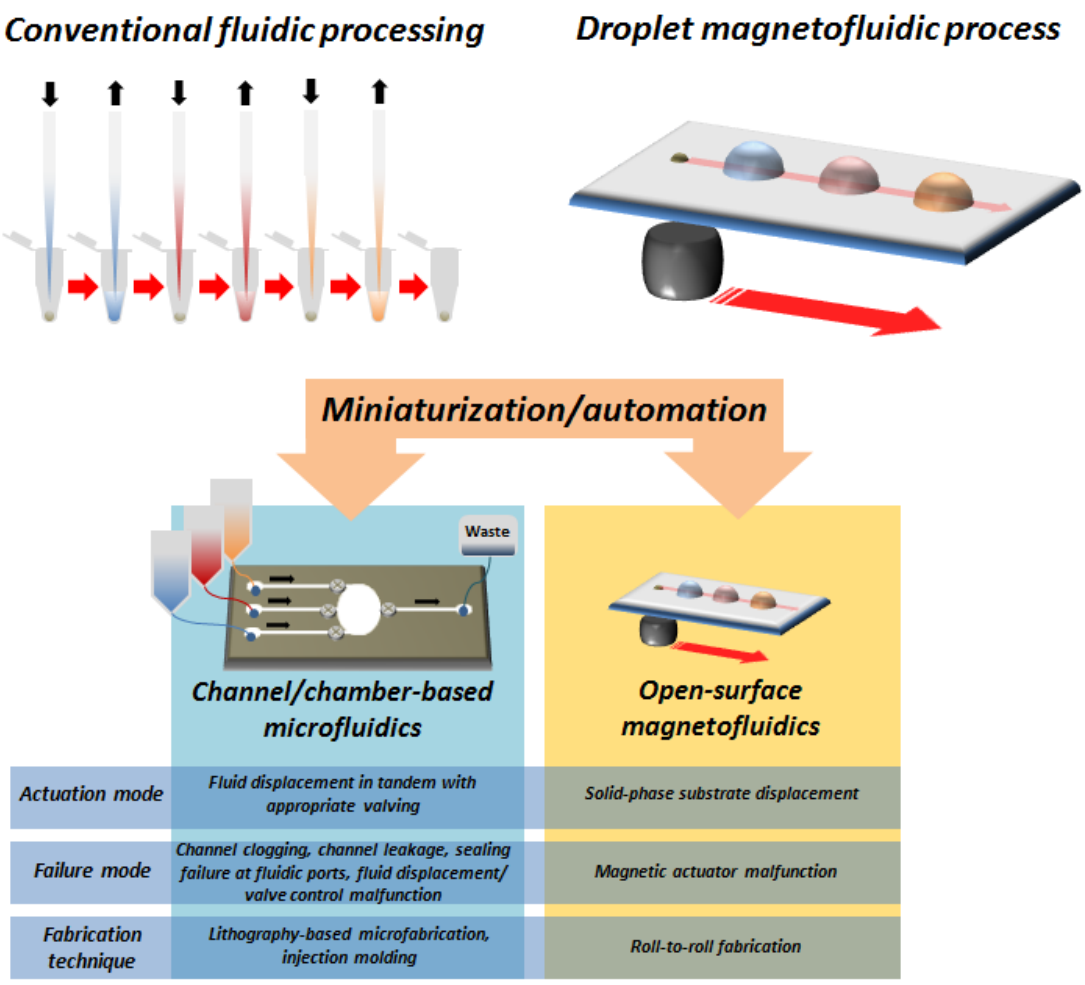
Conventional fluidic processing
Droplet magnetofluidic process
Miniaturization/automation
Waste
Channel/chamber-based microfluidics
Open-surface magnetofluidics
Actuation mode
Fluid displacement in tandem with appropriate valving
Solid-phase substrate displacement
Failure mode
Channel clogging, channel leakage, sealing failure at fluidic ports, fluid displacement/ valve control malfunction
Magnetic actuator malfunction
Fabrication technique
Lithography-based microfabrication, injection molding
Roll-to-roll fabrication

Figure 1.3: Comparison between conventional and magnetofluidic fluidic handling.

Conventional approach based on fluidic displacement in a closed chamber or channel gives rise to a complex fluidic design involving actuators and control systems for valving and fluid displacement, which increases the potential modes of failure and increases the complexity of fabrication process. Meanwhile, droplet magnetofluidic approach is based on solid-phase displacement on a single planar substrate, giving rise to a simple design and a single actuation mechanism using a magnetic actuator.

Chapter 2

2. Single-stream assay design for droplet magnetofluidic platforms

2.1 BACKGROUND

Single-stream assay refers to the streamlining of fluidic processing steps to a linear process involving analyte transfer across stationary buffer reservoirs, driven by a mobile substrate capable of binding and eluting the analyte. This paradigm is in contrast to the conventional bench-top process where an array of discrete reagent handling steps such as aspiration, addition, centrifugation and mixing are required in iterative fashion. As described in the previous chapter, the range of operations facilitated by a droplet magnetofluidic platform makes it especially well-suited to the single-stream assay approach, by replacing the liquid transfer steps with a magnetofluidic transfer of surface-modified magnetic particles across a sequence of liquid reagents.

In this chapter, we demonstrate the concept of single-stream assay workflow in nucleic acid analysis using a droplet magnetofluidic device. In this instance, we focused specifically on PCR-based testing of genetic variation in a target DNA fragment. Genetic testing is a diverse and growing field with applications ranging from diagnostics, newborn screening, and forensics. However, the utility of genetic testing in clinical setting is confined to those with access to core facilities specializing in molecular diagnostic assays. As discussed in the previous chapter, droplet magnetofluidics and associated techniques offer a simple and

tractable alternative to conventional fluidic management with potential towards miniaturization and deployment at the point of care.

As a convenient means of analyzing genetic variations, melting curve analysis has recently emerged as a potential alternative to sequencing [39] or mass spectrometry [40] for genotyping applications. This technique utilizes differences in thermodynamic properties of oligonucleotides to resolve subtle differences in nucleotide sequence. The dissociation characteristics of double stranded DNA during heating can be monitored via the use of DNA intercalating dyes. [41] By monitoring the fraction of double stranded DNA over a positive thermal ramp, thermodynamic properties associated with the sequence are resolved as a function of temperature. Because the stability of DNA double helix is a function of base composition and length, DNA samples containing single nucleotide polymorphisms (SNPs) generate melting profiles that are distinct from their wild-type counterparts. Melting curve analysis benefits from its simple format for genotyping, requiring only a single universal primer pair for product amplification and no additional probes for allelic discrimination, in contrast with other PCR-based genotyping assays such as allele-specific PCR [42] and allele-specific oligonucleotide probes [43].

We present an integrated microfluidic melting curve analysis platform capable of identifying genetic mutation from complex biological samples such as whole blood. Firstly, extraction and purification of nucleic acids from crude biological samples is achieved using a droplet magnetofluidic workflow [14]. Silica-coated magnetic particles are used as a solid phase for DNA extraction and transport, while topographical features raised on the surface of the microchip enable efficient splitting and confinement of reagents. Following DNA extraction, a miniaturized thermal cycling and detection module performs real-time amplification and melting curve acquisition directly from the microchip. Melting curve

profiles were used to demonstrate genotyping capability for heterozygous mutation in K-ras oncogene.

2.2 EXPERIMENTAL DETAILS

2.2.1 Microfluidic device and instrumentation

The microfluidic device **(Fig. 2.1A)** was fabricated by casting polydimethylsiloxane (PDMS) pre-polymer in a computer numerical control (CNC) machined polytetrafluoroethylene (PTFE) mold and curing at 80°C for 60 minutes **(Fig. 2.2)**. This was followed by puncturing a 4 mm aperture in the PCR reagent compartment and bonding with a 100 μm-thick glass coverslip via oxygen plasma activation. Afterwards, the device surface was rendered hydrophobic by dip-coating in 1% Teflon AF 1600 (DuPont, USA). The overall cartridge dimension was 35×43 mm with six identical compartments. The melting curve instrument was a miniaturized epifluorescence detector combined with a PID-controlled thermoelectric element for simultaneous monitoring of fluorescence and temperature **(Fig. 2.3)**. Temperature calibration was achieved by adjusting PID setpoints while monitoring PCR chamber temperature with a secondary thermistor to obtain the desired temperatures on chip **(Fig. 2.4)**. Raw melting curve signals were processed using custom LabVIEW program which implemented curve normalization via exponential background subtraction. [46]

2.2.2 Cartridge priming and assay protocol

The proposed device integrates genomic DNA extraction, real-time PCR, and melting curve analysis using silica-coated magnetic beads as a mobile solid phase extractor. The device was pre-primed with reagents in the form of sessile droplet in the following order: 21.5 μL lysis/binding buffer (10 μL Buffer AL, 10 μL isopropyl alcohol, 1 μL serine protease, and 0.5 μL MagAttract Suspension G), 35 μL wash buffer 1, 30 μL wash buffer 2, another 30 μL wash

buffer 2, and 25 μL PCR mixture (1x LCGreen+ dye, 1x PCR buffer, 3.5 mM MgCl2). All reagents were dispensed into the cartridge using pipettes before the experiment. All droplets were overlaid with mineral oil to prevent evaporation, resulting in aqueous reagent droplets sealed in a continuous oil phase. Lysis/binding and wash buffers were components from commercial DNA isolation kit (BioSprint Kit, QIAGEN). For each extraction process, biological sample was first injected into the lysis buffer droplet and incubated for 10 minutes. During this process, nucleus-containing cells in sample matrix were lysed to release the genomic material. The released genomic DNA then adsorbed to silica-coated surface of magnetic beads in the presence of chaotropic salt in the lysis/binding buffer [47]. After incubation, DNA adsorbed on magnetic beads were transported from the lysis buffer using a permanent magnet and rinsed in a series of washing buffers to remove chaotropes and PCR inhibitors, followed by elution in PCR mixture for 10 minutes at 70°C. The condition of PCR buffer favoured the release of DNA from the silica surface. Lastly, the beads were extracted from the PCR mixture into the waste chamber, and the device was loaded onto the miniaturized instrument for amplification and melting curve analysis.

Droplet operations were facilitated by the use of topographical barriers, which serves a dual purpose of confining aqueous reagents in isolation and enabling splitting of magnetic particles from the aqueous phase. Topographical barriers in the current work were 5×5 mm chambers with ~5 mm height and 1 mm vertical gaps on either side of the chamber. Using a manually operated neodymium magnet positioned ~1 mm below the bottom surface of the cartridge, magnetic particles were removed from the original aqueous phase and available for transport into subsequent reagent solution. During washing and incubation steps, magnet is removed from the device. As the bead surface is silica-coated and therefore

hydrophilic, the beads remained compartmentalized in aqueous buffer phase rather than the surrounding oil phase.

2.3 DNA EXTRACTION CHARACTERIZATION

To demonstrate genomic DNA extraction and amplification using the microchip, we first characterized DNA extraction by performing quantitative PCR from the extracted genomic DNA. Stock of confluent Panc 10.05 cells suspended in 1 mL phosphate buffered saline was serially diluted and quantified using a hemocytometer slide. Afterwards, 10 μL samples were loaded into a lysis mixture and processed on the microchip. In this case, the PCR mixture was replaced with 10 μL elution buffer (BioSprint Kit, QIAGEN), and the isolated DNA was quantified using PicoGreen assay kit (Invitrogen, CA). As shown in **Figure 2.5A**, the DNA yields are linearly proportional to the amount of cells in each dilution. Using a theoretical genome mass of 6.6 pg for each diploid cell, the DNA yield fraction was found to range between 4 to 11% **(Fig. 2.5B)**. The modest extraction yield can be attributed to reduced lysing efficiency due to the lack of incubation at elevated temperatures. Since the white blood cell count is on the order of 10^3-10^4 per μL for normal adults, [48] the extraction yield achieved by this platform is sufficient to capture target genome for amplification.

2.4 ON-CHIP AMPLIFICATION AND MELTING CURVE ANALYSIS

We performed DNA extraction, amplification, and melting curve analysis on chip with crude biological sample to demonstrate genotyping capability of the proposed platform. 10 μL unspun whole blood from male donor with heparin anticoagulant (Biological Specialty Corp, USA) was processed on the microchip using steps described in **Figure 2.1A**. Following genomic DNA isolation, the chip was inserted into the custom instrument for amplification. 167-bp products were amplified using primers listed in **Table 2.1**, as described previously.

[49] Cycling parameters included a 10-minute thermal activation at 95°C, followed by cycling between 95°C for 30 seconds, 60°C for 30 seconds and 72°C for 1 minute for 40 cycles. **Figure 2.6A** shows the real-time fluorescence signals obtained during the anneal phase of each cycle, with a threshold cycle number of 28. At the end of thermal cycling, the sample was cooled to 25°C for 3 minutes, followed by holding at 50°C for another 3 minutes. A positive thermal ramp was applied up to 95°C at a rate of 0.05°C per second. The resulting raw melting curve signal is presented in **Figure 2.6B**. In order to convert fluorescence signal into double-stranded DNA fraction, raw data was normalized using background subtraction method. [46] Background fluorescence intensity is modelled as an exponentially decaying function of temperature. Fitting an exponential curve to the post-melt region and subtracting the curve from raw signal generates a sigmoidal profile that is constant at pre-melt and post-melt regions. Normalization of data between zero and unity generates the final curve as shown in **Figure 2.6C**.

Wild-type genome from a healthy human blood sample was differentiated from the mutant cell line genome using the droplet platform. The adenocarcinoma cell line Panc 10.05 has a heterozygous mutation in K-ras codon 12 (c.35G→A). Sequence information from amplified products was verified by Sanger sequencing using Applied Biosystems 3730xl DNA analyzer **(Fig. 2.7B)**. As shown in **Figure 2.7A**, melting profile generated from wild-type genome is clearly differentiable from the heterozygous mutant. The lower melting point of the heterozygote is attributed to formation of heteroduplex DNA between wildtype and mutant strands, which are less thermally stable than fully complementary DNA [50]. It should be noted that homozygous mutants will generate fully complementary duplexes, whose thermodynamic properties are very similar to wildtype duplexes and are consequently more challenging to differentiate at a single nucleotide resolution. Melting curve analysis is generally conducted with shorter PCR amplicons (<200bp) as described here. The use of

melting profiles in addition to melting temperature during analysis helps to differentiate between PCR products whose amplicon lengths and base pair compositions are similar.

2.5 CONCLUSION

This chapter demonstrates a simple droplet microfluidic platform for performing single-stream genotyping assay via melt curve analysis. The platform is capable of processing crude biological samples such as whole blood. Combined with instrumentation capable of thermal ramp and a suitable normalization algorithm, genetic polymorphisms could be identified in PCR amplicons from biological samples. Due to its simple operation and portability, the platform presents a possible direction for designing decentralized platforms dedicated to mutation scanning from a small aliquot of patient blood sample.

To our knowledge, the study also describes the first integrated droplet magnetofluidic platform applied to genotyping with melting curve from crude biological samples. The additional qualitative information that can be derived from melting curve analysis provides a distinct advantage over previous amplification-based detection method where only binary information can be obtained for each primer pair. Within the context of broader literature, melting curve analysis of pre-prepared samples from a device fabrication perspective has been recently explored in a lab-on-a-foil device [51]. The current work approaches the use of melting curve analysis from a broader scope in combination with sample preparation and amplification, facilitated by magnetofluidic droplet manipulation. Due to the versatility of melting curve techniques, it is anticipated that an increasing number of novel applications will emerge at the intersection between melting curve analysis and microfluidics.

(A)

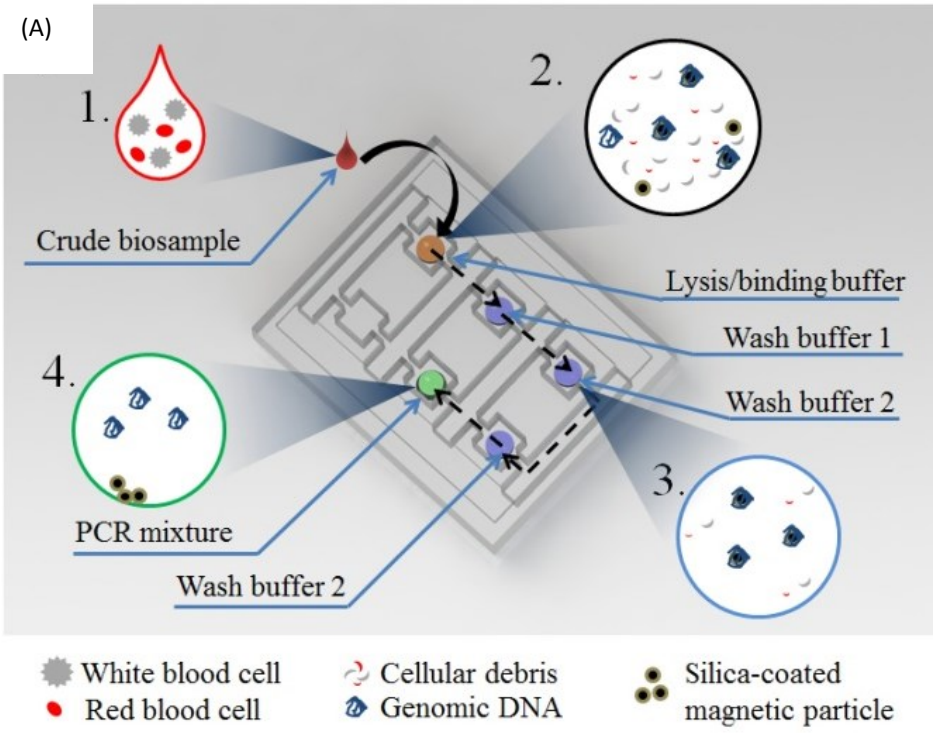
1.
2.
3.
4.
Crude biosample
Lysis/binding buffer
Wash buffer 1
Wash buffer 2
PCR mixture
Wash buffer 2
White blood cell
Red blood cell
Cellular debris
Genomic DNA
Silica-coated
magnetic particle

(B)

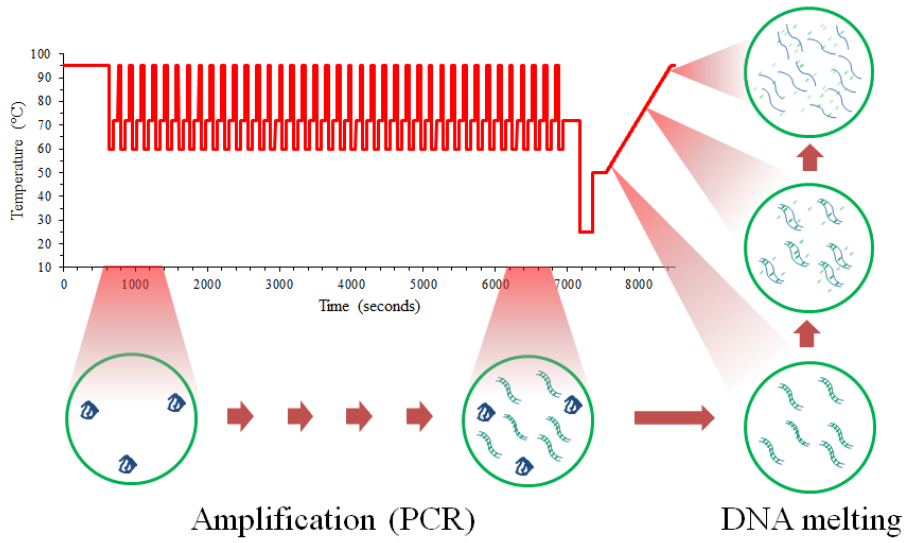
Temperature (°C)
Time (seconds)
Amplification (PCR)
DNA melting

Figure 2.1: Single-stream assay overview.

A) Overview of droplet operation for whole blood processing. Black dashed lines represent the path of magnetic beads. (1) Sample matrix contains red and white blood cells, of which only the white blood cells contain genomic material; (2) Lysis buffer breaks down cells to release genomic DNA, which binds to the silica surface of magnetic beads. (3) Magnetic beads are merged with a series of wash buffers where residual debris from lysis are removed from beads; (4) Washed beads are merged with PCR droplet where DNA is eluted. **B)** PCR droplet from the end of **Fig. 2.1A** is processed through two stages of thermal modulation. The first stage is thermal cycling, which amplifies a segment of DNA specific to primers contained inside the droplet. The second stage generates a positive temperature ramp, at a rate of 0.05°C per second, for melting curve analysis. As duplex DNA begins to denature, dyes are dissociated from denatured bases and strongly quenched in free solution, resulting in a sharp decline in signal.

(A)

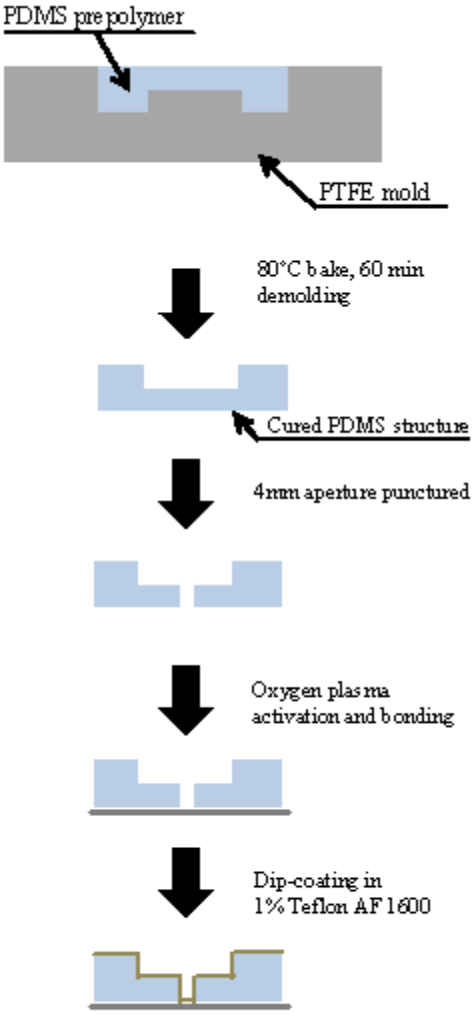
PDMS prepolymer
PTFE mold
80°C bake, 60 min
demolding
Cured PDMS structure
4mm aperture punctured
Oxygen plasma
activation and bonding
Dip-coating in
1% Teflon AF 1600

(B)

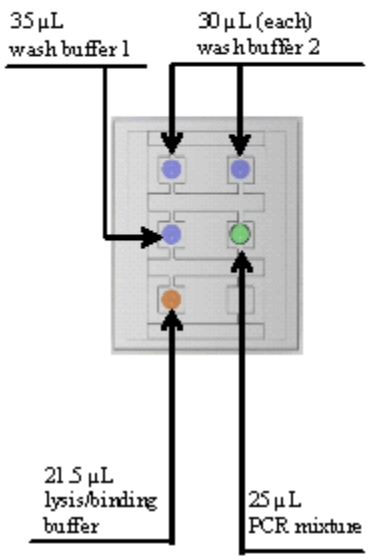
35 µL
wash buffer 1
30 µL (each)
wash buffer 2
21.5 µL
lysis/binding
buffer
25 µL
PCR mixture

(C)

Figure 2.2: Cartridge fabrication overview.

A) Microchip fabrication process. **B)** Reagent priming diagram: 21.5 μL lysis/binding buffer (10 μL Buffer AL, 10 μL isopropyl alcohol, 1 μL serine protease, and 0.5 μL MagAttract Suspension G), 35 μL wash buffer 1, 30 μL wash buffer 2, another 30 μL wash buffer 2, and 25 μL PCR mixture (1x LCGreen+ dye, 1x PCR buffer, 3.5 mM MgCl2). All droplets were overlaid with mineral oil to prevent evaporation. **C)** Photograph of cartridge next to US dime, primed with food dye for visualization.

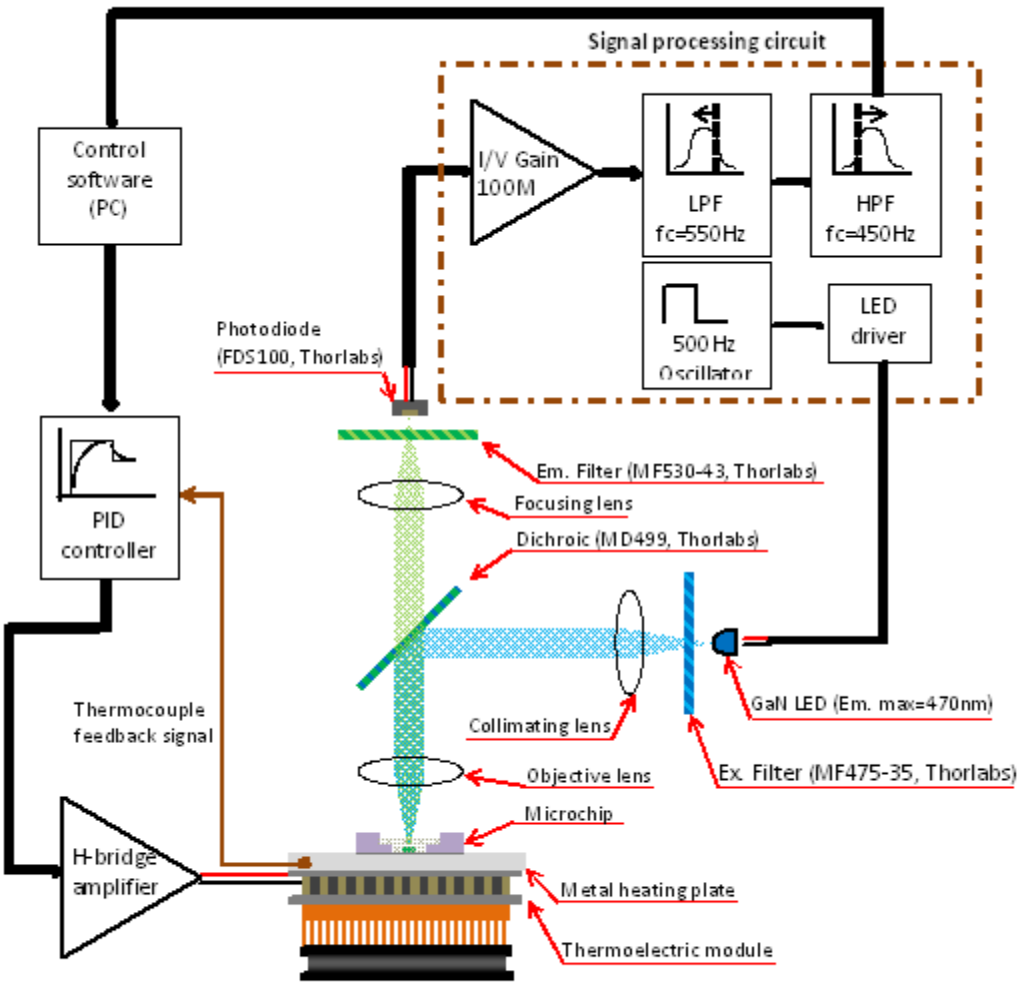
Signal processing circuit
Control software (PC)
I/V Gain 100M
LPF fc=550Hz
HPF fc=450Hz
500 Hz Oscillator
LED driver
Photodiode (FDS100, Thorlabs)
PID controller
Em. Filter (MF530-43, Thorlabs)
Focusing lens
Dichroic (MD499, Thorlabs)
GaN LED (Em. max=470nm)
Thermocouple feedback signal
Collimating lens
Ex. Filter (MF475-35, Thorlabs)
Objective lens
Microchip
H-bridge amplifier
Metal heating plate
Thermoelectric module

Figure 2.3: Layout of miniaturized instrumentation.

(A)

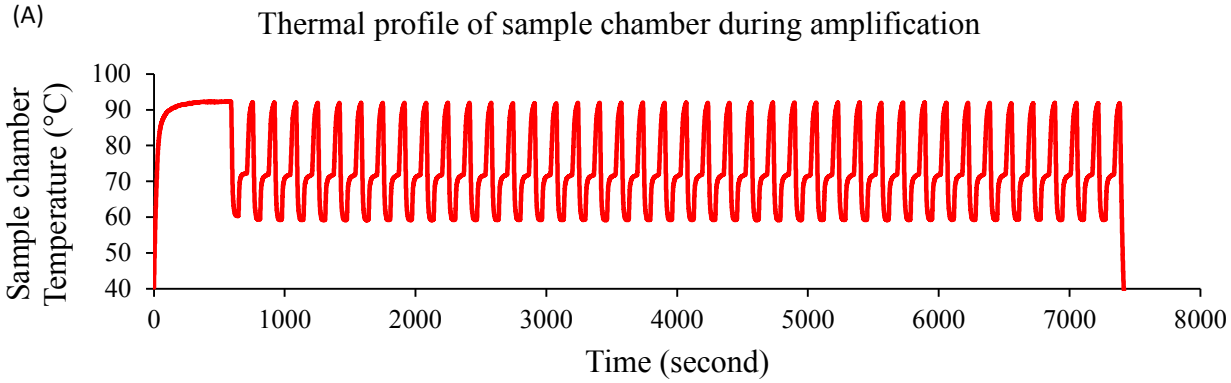
Thermal profile of sample chamber during amplification
Sample chamber Temperature (°C)
100
90
80
70
60
50
40
0
1000
2000
3000
4000
5000
6000
7000
8000
Time (second)

(B)

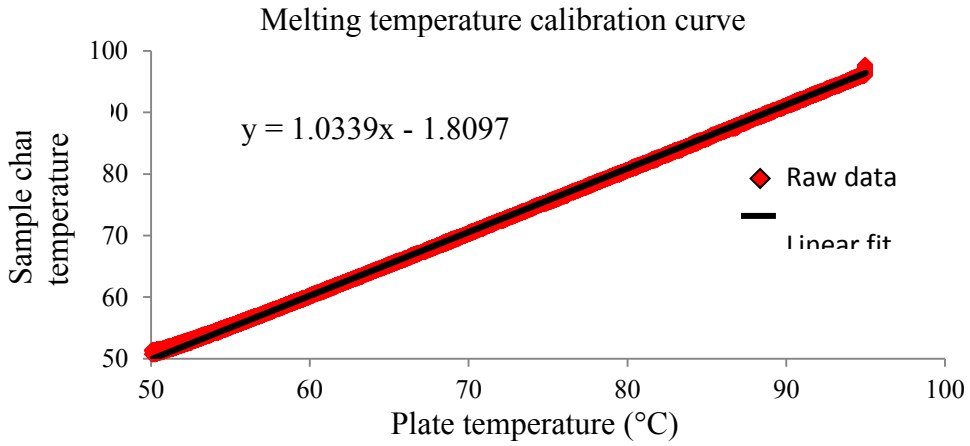
Melting temperature calibration curve
y = 1.0339x - 1.8097
Raw data
Linear fit
Sample chai temperature
100
80
70
60
50
50
60
70
80
90
100
Plate temperature (°C)

Figure 2.4: Thermal characterization.

A) Thermal calibration data for melting curve. **B)** Thermal profile for thermal cycling. Cycling parameters included a 10-minute thermal activation at 95°C, followed by cycling between 95°C for 30 seconds, 60°C for 30 seconds and 72°C for 1 minute for 40 cycles.

(A)

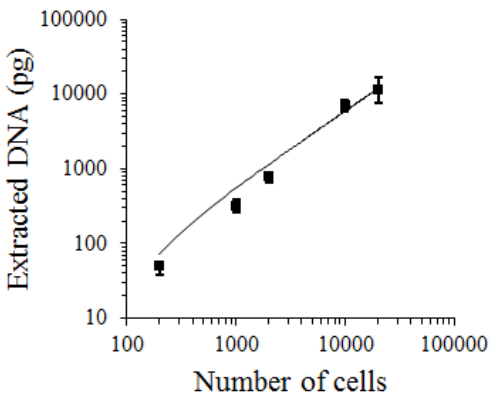
DNA extraction performance
Extracted DNA (pg)
100000
10000
1000
100
10
100
1000
10000
100000
Number of cells

(B)

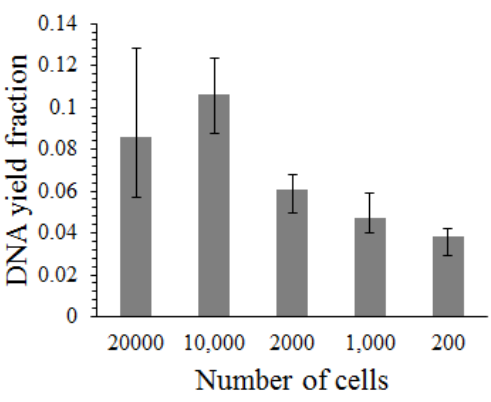
Extraction yield fraction
DNA yield fraction
0.14
0.12
0.1
0.08
0.06
0.04
0.02
0
20000
10,000
2000
1,000
200
Number of cells

Figure 2.5: Characterization of DNA extraction.

Dilutions of Panc 10.05 cell cultures were processed on the microchip and the extracted DNA was quantified using PicoGreen assay (Quant-iT, Invitrogen). The extracted DNA was analyzed as a function of **A)** cell input and **B)** fraction yield based on 6.6 pg DNA per cell.

Oligonucleotide name	Sequence
K-ras forward	**5′- TAAGGCCTGCTGAAAATGACTG -3′**
K-ras reverse	**5′- TGGTCCTGCACCAGTAATATGC -3′**

Table 2.1: Primer sequences

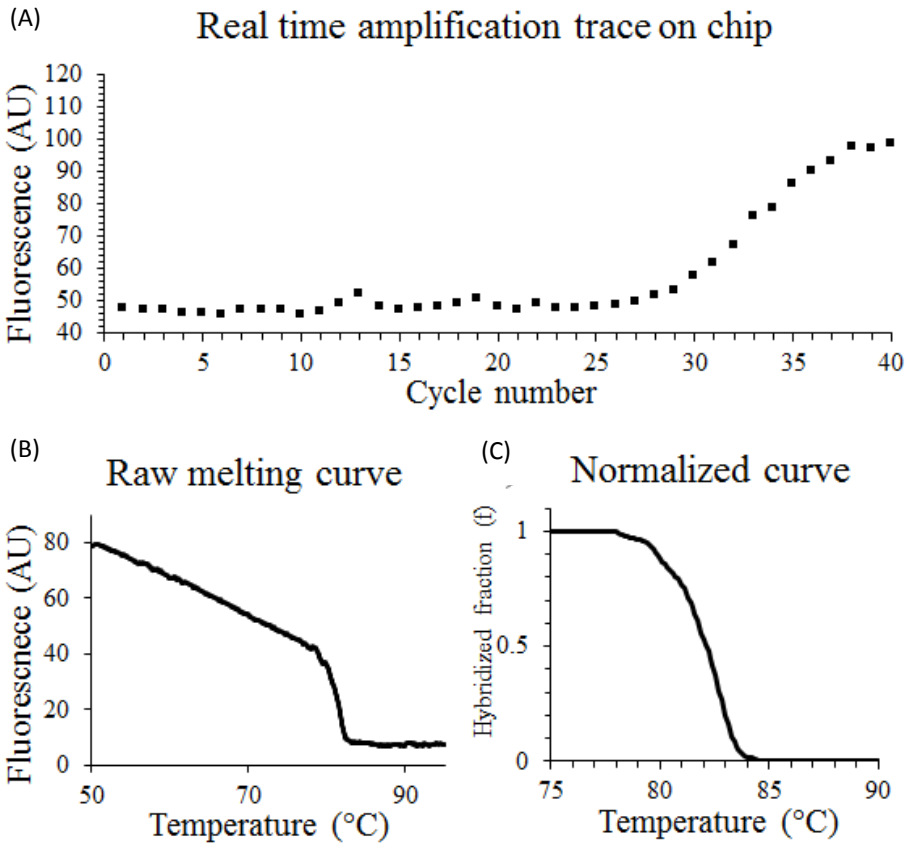
(A)
Real time amplification trace on chip
Fluorescence (AU)
120
110
100
90
80
70
60
50
40
0
5
10
15
20
25
30
35
40
Cycle number
(B)
Raw melting curve
Fluorescnece (AU)
80
60
40
20
0
50
70
90
Temperature (°C)
(C)
Normalized curve
Hybridized fraction (f)
1
0.5
0
75
80
85
90
Temperature (°C)

Figure 2.6: On-chip amplification and melting from crude biological sample.

Genomic DNA was purified from 10 μL human whole blood on the microchip and eluted in the PCR mixture. The microchip was mounted on the miniaturized instrument for thermal cycling and melting curve acquisition. **A)** Amplification enters exponential phase at around 28 cycles. **B)** Raw melting profile obtained after amplification in **Fig. 2.6A**. **C)** Data from **Fig. 2.6B** is processed using custom LabVIEW software to generate a normalized melting profile. Raw signal was processed through Savitsky-Golay filter with a window of 1°C prior to normalization.

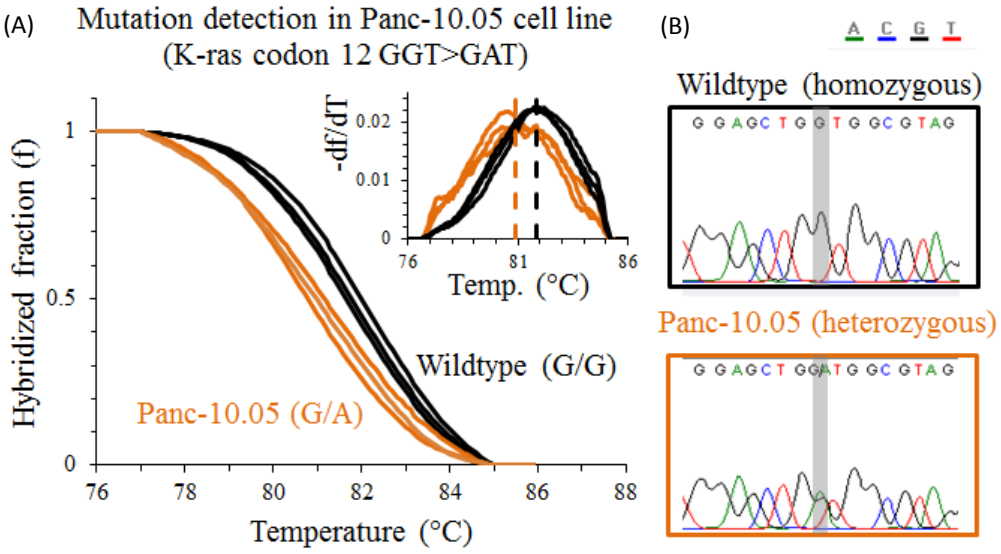
(A)
Mutation detection in Panc-10.05 cell line
(K-ras codon 12 GGT>GAT)
Hybridized fraction (f)
1
0.5
0
76
78
80
82
84
86
88
Temperature (°C)
-df/dT
0.02
0.01
0
76
81
86
Temp. (°C)
Wildtype (G/G)
Panc-10.05 (G/A)
(B)
A C G T
Wildtype (homozygous)
G G A G C T G G T G G C G T A G
Panc-10.05 (heterozygous)
G G A G C T G G A T G G C G T A G

Figure 2.7: Melting curve analysis for K-ras codon 12 mutation.

Adenocarcinoma cell line Panc 10.05 carries a known heterozygous mutation c.25G>A. **A)** Normalized melting profiles from the wildtype and the mutant cell-line genome amplicons. Inset in upper right corner is a derivative plot with dashed lines indicating average melting temperatures, defined as the peak of derivative plot. Approximately 1°C difference is observed between the wildtype and heterozygous mutant. **B)** Genotype of both amplicon set were verified by Sanger sequencing. Panc 10.05 displays a mixture of guanine and adenine signals at the mutated base.

Chapter 3

3. Application of single stream assay design in epigenetic sample processing

3.1 BACKGROUND

Having demonstrated the application of magnetofluidics in a single-stream genetic assay, this chapter extends the application of magnetofluidics to more challenging processes. An important biomedical application can be found in DNA methylation analysis. DNA methylation is a fundamental mechanism in the epigenetic control of gene expression [51]. The close association between hypermethylation and cancer development has led to considerable interest in its use as a promising biomarker for cancer diagnostics, prognostics and prediction to treatment [53-55]. A ubiquitous and essential step in DNA methylation analysis is the bisulfite conversion (BSC) process, which is a biochemical technique used to differentiate between methylated and unmethylated DNA [56]. Through a series of discrete chemical processing steps, the BSC process results in the selective conversion of unmethylated cytosine residues into uracil, while leaving methylated cytosine residues unchanged. Bisulfite conversion ultimately results in the translation of DNA methylation into changes in the primary genetic sequence. The methylation-specific contrast provided by this process can be subsequently assessed through the use of standard DNA analysis techniques in order to determine the methylation status of the original templates.

Bisulfite conversion is currently performed in a benchtop environment using commercially available BSC kits. Despite their widespread use, benchtop processes necessitate an extensive set of manual fluidic handling and centrifugation steps. Furthermore, the microcentrifuge tube-based protocols require relatively large sample volumes for optimal conversion, presenting a substantial constraint when processing small quantities of samples. Dilution of sample volume has substantial drawbacks, as the large surface areas of microcentrifuge tube-based kits have been found to significantly reduce yields for DNA samples smaller than 1 ng [57]. Furthermore, manual fluid transfer between reaction vessels is a highly operator-dependent process that may result in additional sample loss and contamination. Lastly, there is an inherent mismatch in scale that challenges the seamless integration of tube-based sample processing with microfluidic high-throughput analysis platforms. Such concerns make the droplet magnetofluidic platform and the single-stream approach a suitable candidate to simplify and miniaturize the BSC process.

The BSC chemistry also presents several new challenges for the magnetofluidic platform, since it involves multiple thermal incubation steps at various temperatures in addition to fluidic processing steps which do not only require particle extraction but also the addition of liquid buffers across reservoirs. In this chapter, we address these challenges to demonstrate a droplet magnetofluidic device for single-stream bisulfite conversion. We validate our platform using a standard MethyLight assay [58] and demonstrate its performance and advantages over existing benchtop tube processes.

3.2 EXPERIMENTAL DETAILS

3.2.1 Droplet-based bisulfite conversion

In this demonstration, we employed a previously-developed single-tube bisulfite conversion method, methylation on beads (MOB) [57, 59] and adapted it into a microfluidic droplet

format. The bisulfite conversion process in MOB comprises four key sequential steps with intermediate washing steps **(Fig. 3.1A)**. First, the DNA sample is introduced to ammonium bisulfite, resulting in sulfonation and hydrolytic deamination of unmethylated cytosine residues. By contrast, methylation protects the cytosine residue from sulfonation and prevents further chemical modification in subsequent steps. Second, as the unique feature in MOB, silica-coated superparamagnetic beads (SSBs) are employed as a solid phase substrate for tight DNA adsorption, thus allowing DNA capture and transport and facile exchange of buffers across downstream reaction steps. Third, following a brief wash, sulfonated DNA is exposed to sodium hydroxide, during which the uracil sulfonate residues undergo alkali desulfonation to yield fully converted uracil residues. Lastly, the processed DNA is purified via successive washing steps and separated from SSBs, readying recovered DNA for downstream analysis such as quantitative, real-time PCR.

Critically, the use of SSBs enabled the MOB workflow in the microfluidic droplet format because the beads facilitate a robust transport medium for the surface-bound nucleic acids through a lane of isolated droplets, each of which contains a required MOB reagent. An image of the chip with three parallel lanes is shown in **Figure 3.1B**. Each lane consists of one wide and five circular reservoir chambers, each containing aqueous MOB reagent droplets that are isolated within topographic walls. The hydrophobic coating on the bottom surface of the device and the mineral oil pre-loaded in each lane of chip ensures that the aqueous reagents are maintained in droplet form.

In order to convert the MOB process into a magnetofluidics-driven single-stream process, we designed a surface topography-based device that would allow facile manipulation of SSBs to merge droplets, separate from droplets, and disperse within droplets **(Fig. 3.2A)**. In the chamber containing the bisulfite reagent droplet and the binding buffer **(Fig. 3.1B,**

i→ii), the first droplet can be transported across the wide chamber by the SSB cluster for merger with the downstream buffer due to the capillary force on the droplet-oil interface exceeding the magnetic force applied to SSBs. In chambers connected by narrow sieve structures **(Fig. 3.1B, ii→vii)**, SSBs can be effectively separated from reagent droplets and transported into downstream reagent droplets. Such separation is possible because the narrow sieve creates a surface energy barrier to keep reagent droplets in the chamber, while the SSB cluster can be extracted from the reagent due to the significantly higher magnetic force relative to capillary force at the interface. This design provides an efficient and robust means of sequential buffer exchange necessary for bisulfite conversion.

3.2.2 Cartridge priming and assay protocol

On-chip sample processing begins by first mixing 2 µl of extracted genomic DNA (gDNA) with 13 µl of the Lightning Conversion reagent (Zymo) and 5 µl of SSB (Promega Magnesil KF MD), subsequently loading this droplet into the first reservoir **(Fig. 3.2B, step i)**. The sample is subsequently heated to 95˚C for 8 minutes in order to denature the sample into single-stranded DNA (ssDNA). The temperature is then lowered to 54˚C for 1 hour to allow the bisulfite to complete the sulfonation and deamination of unmethylated cytosine into uracil-sulfonate. After this process, the droplet is mixed together with a 60 µl droplet of M-binding buffer **(step ii)** and briefly incubated to allow the DNA to adsorb onto the silica surface of the beads. The SSB are then washed with 40 µl ethanol **(step iii)** to eliminate any remaining bisulfite reagent before being transported into a 20 µl M-desulphonation buffer droplet **(step iv)**. This alkali solution desulfonates the uracil-sulfonate into stable uracil bases. The SSB are washed twice in 40 µl M-wash buffer droplets **(steps v→vii)** in order to remove any residual sodium hydroxide from the solution. Finally, the remaining DNA is eluted from the SSB into Tris-EDTA buffer **(step vii)** and the SSB are decanted into the

previous well to allow the droplet containing purified, bisulfite-converted DNA to be retrieved from the chip for downstream analysis **(step viii)**.

3.2.3 Cartridge design and fabrication

The device consists of a linear array of cylindrical chambers (5 mm diameter), interconnected by sieve structures 1 mm wide and 4 mm long. The total spacing from well center to center is 9 mm in order to facilitate compatibility with standard 96-well microwell plates and multi-channel pipettors. A typical device has a depth of 5 mm. The device is fabricated using only a single piece of PDMS bonded to a thin coverslip, followed by hydrophobic coating. The PDMS pattern was designed using Solidworks 3D CAD (Solidworks Corp.) and translated into a negative acrylonitrile butadiene styrene (ABS) plastic mold generated using a 3D printer (Stratasys Dimension 1200es). PDMS prepared at 1:10 crosslinker-to-base ratio (Sylgard 184, Dow Corning Corp.) is subsequently poured into this mold and incubated at 80˚C for >1 hour. The resulting PDMS structure is bonded to a 2" x 3" coverslip using an oxygen-plasma treatment of the surface. Finally, the chip is coated in Teflon to provide hydrophobic properties to the surface, particularly preventing contact between the reagents and the glass. Heating and cooling of the reagents are performed by regulating the chip temperature via two independent thermoelectric elements, as shown in **Figure 3.3**.

3.2.4 Performance evaluation protocol

In order to evaluate the efficiency and reliability of on-chip conversion, the converted products were assessed using a standard Methylight assay. This assay relies upon carefully designed primers and Taqman probes to quantify the amount of successfully bisulfite-converted target loci. The primers were designed to exclusively amplify only fully-

converted target sequences, resulting in amplification only when complementary template is present.

In the initial assessment of bisulfite conversion on chip, we performed conversion of an unmethylated human gDNA sample using the BSC chip and performed a control experiment using the MOB process in tube. Converted DNA from both processes were analyzed via Methylight assay using primers targeting a locus within the β-Actin gene [60]. An unconverted gDNA sample was used as a negative control. The qPCR master mix was prepared using 300 nM for each primer, 200 nM dNTPs, 500 nM hybridization probe, and 1 unit of Platinum Taq (Invitrogen 10966), 16.7 mM ammonium sulfate, 67 mM TRIS (pH 8.8), 6.7 mM magnesium chloride and 10 mM mercaptoethanol. The relative DNA quantity for both processes was calculated from the CT values using the chip process as the reference value.

Subsequently, we assessed the performance of BSC chip using the average and variability of cycle threshold (CT) values [61, 62]. In order to assess the chip's ability to process a wide range of input DNA in a linear fashion, we used an input DNA ranging from 1ng to 100ng. In order to demonstrate linearity in DNA output from the device for both converted and unconverted DNA, we used a validated set of methylated and unmethylated primers targeting a locus within the promoter region of ADAMTS1 using the same qPCR conditions as described previously [63]. The estimated quantity was normalized using the CT value for 1 ng as a reference.

3.3 COMPARISON OF MANUAL PROCESSING STEPS

The bisulfite conversion on droplet platform significantly reduces both the number of pipetting steps required for the conversion process and the total time required, particularly for multiple simultaneous sample processing. Under the droplet microfluidic approach,

repetitive and operator-dependent pipetting steps required for reagent aspiration and loading is replaced by particle transport across reagent chambers. As a result, pipetting steps are reduced to two steps required for initial loading and final retrieval of DNA sample from the chip. This reduces the number of steps per sample **(Fig. 3.4)** and also enables the use of multi-pipettors for one-step loading and processing of multiple samples in parallel. Compared to a tube-based benchtop process, the BSC chip's capacity for parallelization and simplified fluidic processing steps translate to an overall reduction in sample processing time.

3.4 PERFORMANCE IN DOWNSTREAM ANALYSIS

The converted DNA using the BSC chip platform exhibits comparable performance to the benchtop tube process when analyzed using qPCR. We initially tested the converted DNA using a conversion specific PCR primer set which does not take into account methylation status (β-actin). We found the CT values for the BSC chip process and the tube based process to be 28.34 and 28.45 with a standard deviation of 0.14 and 0.25, respectively **(Fig. 3.5A)**. Similar conversion efficiency was observed between the two processes, suggested by the comparable mean CT value. As expected, bisulfite conversion is required for amplification as indicated by the lack of amplification in the unconverted negative control.

To further assess the device's ability to process DNA without bias towards DNA input quantity or methylation status, we compared the converted output of unmethylated and methylated DNA controls at various concentrations using methylation specific primer sets targeting ADAMTS1 promoter region. The processed DNA concentration **(Fig. 3.5B)** shows a linear relationship with the initial DNA concentration and demonstrates that the BSC chip can operate at high yield across a wide range of sample input quantity. We were able to perform simultaneous conversion on a BSC device with all three lanes to demonstrate low

bias and high reproducibility across replicates **(Fig. 3.5B)**. Importantly, we established that qPCR linearity is preserved across replicate features, indicative of high process fidelity using the droplet device.

3.5 RELIABILITY AND REPRODUCIBILITY

The bisulfite conversion process performed on chip exhibits high reproducibility across runs. The low variability **(Fig 3.5B)** is translated into accurate quantification when used in conjunction with qPCR. This variability is comparable regardless of methylation status. Additionally, this variability is also comparable to that exhibited by the Zymo Lightning Kit when performed in tube.

The reduced processing time required for the conversion reagents from the Zymo Lightning Kit not only significantly reduces the total processing time but also minimizes evaporation **(Fig. 3.6)**. Protection from significant evaporation helps to maintain stable buffer conditions for highly reproducible conversion results. Additionally, there are no visible effects of precipitation of reagents in the droplets due to saturation, which could lead to co-precipitation of DNA and loss as a consequence.

3.6 CONCLUSION

In this chapter, we presented a droplet magnetofluidic approach to performing BSC with a significant reduction in reagent volumes and complexity as compared to the benchtop in-tube process, while maintaining equivalent performance in various performance metrics tested. All necessary steps were performed via droplet merging, droplet separation and mixing within the droplet through magnetofluidic manipulation. The benefit of miniaturization via droplet magnetofluidics is most pertinent the reduction of sample

volume, which enables the analysis of rare samples that are likely to suffer from reduced yield when diluted for processing with the tube-based benchtop protocol.

The modular nature of the device also suggests multiple paths through which the functionality of the BSC chip can be augmented and enhanced. The simplicity of an open-surface droplet design is amenable to facile integration with automation equipment for operator-free sample injection and retrieval, while future iterations of the device may be parallelized at a larger scale for high-throughput sample processing. The chip can potentially interface with other surface droplet solutions. For example, DNA extraction can be performed on the chip prior to conversion [9]. Likewise, the chip can incorporate downstream analysis such as whole genome [64], or locus-specific [21] methylation assessment.

In summary, the robustness of the on-chip BSC in addition to the simplified sample processing workflow and volume reduction demonstrate substantial benefit over existing benchtop processes. Furthermore, the platform's potential for full automation and scalability lays the groundwork for integrating sample pre-processing in high-throughput DNA methylation analyses. As the demand for processing and analysis of macromolecules increases with their potential relevance as biomarkers, it is anticipated that investigations such as our own will continue to demonstrate the utility of a magnetofluidics-driven single-stream approach as an alternative to the conventional fluidic process with flexibility for miniaturization and parallelization.

(A)

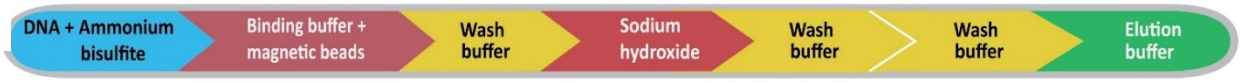
DNA + Ammonium bisulfite
Binding buffer + magnetic beads
Wash buffer
Sodium hydroxide
Wash buffer
Wash buffer
Elution buffer

(B)

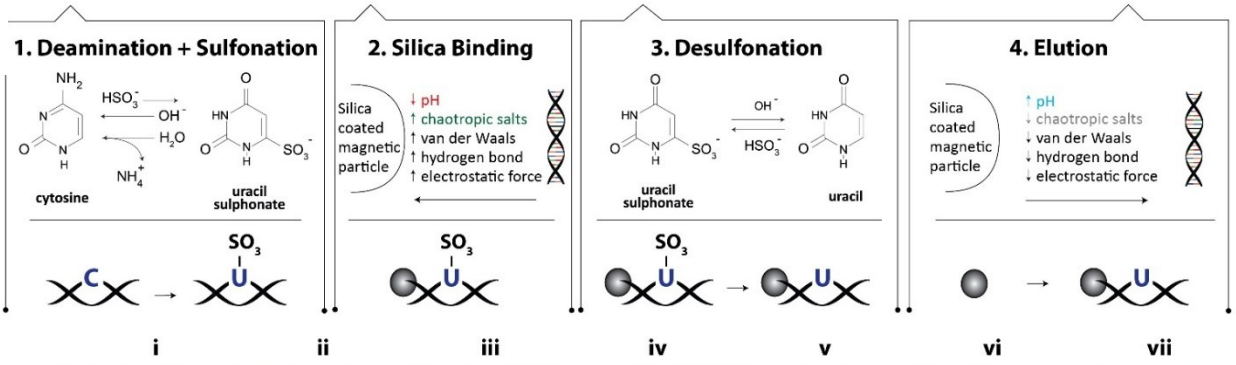
1. Deamination + Sulfonation
cytosine
uracil sulphonate
2. Silica Binding
Silica coated magnetic particle
↓ pH
↑ chaotropic salts
↑ van der Waals
↑ hydrogen bond
↑ electrostatic force
3. Desulfonation
uracil sulphonate
uracil
4. Elution
Silica coated magnetic particle
↑ pH
↓ chaotropic salts
↓ van der Waals
↓ hydrogen bond
↓ electrostatic force
i
ii
iii
iv
v
vi
vii

(C)

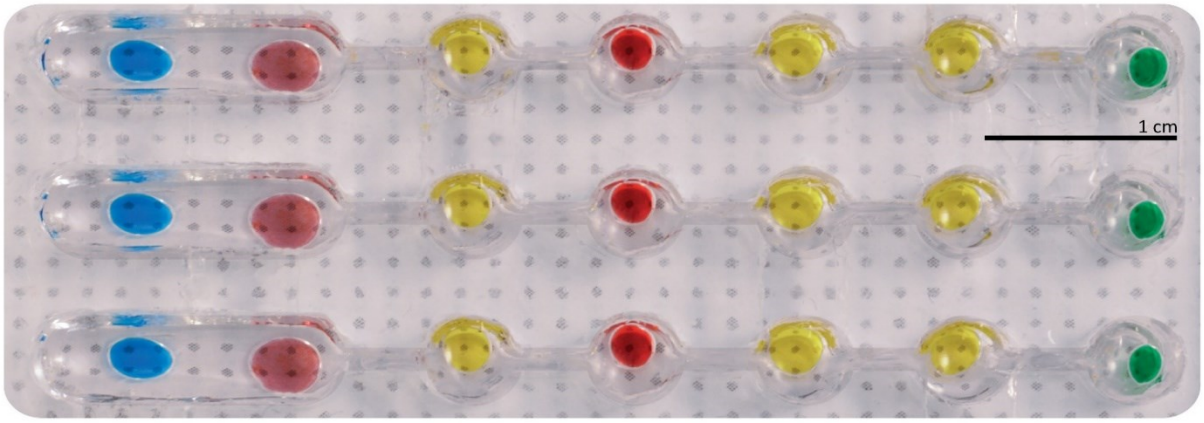
1 cm

Figure 3.1: Single-stream bisulfite conversion workflow.

A) Outline of bisulfite conversion chemistry. Bisulfite conversion allows the discrimination of methylated from unmethylated cytosine by transforming the latter into uracil. Methylated cytosine (represented as mC) is protected from this conversion, resulting in changes in primary sequence that can be analyzed by various DNA analysis methods. **B)** The bisulfite conversion on-chip process, as performed using a series of buffers contained within the chip. **C)** Photograph of aqueous reagents loaded onto a single lane of droplet chip. Each reagent is contained in a round well that holds the droplet within it. The wells are connected either by a single open channel (i.e. between I and II) to merge the droplets or a narrow sieve (II through VII) to separate the beads from the droplet by surface tension.

(A)

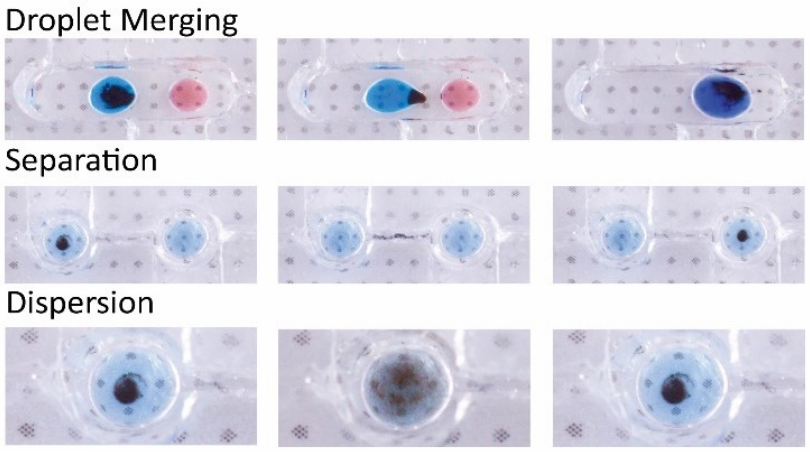
Droplet Merging
Separation
Dispersion

(B)

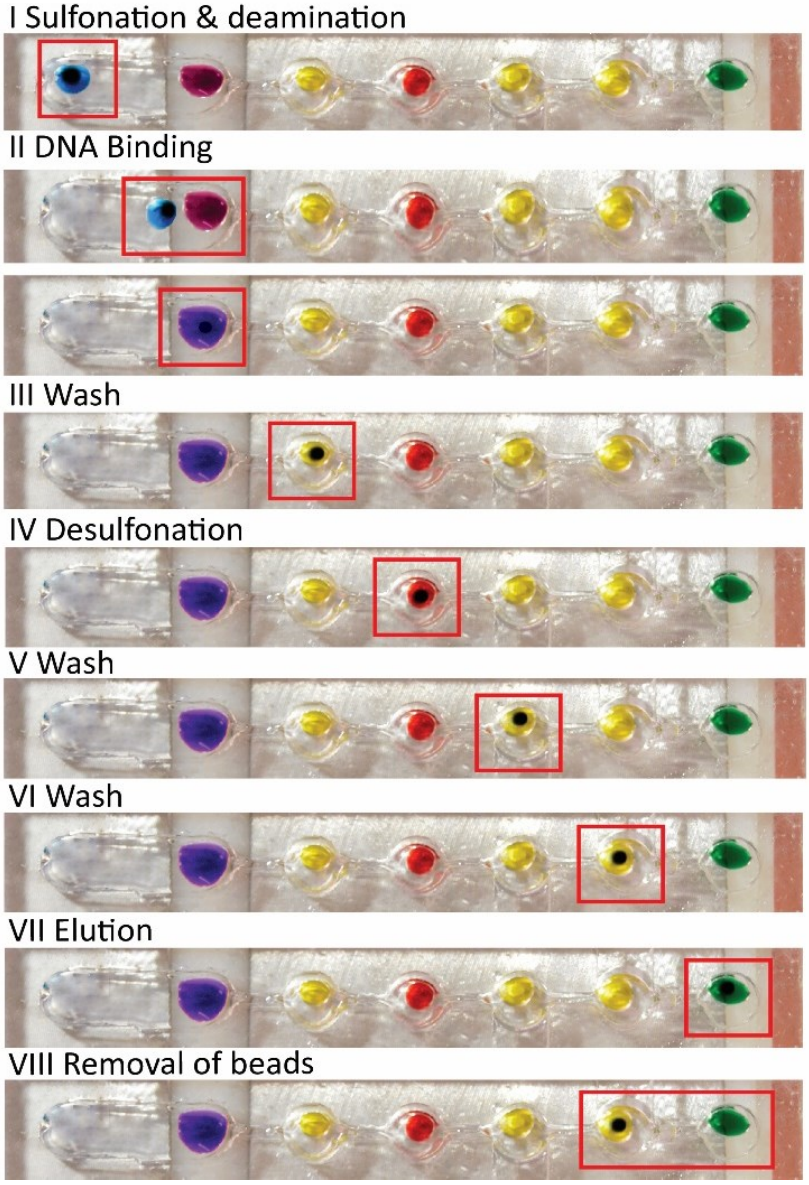
I Sulfonation & deamination
II DNA Binding
III Wash
IV Desulfonation
V Wash
VI Wash
VII Elution
VIII Removal of beads

Figure 3.2: Droplet processing sequence.

A) The steps required for bisulfite conversion are demonstrated in their corresponding reagent droplets. As the beads and DNA (red frame) are transported across the chip surface, the DNA is exposed to each subsequent reagent of the BSC process. **B)** There are three main modes of transportation for the beads. Droplet merging is done across an open channel, where the lower surface energy allows the droplet to be transported with the bead cluster. The separation process is achieved by moving the beads across a sieve where the droplet is retained while the SSB cluster can move. Dispersion is performed by removing the magnetic force and allowing the magnetic beads to resuspend via Brownian motion.

(A)

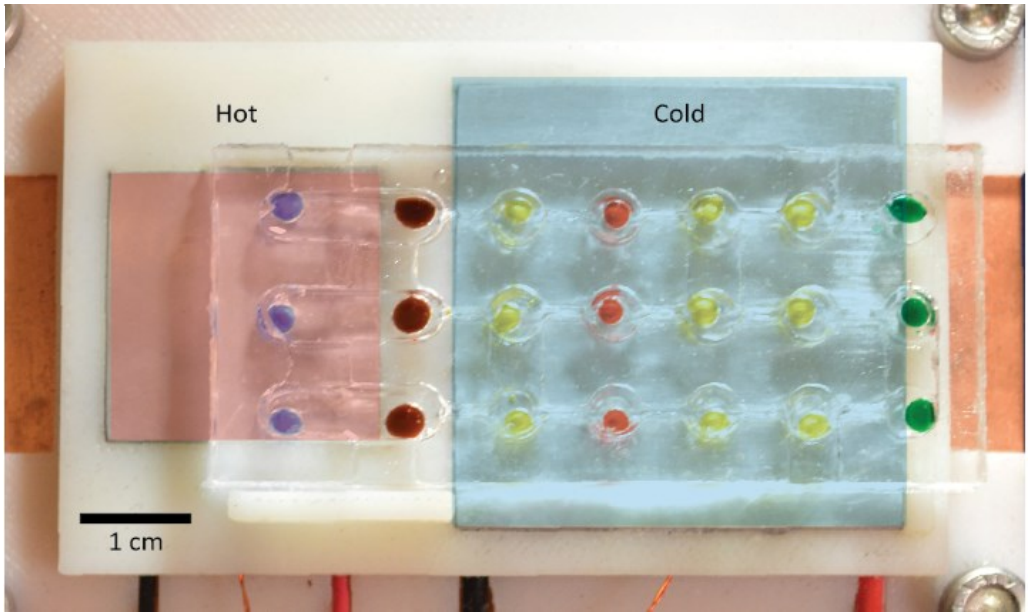
Hot
Cold
1 cm

(B)

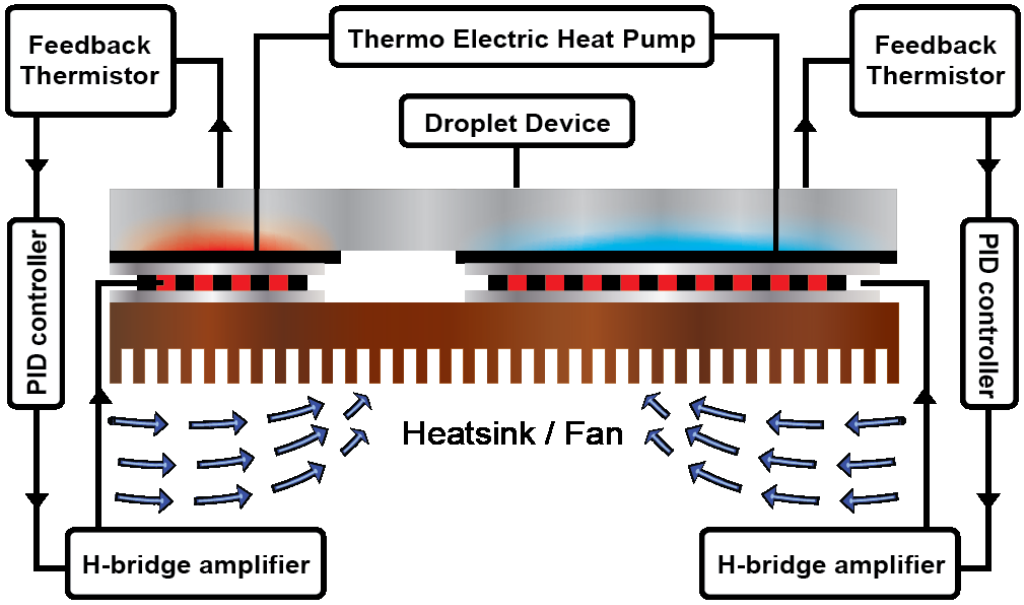
Feedback Thermistor
Thermo Electric Heat Pump
Feedback Thermistor
Droplet Device
PID controller
PID controller
Heatsink / Fan
H-bridge amplifier
H-bridge amplifier

Figure 3.3: Thermal control instrumentation.

A) The temperature is controlled via a dual thermal controller setup. The thermoelectric pump on the left can heat the sample (red) while the pump on the right maintains the rest of the chip at a lower temperature (blue). **B)** The first thermoelectric element is used to heat the incubation region (highlighted in red) while the second maintains the rest of the chip at room temperature (blue) to prevent evaporation of the wash and desulfonation buffers during all heating steps. The thermoelectric elements are controlled by a proportional-integral-derivative (PID) controller, which monitors the heating surface temperature via a thermistor. The use of two temperature zones ensures that reagent temperatures at incubation zones do not adversely affect other reagents due to thermal conduction.

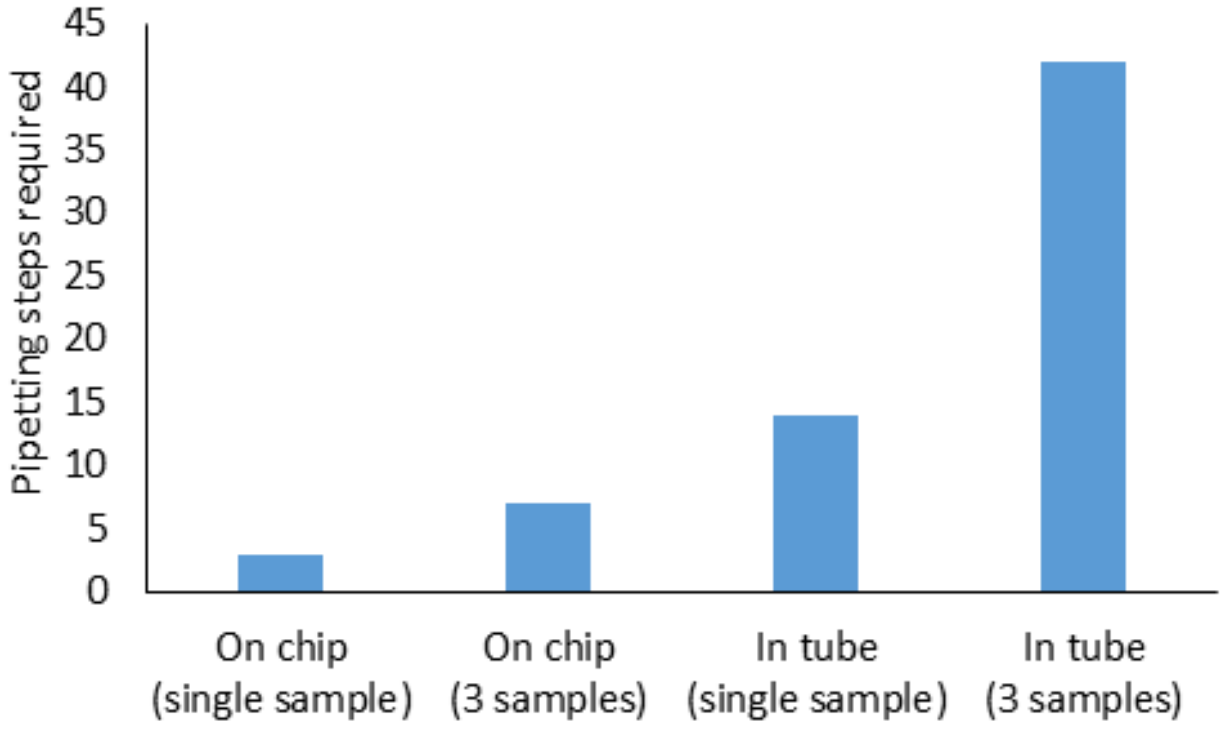
Pipetting steps required
45
40
35
30
25
20
15
10
5
0
On chip (single sample)
On chip (3 samples)
In tube (single sample)
In tube (3 samples)

Figure 3.4: Comparison of manual processing steps.

The BSC chip greatly reduces the number of manual pipetting steps, particularly when processing multiple samples in parallel. Tube-based benchtop process require numerous liquid transfer steps into and out of the tube, while the BSC chip reduces the essential number of liquid transfers to sample loading and retrieval.

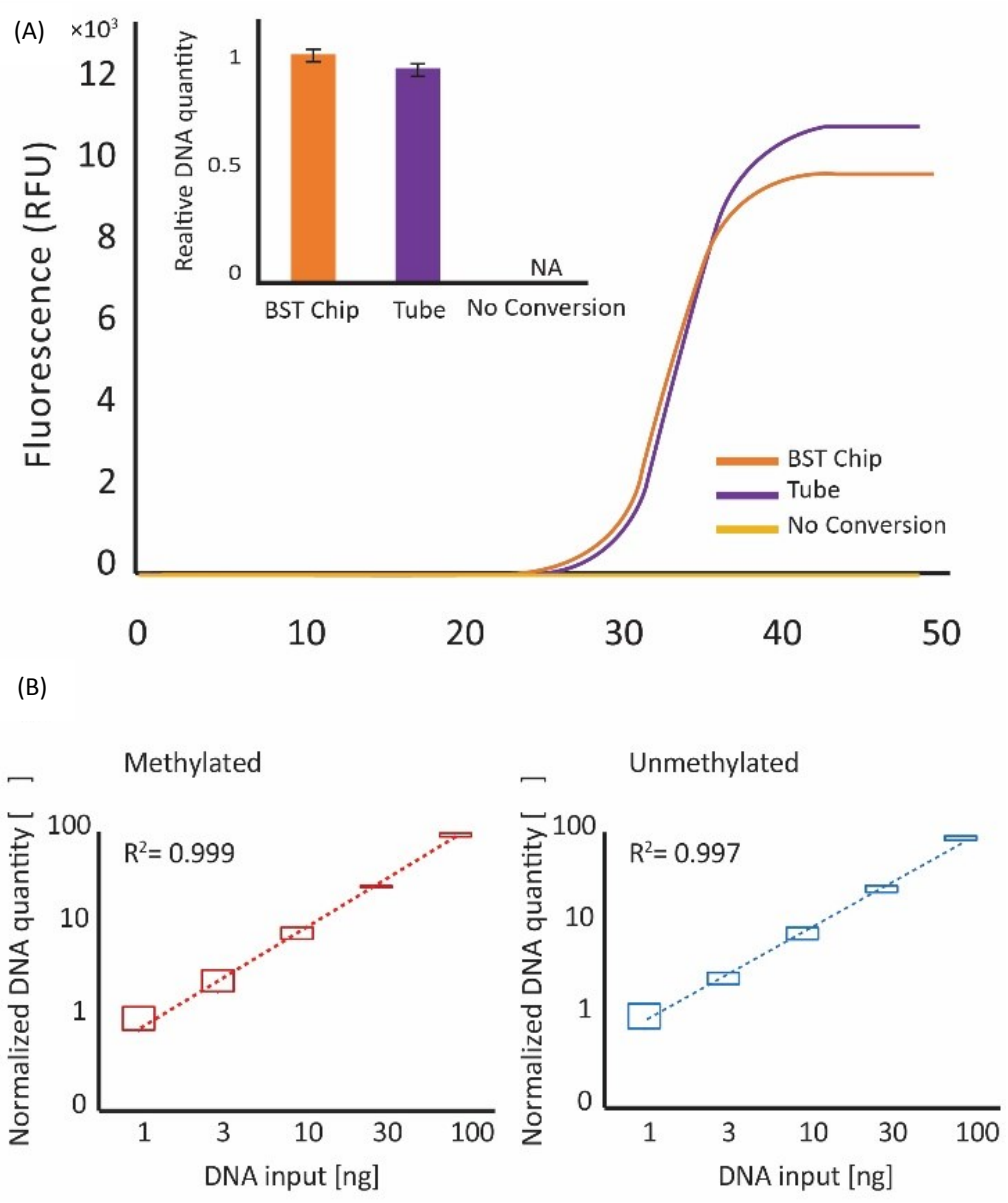
(A)
×10³
Fluorescence (RFU)
12
10
8
6
4
2
0
0
10
20
30
40
50
Realtive DNA quantity
1
0.5
0
NA
BST Chip
Tube
No Conversion
BST Chip
Tube
No Conversion
(B)
Methylated
Normalized DNA quantity [ ]
100
10
1
0
R²= 0.999
1
3
10
30
100
DNA input [ng]
Unmethylated
Normalized DNA quantity [ ]
100
10
1
0
R²= 0.997
1
3
10
30
100
DNA input [ng]

Figure 3.5: Comparison between chip and tube performance.

A) The qPCR amplification curve for the tube process (shown in purple) is compared to the chip process (shown in orange). **B)** The calculated DNA recovery (based on CT value and normalized to 1 ng) for varying quantities of DNA are compared across methylated and unmethylated sequences. The top and bottom bars reflect the variability across multiple devices and different channels.

SIDE

Initial state	After 8min @ 95 °C	After 60 min @ 54 °C
		
20.0 µl	19.8 µl	19.7 µl

Figure 3.6: Evaluation of droplet size after incubation.

The droplet showed a 1% reduction after the 8 minutes of heating at 95 ˚C and a 0.5 % reduction after an hour at 60 ˚C, for a total of 1.5% volume reduction.

Chapter 4

4. Sample-to-answer process automation with droplet magnetofluidics

4.1. BACKGROUND

In the last two chapters we demonstrated the concept of single-stream assay workflow using droplet magnetofluidics, highlighting the transformation of multiple fluidic handling steps into a sequential process of magnetic particle translocation. The benefit of this workflow is more clearly apparent when the operator can appreciate the scale of miniaturization that can be attained not only in cartridge design, but the operating instrument as well. Process integration and automation are inseparable goals in designing a platform that can be operated by an untrained person in the absence of laboratory infrastructure. The ASSURED guideline for POC tests set by the World Health Organization (WHO) stipulates operability by untrained person and delivery to end users as its criteria [65]. In order to gauge the prospects for achieving this task, we set out to develop methods of process automation for droplet magnetofluidic assays.

Movable permanent magnets have been used to successfully perform transport, splitting, merging of droplets in previous investigations [10, 11, 14] as well as our own described in the preceding chapters. Automation via translational stages can facilitate automation of this process in a manner that is analogous to robotic pipettors for conventional fluidic processing. While straightforward in principle, this approach raises a number of potential

challenges. Due to the presence of supporting components such as the stepper motor, controller module and power supply, translational stages occupy a considerable footprint and weight that may not be suitable at the point of care. The need for regular maintenance of lead screws also limits the accessibility of such instruments in the hands of an untrained user. In addition, permanent magnet-actuated platforms with a single plane for the exertion of magnetic field generally lack strategies for bead agitation. Addressing these limitations, planar coils have been demonstrated to be capable of generating effective magnetic fields for long-range transport and manipulations of droplets [8, 66], providing a largely maintenance-free electronic apparatus for droplet operations.

In this chapter, as illustrated in **Figure 4.1**, we present an electromagnetic droplet platform for PCR-based genetic testing in which magnetic particles are automatically processed using coil array-induced magnetic field gradients and are assisted by topographical barriers for splitting operations. The combination of electromagnetic coils and topographical barriers enables efficient and automated manipulations of droplets from a wide variety of buffers and reagents – including lysis, binding, wash, elution buffer and PCR reagent – required for carrying out the entire process of genetic detection assays. As we will discuss further, optimizing various parameters of the assay cartridge presents unique challenges when the magnetic field gradient is generated by sources substantially weaker than rare-earth permanent magnets, such as an electromagnet. We demonstrate the functions of our droplet manipulation platform by performing all processing steps between whole blood sample input and real-time amplification detection on a single cartridge.

4.2 EXPERIMENTAL DETAILS

4.2.1 Cartridge fabrication

The cartridge consisted of seven compartments connected serially by six sieve structures **(Fig. 4.1)**. Each sieve was designed with a radius of curvature of 1.5 mm and a gap width of 750 µm. Outer dimensions of the cartridge were approximately 56 × 15 × 6 mm. ABS molds were generated by 3D rapid prototyping (Dimension 1200es, Breakaway Support Technology, USA). PDMS (Sylgard 184, Dow Corning Corp., USA) prepared with base-to-crosslinker ratio of 9:1 was cast into the mold and cured at 80°C for 30 minutes. The demolded structure was covalently bonded to a glass cover slip with a thickness of 100 µm (GOLD SEAL cover glass, Electron Microscopy Sciences, USA) following standard O_2 plasma treatment process. The device was subsequently dip-coated in a 1% w/w Teflon AF 1600 (DuPont Corp., USA) in FC-40 solvent (3M Company, USA) and baked overnight at 80°C. Teflon coating was applied in order to protect against surface adsorption of biomolecules and to prevent spreading of reagent droplets on the cartridge surface. The completed prototype is shown in **Figure 4.1A**.

4.2.2 Magnetic bead manipulation system

Figure 4.1B depicts the schematic assembly of the magnetic bead manipulation system. The fabricated device was attached on top of PCB containing a linear array of planar coils that were used as electromagnets to manipulate the magnetic beads. The sieve structures were aligned to the coils as shown in **Figure 4.1C** to ensure proper droplet manipulation. The magnitude of coil-induced magnetic fields was controlled by modulating the amplitude of driving current source, while the directions of fields generated by each coil were controlled by an H-bridge circuit. Custom software written in LabVIEW (National Instruments, USA) was used to sequentially control the magnitude, duration and direction of magnetic fields. Automated operations were achieved by programming a complete routine for particle splitting and agitation operations in each reagent for DNA extraction and PCR.

A set of permanent magnets were placed on top of a soft magnetic steel plate, generating a 50×10 mm plane of uniform transverse magnetic field measuring approximately 50 mT. Magnetic field gradients were adjusted by a two-layer, 200 μm thick PCB. The PCB contained 7 coils on the top layer and 6 coils on the bottom layers, in which there was a partial overlap of adjacent coils with the center-to-center distance of 3 mm. Each coil was designed in a square profile with 8 windings. The height, width, and pitch of the copper lines were 35 μm, 150 μm, and 150 μm, respectively.

A thermoelectric module (Custom Thermoelectric Inc, USA) was placed underneath the PCB as a cooling pad to alleviate the effects of Joule heating on thermally sensitive reagents such as the PCR mixture, which contains heat-activated enzymes. Cooling temperature was feedback controlled by using a commercial PID controller (Accuthermo Technology, USA) and a K-type thermocouple (Omega Engineering Inc, USA) mounted on the surface of the module.

4.2.3 Cartridge priming and assay protocol

The on-chip procedure for the cell lysis, extraction and purification of nucleic acids followed the standard protocol based on solid phase extraction methods using commercially available silica-coated magnetic particles. Magnetic particles and reagents for nucleic acid extraction were purchased from Roche (MagnaPure LC DNA Isolation Kit I, Roche Diagnostic Corporation, USA). Unspun human whole blood from male donor containing heparin anti-coagulant was purchased from Biological Specialty Corporation (Colmar, PA, USA). The cartridge described previously was first filled with mineral oil (M5904, Sigma-Aldrich, USA) containing 0.5% w/w of surfactant Span-80 (Sigma-Aldrich, USA) to prevent the evaporation of reagents. Sessile reagent droplets (10-30 μL) corresponding to each step of the assay protocol were loaded sequentially into the compartments. 5 μL of whole blood

was transferred into a mixture containing 10 µL lysis/binding buffer (LSB), 5 µL Tris-EDTA buffer, 1 µL Proteinase K (20 mM) and 3 µL of magnetic particles, and the mixture was dispensed into the first compartment of the device. Compartments 2 through 6 were sequentially loaded with the following reagents: 15 µL washing buffer 1 (WB1a), 15 µL washing buffer 1 (WB1b), 15 µL washing buffer 2 (WB2a), 15 µL washing buffer 2 (WB2b), and 10 µL PCR reagent mixture, as illustrated in Scheme 1D. The lysis mixture in the first compartment was incubated on chip for 5 minutes with 100 cycles of agitation. Each washing step consisted of merging particle with the wash buffer, 15 cycles of mixing/agitation for 45 seconds, and splitting of particle into the next reagent droplet. Lastly, genomic DNA was eluted into the PCR mixture droplet by incubating the magnetic particles for 5 minutes with continuous agitation. The last compartment was intentionally left empty as a waste collection reservoir. PCR reagent mixture was prepared using QIAGEN HotStarTaq Core Kit (QIAGEN N.V., Netherlands). Total time required for electromagnet-actuated sample preparation was 15 minutes including all incubation steps, only a fraction of time required for manual extraction by a technician (Dundas et al., 2008).

4.2.4 Nucleic acid amplification and detection

After sample preparation was performed using the magnetic droplet manipulation system, the cartridge was transferred to a custom-built instrument for thermal cycling and fluorescence detection **(Fig. 4.2)**. Thermal cycling was performed using a thermoelectric module and PID controller in a similar arrangement used for Joule heat management. In order to account for transition times and temperature offsets between the surface of thermoelectric module and the droplet, thermal cycling conditions were calibrated to temperature profile obtained by monitoring a 10 µL PCR mixture with a secondary thermocouple. Temperature profile obtained during calibration is presented in **Figure 4.3**.

Primers targeting codon 12 of exon 2 of the KRAS oncogene was used as previously described (Ho et al., 2004). Primers were synthesized by Integrated DNA Technologies Inc. (Coralville, IA, USA) and 1x LC Green Plus+ (Idaho Technologies Inc, USA) was used as the double-stranded DNA binding reporter dye. Primer sequences are presented in **Table 2.1**.

Fluorescence was detected using a custom-built, portable optical instrument in epifluorescence configuration consisting of a blue light-emitting diode (LED) source (λ_{max}=470nm) and photodiode. Briefly, pulsed light from LED was passed through an excitation filter, reflected by a dichroic mirror, and was then focused onto the PCR reagent mixture droplet. Fluorescence emission from the reporter dye bound to genomic target was passed through an emission filter and focused onto a frequency-sensitive detector. The signals from the detector were recorded using analog-to-digital acquisition (USB-6229, National Instruments, USA) at a 5-second interval with a bin time of 150 ms. Signals obtained over the last 25 seconds of each annealing phase was averaged and plotted to generate a real-time amplification profile.

Agarose gel electrophoresis was performed to verify product amplified on droplet platform. Gels were run at 8 V/cm for 60 minutes. DNA was stained using GelStar nucleic acid gel stain (Lonza Rockland Inc, USA) and imaged under an epi-illumination configuration using a Kodak Gel Logic 200 Imaging System (Kodak, USA).

4.3 OPERATING PROCEDURE

In this droplet cartridge (**Fig. 4.1D**), genomic DNA extraction from whole blood and subsequent real-time amplification were integrated into a single process on the cartridge. First, whole blood sample was loaded to the initial compartment containing lysis buffer mixture and incubated. During this process, the white blood cells in sample matrix were lysed to release the genomic material. The released genomic DNA was adsorbed to silica-

coated surface of magnetic particles in the presence of chaotropic salt in the lysis/binding buffer. After incubation, magnetic particles were split from the lysis buffer using coil-induced field gradient and merged into a series of washing buffers. The magnetic particles were then merged with the last droplet reagent containing PCR mixture and incubated. The lower concentration of salt present in a PCR mixture enables the genomic DNA bound on the particle surface to be released into the mixture. Afterwards, the magnetic particles were split from the PCR mixture into the waste chamber and the entire cartridge was loaded onto a custom-built thermal cycler and optical detection instrument for real-time amplification on chip.

4.4 PCB COIL ARRAY-BASED DROPLET MANIPULATION

Droplet kinematic behaviors were governed by the interaction between two forces. The first was the magnetic force acting on the magnetic particles within the droplet, while the second was the capillary force induced by droplet deformation [20]. The proposed droplet manipulation strategy employed on-cartridge topographic features to control capillary forces, with an external actuation mechanism to control magnetic force on particles. Actuation of magnetic particles is realized on this platform using planar coil-induced magnetic field gradients in presence of uniform static field [8]. Briefly, this mechanism utilizes a large, uniform transverse magnetic field B_0 to strongly polarize the magnetic moments of magnetic particles (**Fig. 4.4A**). Planar coils are used to induce small magnetic fields in parallel with B_0. Since the magnetic force acting on each particle is described by the dot product of magnetic moment and the applied field gradient [38], force is generated towards the direction where the transverse component (B_z) of field generated by planar coils is maximized. Controlling the direction of driving current allows switching of the polarity of coil-induced field, resulting in magnetic field gradient that can be made both

positive and negative. This enables both attractive and repulsive forces which is necessary to perform transport, splitting and agitation of magnetic particles.

Meanwhile, capillary force is controlled using sieve structures to facilitate droplet splitting. Capillary force has two components, the Laplace force and the interfacial tension force [67]. As illustrated in **Figure 4.4A**, sieve structures were incorporated between reagent compartments to facilitate droplet deformation during splitting. When the magnetic droplet was actuated through the sieve, the droplet was deformed to attain negative mean curvature resulting in negative Laplace force. This phenomenon mitigates the effective capillary force, enabling droplet fission with a relatively low magnetic force.

4.5 DROPLET SPLITTING AND MERGING

To split magnetic particles from the droplet with maximal retention of particles, a magnetic field gradient was generated by applying a positive, zero, and negative current to three consecutive coils, respectively **(Fig. 4.4B)**. The magnetic fields were simulated numerically using commercial software (CFD-ACE+, CFD-RC, USA) and further characterized by measuring the coil-generated fields **(Fig. 4.5A and B)**. The resulting magnetic force was sufficient to overcome the capillary force and cause droplet fission. In order to mitigate the effects of Joule heating on interfacial tensions and thermally sensitive reagents such as the PCR mixture, the temperatures inside the droplet during the splitting process were maintained below 30°C by using a thermoelectric cooler located below the PCB. Joule heating is characterized and presented in **Figure 4.5C**.

Droplet splitting is primarily influenced by the interfacial tension between the droplet and the surrounding medium, as well as the magnetic force. In the proposed assay, we observed three levels of interfacial tensions between different reaction droplets and surrounding oil medium: 1) lysis mixture containing the lysis/binding buffer (LBS), which includes 20-30%

w/w Triton X-100, 2) washing buffers 1 and 2 (WB1 and WB2) containing 30-60% w/w ethanol, and 3) the PCR master mixture mostly composed of water and salts. Experimental conditions were optimized such that consistent splitting and merging could be achieved in all three types of reagents. Splitting conditions were adjusted by varying three factors: 1) magnetic particle load, 2) surfactant concentration in surrounding oil medium, and 3) sieve gap. Topography-assisted splitting enabled us to apply a wide range of particle load to optimize the splitting conditions simultaneously for the reagents with several different interfacial tensions. If particle load was less than 200 μg, the magnetic force applied to the beads was insufficient to overcome interfacial tension of the parent droplet. With particle load in excess of 600 μg, the separated bead plug carried a substantial amount of buffer from the parent droplet. Particle loads between these limits were examined to qualitatively assess the splitting capability from various reagents. Higher surfactant concentration was observed to cause droplet instability indicated by difficulty in priming the device with reagents, while lower surfactant concentration was accompanied by increased difficulty in splitting. Variation in sieve gap size demonstrated poor repeatability in splitting operation with gap sizes smaller than 500 μm, due to the increased resistance to particle extraction from topographical barrier. Gaps larger than 1000 μm resulted in large amounts of buffer carryover, as the particles were unable to dissociate from the parent droplet. An intermediate gap size of 750 μm showed high repeatability with low carryover volume.

Figure 4.6 shows a photographic sequence of surface topography-assisted droplet splitting process, where a droplet containing magnetic particles is deformed through the sieve structures and dissociated into a small plug carrying trace amount of aqueous material from the parent droplet. As field maximum was generated at the destination compartment, magnetic particles were collected into a plug and pulled through the sieve structure until scission occurred at the elongated neck (**Fig. 4.6D**). After splitting from the parent droplet,

magnetic particles were merged with the subsequent droplet. At the optimal concentration of surfactants, magnetic particle plug could be brought into close proximity with subsequent droplet without immediate merging upon contact. The resulting conditions enabled the droplet compartments to be packed more compactly on a smaller cartridge footprint. Droplet merging could be actively induced by generating field maximum at the center of current compartment, resulting in merger of the magnetic plug with the target droplet and collection of magnetic particles at the center of the droplet (**Fig. 4.6E**).

4.6 PARTICLE AGITATION

One of the advantages of this platform is that efficient mixing can be achieved by agitating magnetic particles under alternating attraction and repulsion forces, as illustrated in **Figure 4.7C**. Particle agitation involves a single coil centered on the droplet. When the direction of coil-generated magnetic field is parallel to background field, the maximal field occurs at the center of coil and particles are concentrated at the center of droplet. When the current is reversed, coil-generated field is antiparallel to background field; the center of droplet becomes a local field minimum, and particles are dispersed towards the fringes of the droplet. The particles can be repeatedly agitated inside the droplet by alternating the polarity of current.

Particle agitation was performed by applying a current of 1.5 A with alternating frequency of 0.5 Hz. Performance was evaluated by comparing the diffusion process of the dark blue food dye in water in presence and absence of agitation. Inner convective flow was introduced with the assistance of agitation and accelerated the mixing process, as shown in **Figure 4.7B**. Mixing of food dye with water was achieved in 2 seconds. Conversely, hardly any mixing was observed over the span of 50 seconds when the process was left to diffusion alone, as shown in **Figure 4.7C**. In contrast to the permanent magnet-based actuation

scheme, in which the magnetic particles are anchored to the surface due to magnetic attraction or higher specific gravity, mixing efficiency can be enhanced by means of magnetic agitation in the proposed system.

4.7 PARTICLE WASHING

When crude biological samples are lysed, the buffer carried over by the magnetic clusters contains PCR inhibitors including hemoglobin and DNA-binding proteins [68]. Performance of washing process was evaluated by estimating the volume of buffers being carried over between each reagent droplet. Washing process was defined as a combination of droplet splitting with subsequent merging. Owing to the presence of a dark blue dye in lysis/binding buffer, it is a suitable indicator of cleanness after each washing step. A reference curve was first generated by measuring the mean gray value of color of lysis/binding buffer against serial dilutions to evaluate the effect of washing **(Fig. 4.8)**. Afterwards, the magnetic particles were split from LSB droplet and were subsequently washed in WB1a, WB1b, WB2a, and WB2b, as demonstrated in **Figure 4.9A**. **Figure 4.9B** presents the mapped grey values of LSB, WB1a, WB1b, and WB2a on the reference curve with dye concentrations of 83.9% (C_{LSB}), 6.1% (C_{WB1a}), 0.5% (C_{WB1b}), and less than 0.1% (C_{WB2a}), respectively.

Based on a previous investigation by Lehmann et al., a simple dilution calculation was performed using the following equation:

$$V_C \times C_{LSB} = C_{WB1a} \times (V_C + V_{droplet})$$

The carryover volume (V_C) after the first wash step was estimated to be around 1.2 µL that is merged with a subsequent droplet of a volume ($V_{droplet}$) of 15 µL. Similarly, the carryover volume after the second washing was estimated to be around 1.3 µL. Volume occupied by

the magnetic particles (< 0.1 μL) was considered to be negligible. It is reasonable to estimate that each washing on the device step results in >10 fold dilution, meaning that the lysis buffer residue and PCR inhibitors carried alongside magnetic particles are attenuated 10^4-fold or greater in the PCR reaction buffer after the four washing steps.

4.8 DNA EXTRACTION AND ON-CHIP AMPLIFICATION

In order to test the feasibility of applying our fluidic platform to PCR-based diagnostic assays, we first characterized DNA extraction from mammalian cells. Human adenocarcinoma cell line culture (Panc-1) was suspended in phosphate buffered saline and concentration was measured by calculating the average of five aliquots on a hemocytometer slide. The cells were serially diluted over three orders of magnitude ($10^4 \sim 10^2$ cells per 10 μL aliquot), and processed in triplicates of 10 μL aliquots using the electromagnetic coil platform. Elution buffer from the DNA extraction kit replaced PCR reagents in this experiment. The amount of eluted DNA was quantified using a standard PicoGreen assay (Quant-iT, Invitrogen). In general, extraction yield on the order of 10~20 pg genomic DNA per 10^2 cells was observed. Higher yields may be possible by further optimizing cell lysis and elution conditions in the future.

Afterwards, real-time amplification detection of the KRAS oncogene was performed on the droplet platform using 5 μL of human whole blood as the biological sample input. Genomic DNA was first isolated from whole blood using automated processing described in an earlier section and eluted directly into a PCR reagent mixture droplet containing 1× LCGreen+. The processed cartridge was subsequently mounted on a custom thermal cycling and detection module and amplified while monitoring the fluorescence emission of the droplet.

Figure 4.10A shows the real-time PCR signal from KRAS detected within the droplet. We observed a high threshold cycle number that was attributed to lower amplification

efficiency, associated with long transition times between temperature zones and the effect of thermal gradient across the droplet. In order to verify that the amplification signals were associated with the target region rather than primer dimers or unspecific products, the amplified product was analyzed using 2% agarose gel electrophoresis. Positive control samples were generated by thermal cycling PCR mixtures spiked with 2 ng male genomic DNA (Promega Corporation, USA) under similar cycling conditions on a conventional thermal cycler, while negative control was generated by thermal cycling the same mixture without genomic targets (no template control). As shown in **Figure 4.10B**, gel results show that the products were of expected length (Lane 1), which confirmed amplification of target product from the sample.

4.9. CONCLUSION

This chapter demonstrates an automated magnetic droplet-based platform for whole blood genetic testing, integrating nucleic acid extraction from crude samples, nucleic acid amplification, and real-time fluorescence detection on a single disposable cartridge. Topographical barriers on the cartridge were used in tandem with magnetic coil-based instrument to create a simple and efficient droplet manipulation scheme. Planar coil structures provided a ubiquitous actuation mechanism for the splitting, transport and agitation/mixing of magnetic particles, while topographical barriers enabled efficient splitting and isolation of reagent droplets with varying interfacial tensions. A major strength of the proposed droplet manipulation platform is its flexibility, as the platform can simultaneously handle a diverse range of reagents and could be extended to perform other assays using magnetic particles as a substrate for biomolecule isolation and detection.

We also recognized a number of its limitations that are abstracted in the laboratory demonstration process. First, the use of topographical barriers in an open-top design

overlooks potential challenges for storage and handling. Secondly, while the instrumentation may suggest a considerable step towards miniaturization in comparison with automated pipettors, the substantial power requirement for operation presents a challenge when mobility is considered. These questions raise a common concern shared among technologies developed in the context of laboratory research, which is the scalability of the concept to real-world application. In the next chapter, we discuss these and other factors in greater detail in an effort to highlight the key challenges that should be overcome in order to enhance the relevance of magnetofluidic technology in biomedicine.

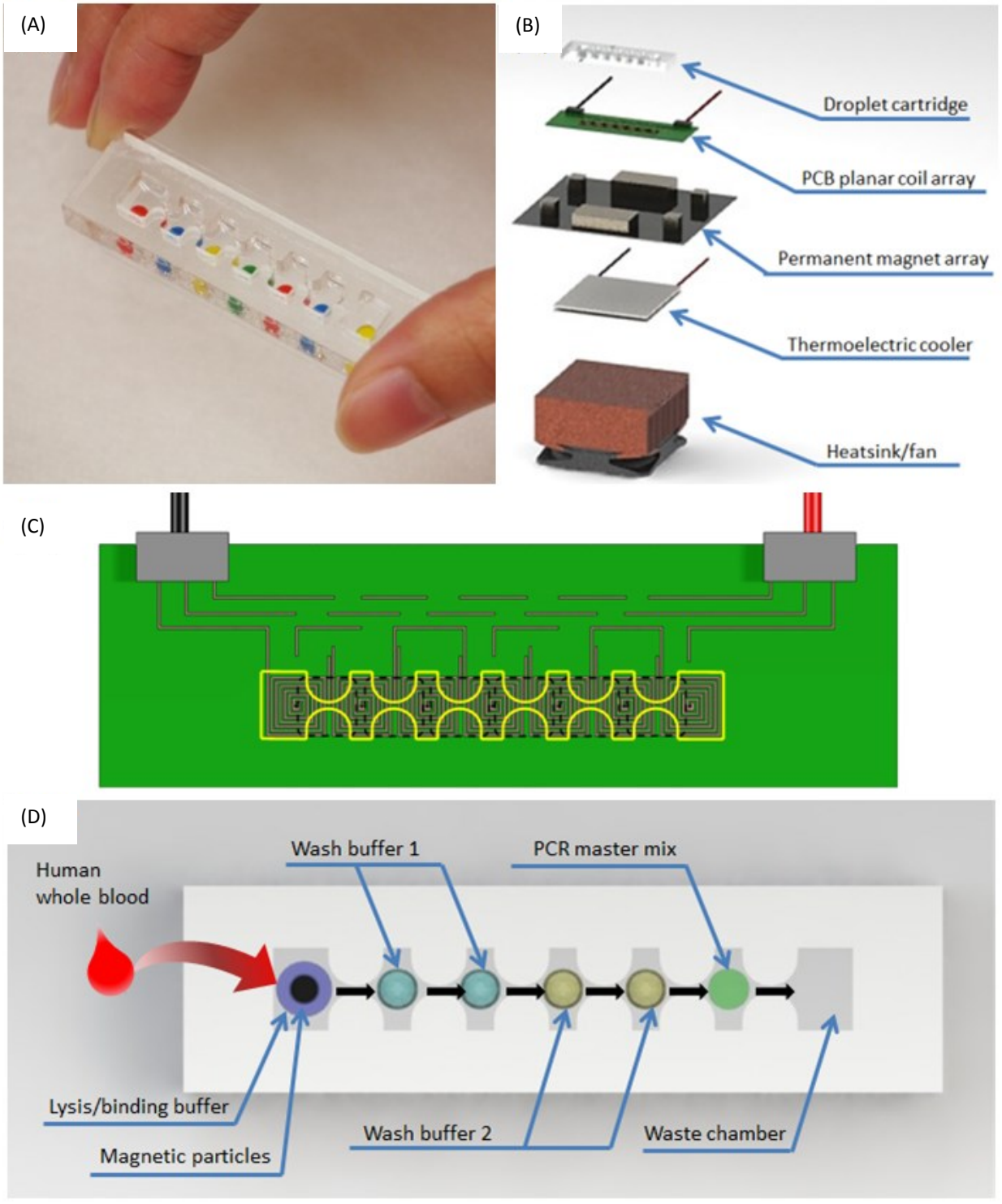
(A)
(B)
Droplet cartridge
PCB planar coil array
Permanent magnet array
Thermoelectric cooler
Heatsink/fan
(C)
(D)
Human
whole blood
Wash buffer 1
PCR master mix
Lysis/binding buffer
Magnetic particles
Wash buffer 2
Waste chamber

Figure 4.1: Cartridge and system layout.

A) Photograph of the disposable chip containing aqueous food dyes pre-injected in each compartment. **B)** Schematic illustration of magnetic droplet manipulation system composed a disposable chip and actuation module for automated nucleic acid extraction. **C)** Diagram illustrating alignment of droplet cartridge on coil PCB. Top layer of coils were centered at each droplet compartments (yellow, solid lines), which would automatically align the bottom layer of coils (black, dashed lines) to the centers of sieve structures. **D)** Layout of droplet cartridge and sample processing order indicated by black arrows. Droplet cartridge was composed of seven compartments separated by sieve structures to facilitate droplet splitting. Each compartment was primed with reagent droplets and overlaid in mineral oil. The magnetic particles were split from the lysis/binding buffer droplet and transferred to washing buffers WB1a, WB1b, WB2a, and WB2b for DNA extraction. Afterwards, the particle-bound DNA was directly eluted in PCR reagent droplet, followed by extraction of particles into the last compartment.

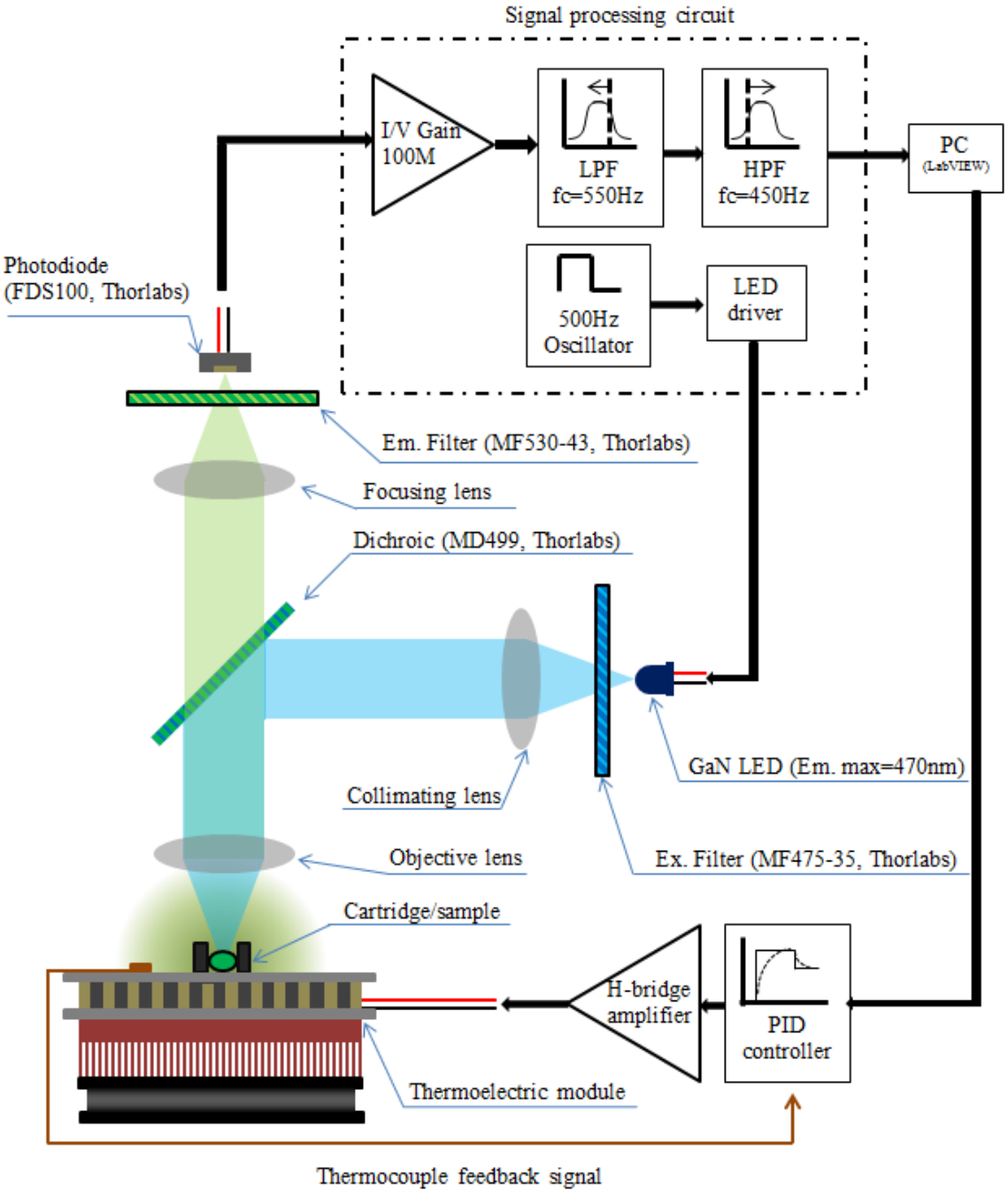
Signal processing circuit
I/V Gain
100M
LPF
fc=550Hz
HPF
fc=450Hz
PC
(LabVIEW)
Photodiode
(FDS100, Thorlabs)
500Hz
Oscillator
LED
driver
Em. Filter (MF530-43, Thorlabs)
Focusing lens
Dichroic (MD499, Thorlabs)
GaN LED (Em. max=470nm)
Collimating lens
Objective lens
Ex. Filter (MF475-35, Thorlabs)
Cartridge/sample
H-bridge
amplifier
PID
controller
Thermoelectric module
Thermocouple feedback signal

Figure 4.2: Layout of instrumentation for thermal cycling and optical detection.

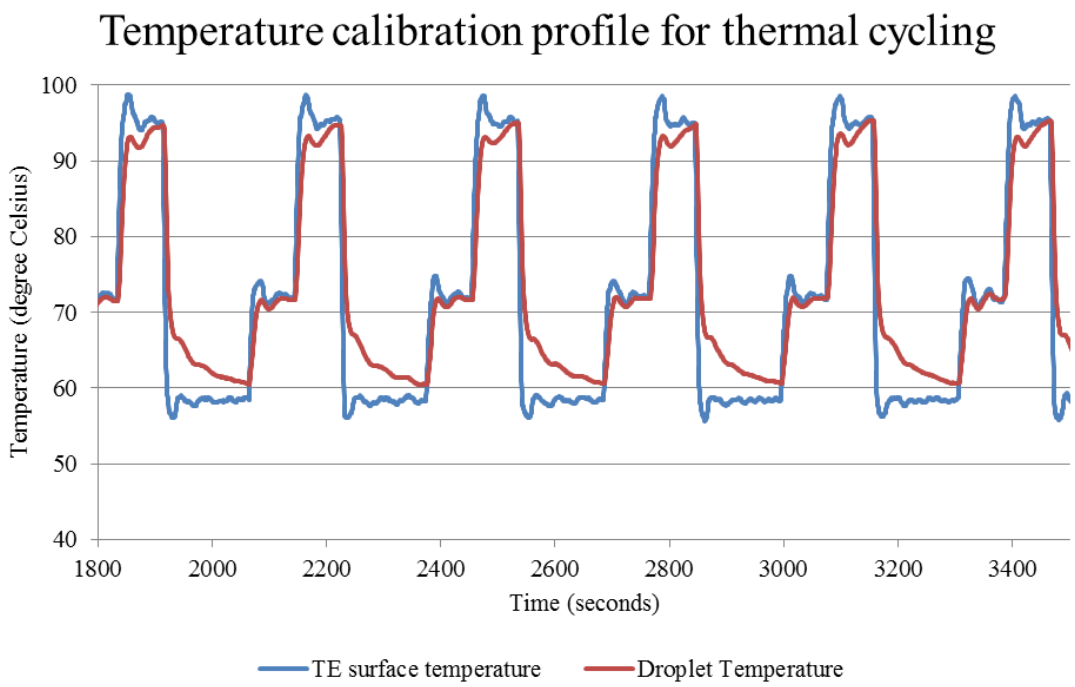
Temperature calibration profile for thermal cycling
Temperature (degree Celsius)
100
90
80
70
60
50
40
1800
2000
2200
2400
2600
2800
3000
3200
3400
Time (seconds)
TE surface temperature
Droplet Temperature

Figure 4.3: Temperature calibration profile for thermal cycling on chip.

Target cycling parameters were as follows: denaturation (90~95˚C for >30 seconds), annealing (60~64˚C for >30 seconds) and extension (72˚C for >30 seconds). Cycling on chip involved 15 minute enzyme activation at denaturing temperature, followed by 50 cycles of thermal cycling and 3 minutes of extension.

(A)

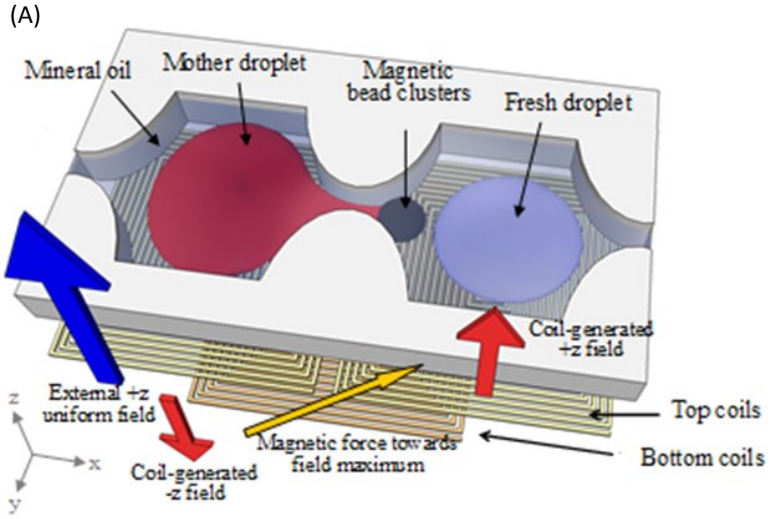
Mineral oil
Mother droplet
Magnetic bead clusters
Fresh droplet
Coil-generated +z field
External +z uniform field
Top coils
Magnetic force towards field maximum
Bottom coils
Coil-generated -z field
z
x
y

(B)

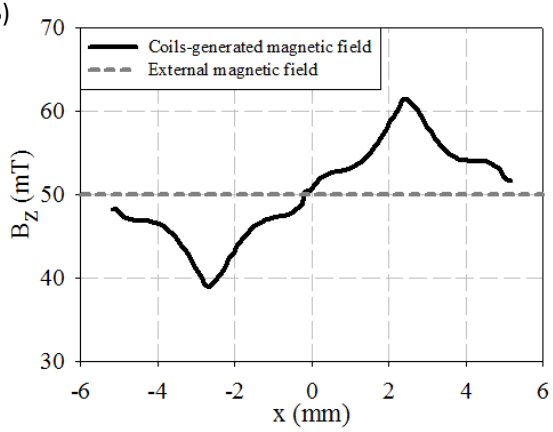
Coils-generated magnetic field
External magnetic field
B_Z (mT)
x (mm)

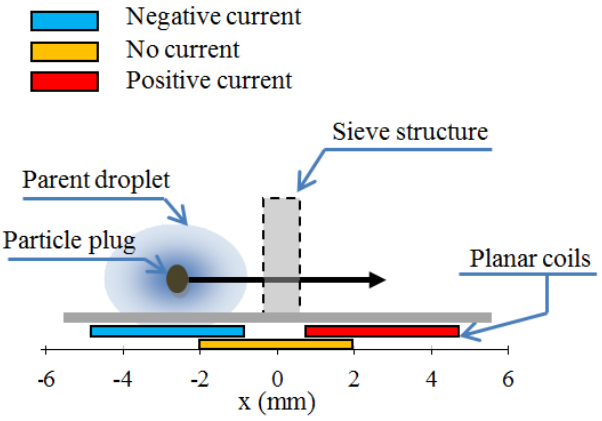
Negative current
No current
Positive current
Sieve structure
Parent droplet
Particle plug
Planar coils
x (mm)

(C)

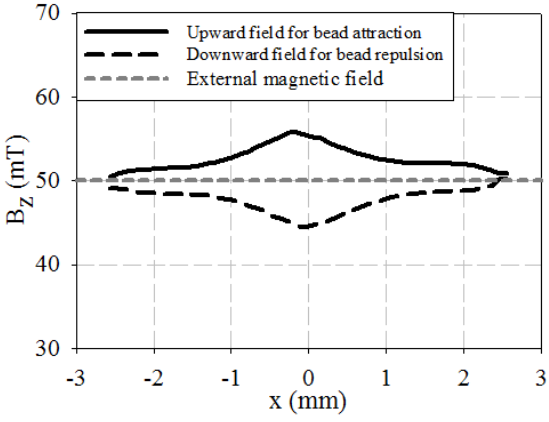
Upward field for bead attraction
Downward field for bead repulsion
External magnetic field
B_Z (mT)
x (mm)

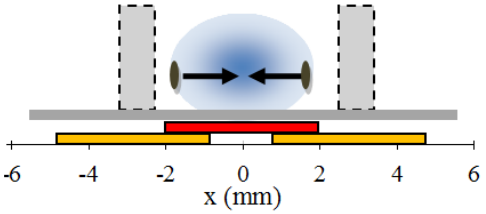
x (mm)

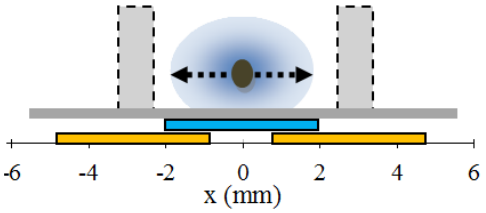
x (mm)

Figure 4.4: Droplet manipulation platform.

A) Topography-assisted droplet splitting. Magnetic particle cluster was extruded from the parent droplet as the magnetic attraction moved the cluster through a sieve structure. A wide-range field gradient was generated by creating magnetic fields of opposing polarity on two adjacent coils. **B)** Splitting is achieved by applying a strong field gradient between two droplet compartments. Negative, zero and positive polarity currents are applied in 3 consecutive coils to generate field maximum at the center of destination droplet and field minimum at the center of current droplet. The resulting force applied on magnetic particles facilitates droplet splitting. **C)** Agitation is achieved by alternating between two polarities of current applied to a single coil directly below the droplet containing magnetic particles. When the field is directed upward, gradient maximum is located at the center of the droplet and particles are concentrated. In reverse polarity, gradient is directed away from the center of the droplet and force is applied on particles to move towards the fringes of the droplet.

(A)

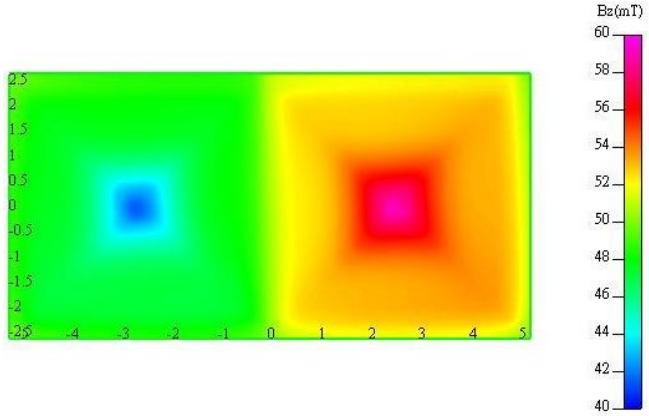
Bz(mT)
60
58
56
54
52
50
48
46
44
42
40
2.5
2
1.5
1
0.5
0
-0.5
-1
-1.5
-2
-2.5
-5
-4
-3
-2
-1
0
1
2
3
4
5

(B)

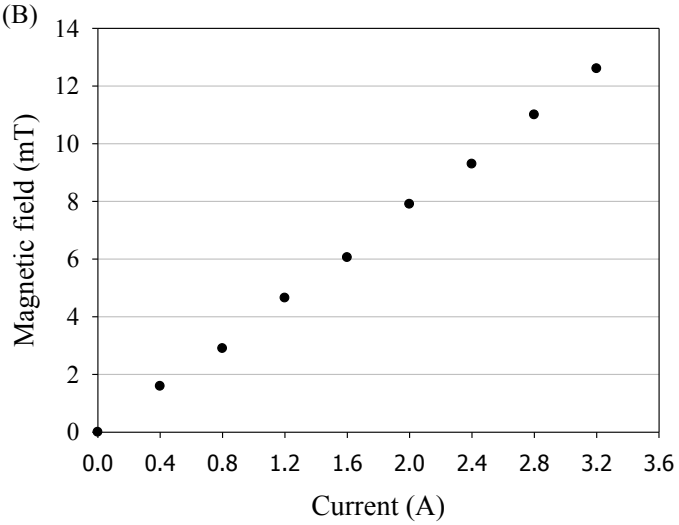
Magnetic field (mT)
0
2
4
6
8
10
12
14
0.0
0.4
0.8
1.2
1.6
2.0
2.4
2.8
3.2
3.6
Current (A)

(C)

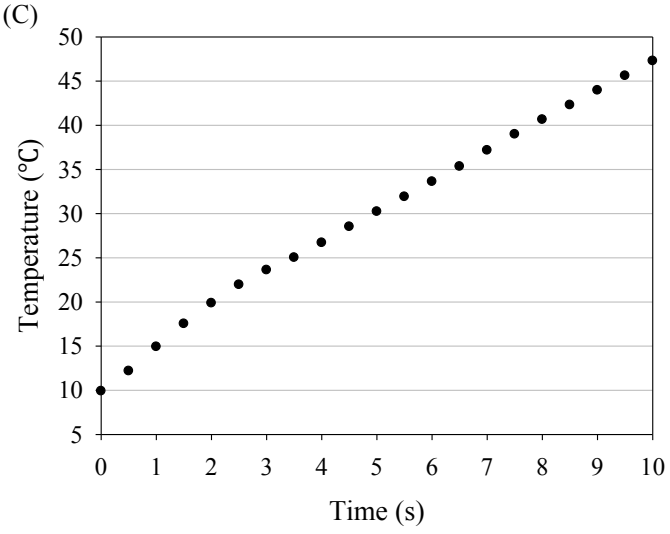
Temperature (°C)
5
10
15
20
25
30
35
40
45
50
0
1
2
3
4
5
6
7
8
9
10
Time (s)

Figure 4.5: PCB coil array characterization.

A) Simulation of the coil-generated magnetic field topology with one positive phase and one negative phase. The simulated magnetic field gradient between two adjacent coils on the same layer was around 4 T/m at an elevation of 100 μm and coil input current of 3 A. **B)** Characterization of magnetic field generated by a single planar coil on a printed circuit board as a function of driving current. **C)** Characterization of Joule heating as a function of time, for driving current of 3 A.

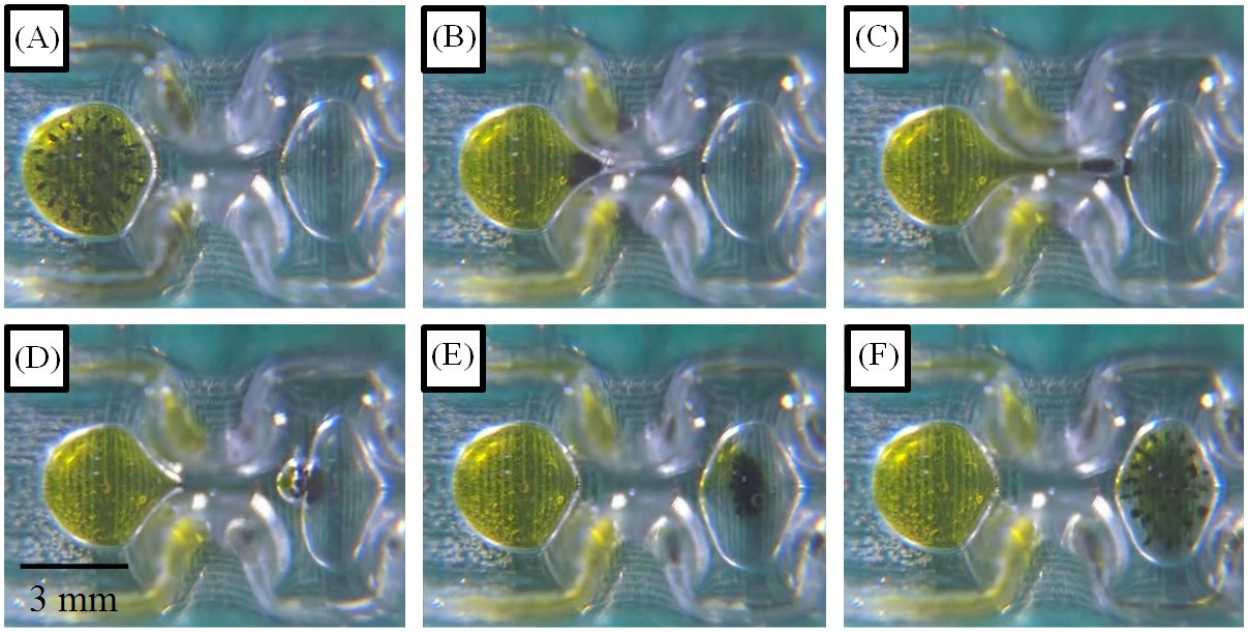
(A)
(B)
(C)
(D)
(E)
(F)
3 mm

Figure 4.6: Droplet splitting and merging assisted by a sieve structure.

From left to right: **A)** magnetic particles were dispensed into the parent droplet containing yellow food dye, forming columns due to magnetization under large transverse B-field; **B)** magnetic particles collected towards the maximum of coil-generated field gradient, located at the center of the sieve structure; **C)** field gradient maximum was changed to the center of the adjacent droplet, causing magnetic particles to pull through the sieve structure; **D)** this process formed a long neck, which reduces capillary force until a sessile plug containing magnetic particles was formed; **(E-F)** the separated plug was magnetically transported and merged with the adjacent droplet.

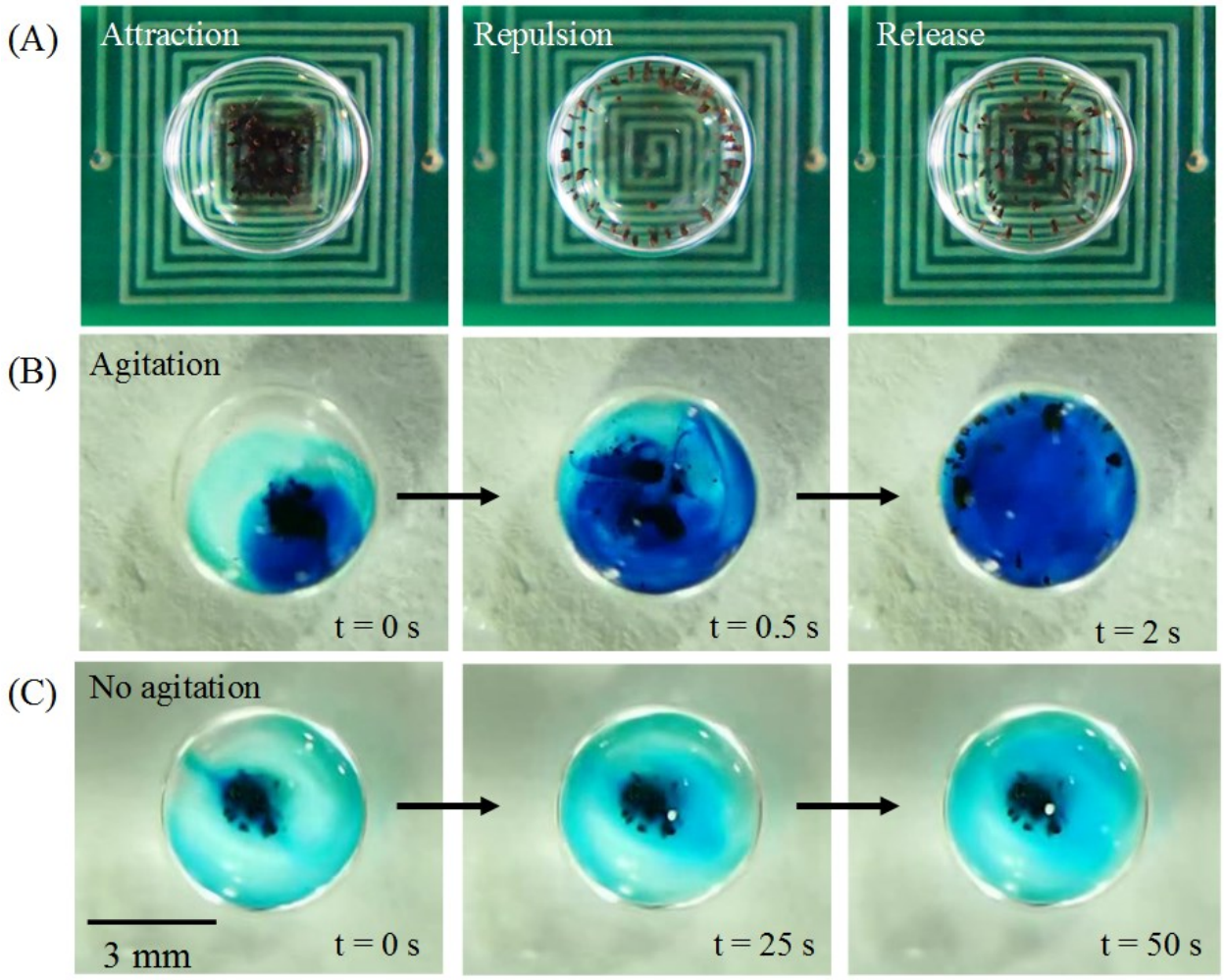
(A)
Attraction
Repulsion
Release
(B)
Agitation
t = 0 s
t = 0.5 s
t = 2 s
(C)
No agitation
3 mm
t = 0 s
t = 25 s
t = 50 s

Figure 4.7: Photographic sequences showing droplet agitation.

A) Left: magnetic particles attracted towards the center of the droplet. Center: particles dispersed towards the fringes of the droplet. Right: particles dispersed inside the droplet when no current is applied to the coil. **B)** Mixing of blue food dye in water droplet with the assistance of agitation. **C)** Diffusion of blue food dye in water droplet in absence of agitation.

(A)

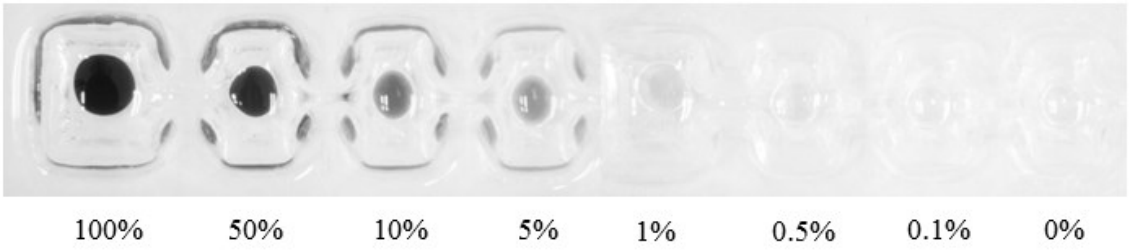
100%
50%
10%
5%
1%
0.5%
0.1%
0%

(B)

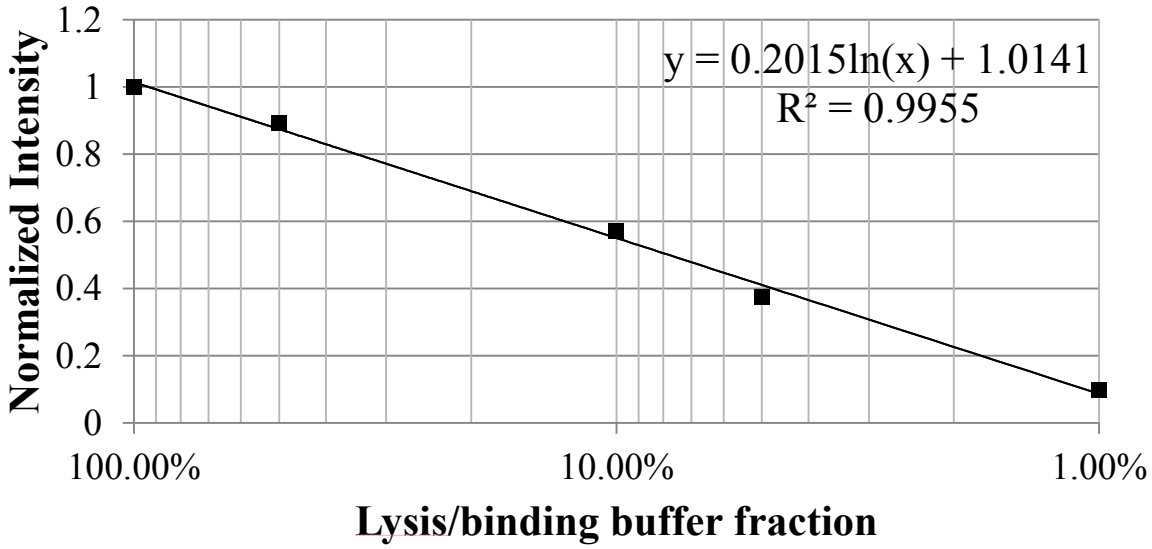
y = 0.2015ln(x) + 1.0141
R² = 0.9955
Normalized Intensity
1.2
1
0.8
0.6
0.4
0.2
0
100.00%
10.00%
1.00%
Lysis/binding buffer fraction

Figure 4.8: Reference data for washing efficiency characterization.

A) Standard droplets with known volume fraction of LSB in transparent solution. **B)** Plot of standard curve used to correlate normalized mean gray value of droplet to expected fraction of LSB present in the mixture.

(A)

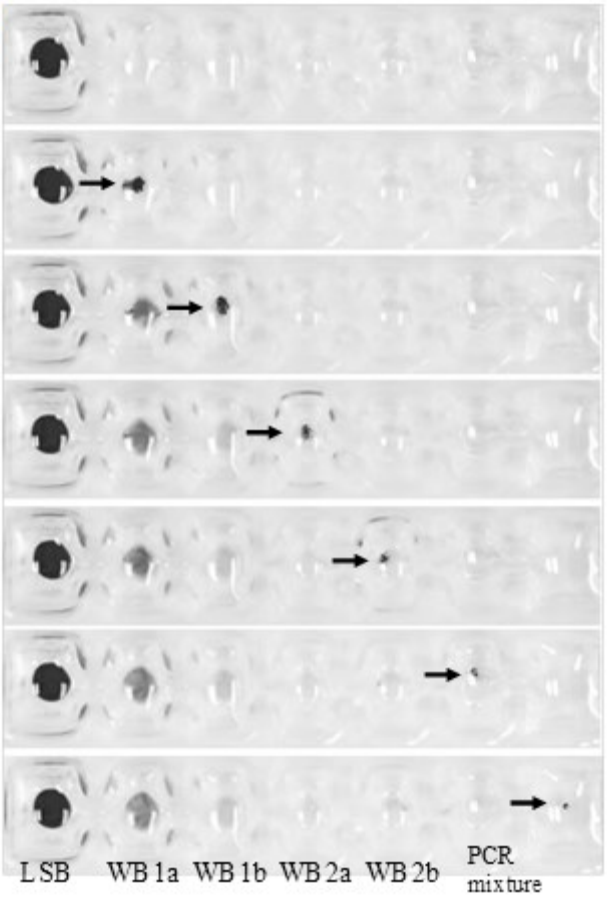
LSB
WB1a
WB1b
WB2a
WB2b
PCR mixture

(B)

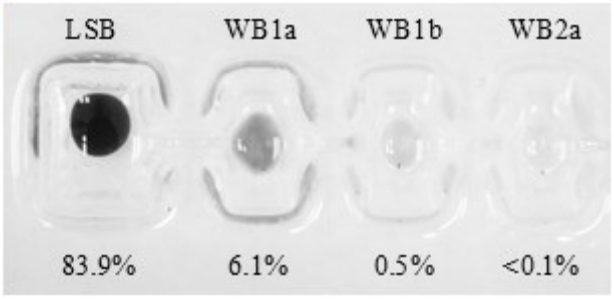
LSB
WB1a
WB1b
WB2a
83.9%
6.1%
0.5%
<0.1%

Figure 4.9: On-chip droplet manipulation for sample washing.

All images were converted to gray scale for analysis. **A)** Photographs of sequential splitting, merging, and washing performed in an automated fashion. The arrows indicate magnetic particle clusters. **B)** Potential carryover of PCR inhibitors can be minimized by successive washing steps. Droplet manipulation in the demonstration above was performed with 300 μg particle load and 15 μL reagent droplets each.

(A)

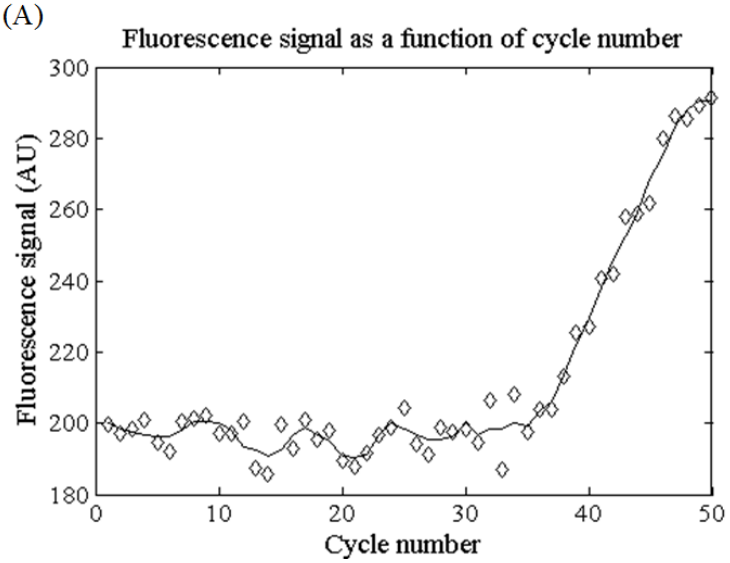
Fluorescence signal as a function of cycle number
Fluorescence signal (AU)
Cycle number
300
280
260
240
220
200
180
0
10
20
30
40
50

(B)

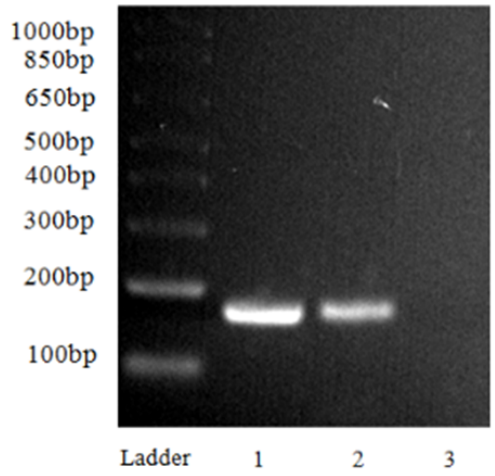
1000bp
850bp
650bp
500bp
400bp
300bp
200bp
100bp
Ladder
1
2
3

Figure 4.10: Amplification signals obtained from PCR on chip.

A) Real time PCR amplification curve. Amplification curve (black solid line) is generated by smoothing raw signal (◊) with 8th order Savitsky-Golay filter. **B)** Gel electrophoresis image of PCR products. The amplified products (Lane 1) were verified by comparing against positive controls (Lane 2) and no-template controls (Lane 3) amplified from male genomic DNA on a conventional thermal cycler using 2% agarose gel electrophoresis. Products are 167bp in length.

Chapter 5

5. Bridging the gaps: key considerations in magnetofluidic platform design

5.1 BACKGROUND

The previous chapters outlined the principles of droplet magnetofluidics and demonstrated the single-stream assay concept as a facile alternative to conventional fluid handling for nucleic acid analysis. Process integration and automation via instrumentation as illustrated in Chapter 4 showcases the potential of the magnetofluidic approach, where a single cartridge can internally process raw biological sample to perform real-time PCR. While these developments are encouraging, it is still essential to recognize the design limitations of a proof-of-concept study.

Translating laboratory findings to create a field-deployable prototype requires scalability of essential design elements. An example is the experimental open-surface droplet cartridge with an open top as described in the preceding chapters, which immediately present a challenge when one considers transportation outside the immediate vicinity of the laboratory environment. A more scalable design calls for packaging of cartridges such that the droplets are enclosed for ease of handling and transport. Planar construction based on glass slides may be too fragile, necessitating a modification of cartridge material and fabrication process. It is important to recognize that all design elements are closely interconnected, which makes the independent optimization of components untenable without first outlining the specifications of the instrument, the cartridge and the biochemical assay simultaneously. For example, thermal control of droplet cartridges

must cohabit instrumentation for magnetic actuation and places a critical constraint on the possible designs for a fully functional magnetofluidic workstation.

This chapter summarizes the design considerations that are involved in developing an assay platform that is fully portable and easy to perform. These findings are a summary of important parameters that has accumulated through an iterative process of major design changes alternating between the instrument, the cartridge, and the assay itself. Specific discussions will revolve around cartridge design, instrument design and assay design, where each component will be reviewed on the basis of material from other investigators as well as our own. This chapter serves an important heuristic purpose for readers who are interested in designing their own magnetofluidic assay systems.

5.2 INSTRUMENT DESIGN

Designing and realizing an integrated bioassay platform from the basic principles highlighted in the preceding section requires several engineering problems to be addressed. Firstly, the device must have a mechanism to facilitate extraction and transport of magnetic solid substrates across multiple reagents in a robust manner. Secondly, the magnetic particles must be actuated by a mechanism that is robust and operator-independent. Lastly, appropriate supporting instrumentation for thermal incubation and signal acquisition must be in place. In this section, the discussion will focus on the modes of magnetic actuation, device fabrication, thermal control and signal acquisition.

5.2.1 Magnetic particle actuation mechanism

An elegant approach to magnetic actuation is by using an array of electromagnets to control the magnetic field across the device surface in an addressable manner. The lack of mechanical components and the ease of access to customized printed circuit boards make this an attractive approach from both miniaturization and manufacturing standpoint. In Chapter 4, we demonstrated

the use of topographical barriers in combination with coil-based magnetic transport in order to recreate the entire workflow for a real-time PCR assay from a biological sample [16]. While electromagnetic manipulation is capable of miniaturizing the actuation mechanism, several technical limitations should be recognized. The requirement for generating a field gradient of sufficient magnitude in order to overcome the other two force components acting on the droplet implies the use of high current to drive the coils, which also increases the effect of resistive heating. This dual constraint of power and thermal management challenges the applicability of electromagnetic actuation in portable instruments.

In light of this conundrum, we revisited methods for mechanical manipulation of rare earth magnets such as neodymium alloy ($Nd_2Fe_{14}B$) to actuate the magnetic particles. Translational stages have been used in quantitative investigation of droplet kinematics due to their ability to precisely control the position and velocity of the magnet [11, 20, 20], although we have noted their size and power requirement as bottlenecks for miniaturization. Alternatively, a stepper motor with a permanent magnet mounted on the rotor may be employed to facilitate magnetic particle actuation in a circular motion [12, 13] as shown in **Figure 5.1**. Its independence from lead screws, stages and other hardware necessary for linear actuation makes rotary actuation a promising candidate for miniaturization. In our own investigation, we found that further reduction in power requirement and device footprint could be achieved by using servomotors in place of stepper motors **(Fig. 5.1C)**. Power requirement was reduced to such an extent that the motor could be powered and programmed using a microcontroller and a standard phone charger (5V/150mA). As with all rotary actuators, this mode of actuation requires that the cartridge being processed is designed with an arc-shaped particle trajectory.

While actuation via a permanent magnet is the most intuitive method, there are some limitations. Firstly, the permanent magnet itself is not capable of switching polarity in a manner that can allow the particles to disperse. Although mixing of constituents in a single droplet may be

achieved through internal flow introduced by oscillation of the magnetic particle or by droplet transport [18, 31], this effect was found to be valid only in small droplets during our investigation **(Fig. 5.2)**. Efficient sampling of the entire droplet volume by the magnetic particles would require an active mechanism for agitation. To address this, we looked to two examples from other investigators as sources of inspiration. The instrument proposed by Shikida *et al* [12] utilizes a stepper motor with two spokes attached with a permanent magnet and a coil electromagnet respectively, where the electromagnet is able to induce particle agitation and supplement the limitations of the platform solely based on permanent magnet actuation. In the method proposed by Tsuchiya *et al* [11] **(Fig. 5.3A)** two linearly actuated magnets on opposite sides of the droplet are used in to facilitate agitation of magnetic particles. Because the magnetic particles can be gathered in two opposing directions inside the droplet, the droplet volume can be sampled more thoroughly by the particles. In our investigation, we devised a synthesis of the two approaches by attaching two spokes to a single rotor, each mounted by a magnet **(Fig. 5.3B)**. With one magnet applying the field from the top of the cartridge and the second magnet applied magnetic field from the bottom, it was possible to induce particle mixing by generating particle motion perpendicular to the device. As it may be apparent, this actuation mechanism requires a modification of cartridge design such that both the top and bottom of the cartridge is accessible to an external magnetic field, necessitating a modification of open-top cartridge designs described in the earlier chapters.

5.2.2 Thermal control

Thermal control is an important parameter in assays which require incubation at elevated temperatures for enzymatic reactions. In particular, PCR requires cycling of reagent temperature between approximately 60˚C and 95˚C for primer annealing and duplex DNA denaturation. Thermal cycling for microdevices has been achieved using various mechanisms including contact heating elements [69-74] and non-contact modes such as infrared heating [75, 76] and microwave

heating [77]. In the context of open-surface droplet platforms, two directions have been explored **(Fig. 5.4A and B)**. In the first instance, thermal cycling is achieved in the manner of zone heating, where spatially separated zones are maintained at different temperatures required for thermal cycling. This method is more commonly found in channel-based microfluidic platforms [71-73] since flow-based transport of reagents lends itself to thermal cycling via zone heating, although systems using a static heating chamber have also been reported [74, 75]. The liquid reagent is transported repeatedly across different temperature zones to alter the temperature. Implementation of this technique on a magnetic droplet platform requires the system to operate under droplet transport mode to ensure that transport of the droplets across temperature zones can be performed without accidental particle extraction. Neuzil et al demonstrated a circularly actuated device with temperature zones maintained by microfabricated heating elements [6], while Ohashi et al demonstrated a linearly actuated droplet device for thermal cycling reactions with a temperature gradient established by heating one edge of an aluminum plate [21].

In the second instance, thermal cycling is achieved by a single heating element placed in contact with static incubation chamber which transitions through target temperatures in a manner that is analogous to a conventional thermal cycling instrument [69, 70]. This approach consumes smaller device footprint due to the static nature of the incubation zone and is also suitable in applications where an array of samples must be thermally controlled simultaneously [78]. In a micro-PCR platform developed by Angione *et al* [69], thermal cycling is achieved directly on a Teflon-coated indium tin oxide (ITO) substrate via resistive heating. While this type of arrangement requires an integrated heater for each PCR device, the scheme adapted by Xiang *et al* [70] utilizes a glass-PDMS chamber cartridge that is loaded onto an external thin-film heater for thermal cycling. Similar approaches have been adopted by Zhang *et al* [14] and our own investigations in chapters 2 and 4 for thermal cycling of genomic DNA extracted on the cartridges.

There are several considerations in implementing temperature control elements in a droplet magnetofluidic platform. In order to facilitate rapid transition of the reagent between temperatures, it is imperative that the thermal mass of the incubation region is minimized. In contrast to thermal cycling of the entire device, integrated microheaters placed directly in contact with the reagent can minimize the thermal mass involved to the reagent and its immediate vicinity. However, the integration of a microfabricated heater and temperature sensor may contribute significantly to the cost of each assay cartridge, and it may be prudent to incorporate heating elements on the instrument instead. When heating elements are placed outside the microfluidic device, care must be taken to thermally insulate the incubation zone and ensure proper thermal contact between the heating element and the device. In addition, careful thermal calibration using external probes is necessary in order to obtain correct temperatures inside the reaction chambers **(Fig. 5.4C)**.

5.2.3 Signal acquisition

While open-surface fluidic manipulation can be made compatible with various biosensor technologies, optical modes are conveniently integrated into these platforms without affecting the droplet kinematics due to their non-contact nature. Furthermore, the prevalence of fluorescent probes and indicator dyes in bioassays has encouraged development of either luminescence or fluorescence-based approaches for signal acquisition. A typical acquisition system involves detectors such as photomultiplier tubes [69], silicon photodiodes [14] or charge-coupled devices (CCD) [70], while illumination sources may range from light-emitting diodes (LED) [14] to halogen lamps [69]. Optical setups for collection of fluorescence from a single collection spot are configured in an epifluorescence microscope configuration, where a dichroic beamsplitter is used to route excitation and emission light along the same objective lens **(Fig. 5.5A)**. This arrangement lends itself to compact detector design suitable for portable instrument as demonstrated by Novak *et al* [79] and recreated in our own investigation **(Fig. 5.5B)**.

Image-based data acquisition is another strategy that has recently gained much academic interest. With the widespread integration of CMOS camera devices in consumer electronics such as mobile phones, coupling this technology to signal acquisition has been studied for their potential in assessing colorimetric indicators [80] and fluorescence [81]. In the context of droplet magnetofluidics, we devised a simple fluorescence acquisition setup for smartphone-based data acquisition **(Fig. 5.5C)**. Such design enables a laboratory-free setup for data acquisition and signal processing when coupled with an appropriate software designed for the mobile phone.

5.3 CARTRIDGE DESIGN

5.3.1 Design considerations

On an open hydrophobic surface, magnetofluidic droplet manipulation can achieve three operations including particle extraction, magnet disengagement and droplet transport as described by Long *et al* [20]. However, velocity is a difficult parameter to control precisely, and a more robust mode of particle extraction is desirable for platforms designed to perform biomolecular assays. In order to aid this process, passive elements may be placed on the device substrate. Passive elements on these platforms are analogous to valves in the sense that the movement of fluid is regulated such that only the magnetic particles with analytes of interest can be transferred to subsequent reagents. Two broad approaches to generating passive elements include topographical features and surface patterning, which will be discussed in the next subsection.

One critical parameter in cartridge design is thermal control. As demonstrated in previous chapters, thermal incubation and cycling are essential operations in a conventional biochemical assay. However, the smooth continuous design necessitated by magnetofluidic process makes thermal regulation of specific droplets on the cartridge a challenging task. In a prototyping stage, generating a smooth surface is typically achieved using a planar design in a layer-by-layer assembly. Such designs are poorly adapted to rapid thermal control of reagents, detrimental to

applications such as PCR. This constraint is compounded by the need for thermal isolation of some reagents from evaporation through approaches such as having multiple temperature-controlled zones, as was the case in the instrumentation used for magnetofluidic bisulfite conversion presented in Chapter 3. A related constraint is thermal mass, which negatively impedes thermal change. Devices of substantial thickness and large internal volumes suffer from this constraint, resulting in thermal cycling properties that are impractical for field use. Such challenges favor the design of small cartridges with thin walls on the heating surface, as well as streamlined designs which isolate the thermal mass of a thermally sensitive reagent from the rest of the cartridge. Prudence is also required in the selection of immiscible oil phase for prevention of evaporation, as fluids may contribute significantly to thermal mass. Immiscible fluids with very low thermal conductivity may provide the necessary insulation to minimize thermal crosstalk between reagent droplets.

Another important parameter is cartridge interface with external instrumentation. In the examples that were discussed in the previous chapters, external instrumentation was developed in order to demonstrate one aspect of process control, either particle actuation or thermal incubation and fluorescence data acquisition. In a fully integrated system, both processes must be implemented on a single instrument. Since all previously demonstrated examples of cartridge design have only a single planar surface for these functions, this becomes a potential bottleneck to integration. Manual handling steps obviate this problem at the expense of the user, making this approach not suitable for a platform targeted point of care applications. Automated switching mechanism between particle actuation and thermal incubation may be implemented, only at the expense of instrument complexity that contributes to instrument cost and mode of failure. In order to address these concerns, cartridges may be designed with two functional surfaces with a dedicated thermal control on one surface and particle actuation on the opposite surface.

5.3.2 Device elements and fabrication strategies

Topographical patterns as shown in **Figure 5.6A** are capable of serving dual roles as storage wells for the aqueous reagents and physical barriers to restrain the droplets during particle extraction [14]. During particle extraction, the narrow sieve structures formed between topographical barriers provide an outlet port for magnetic particles to be transferred across. Because the maximum capillary force at the sieve neck is insufficient to maintain cohesion of the entire droplet past the barrier, droplet fission takes place and particle is extracted. In the regions that are not compartmentalized by topographical barriers, droplet transport can be performed without hindrance under a slow-moving magnetic field [20]. Fabrication of topographical patterns can be achieved using various techniques. In an earlier work demonstrating the use of physical obstruction for particle extraction, Shikida *et al* constructed devices by bonding layers of glass plates together with phenol resin, followed by hydrophobic surface treatment [7]. However, glass devices are generally difficult to manufacture and prototype on a regular basis. Using an alternative approach, a more convenient soft lithography-based fabrication has been proposed by Zhang *et al* [14] and also utilized in a similar fashion by Berry *et al* [15]. In this process, master molds with depth on the order of 10^{-4} m are fabricated using SU-8 negative photoresist with planar features defined by a conventional photolithography process. The mold is subsequently cast with curable polymer such as PDMS, which can be permanently bonded via oxygen plasma activation to a glass substrate and dip-coated in amorphous Teflon in order to render the device surface hydrophobic. Alternatively, in Chapter 2 we demonstrated the use of a computer numeric controlled (CNC) machined PTFE mold for fabrication of pillar features on the order of 10^{-3} m to be utilized as topographical barriers **(Fig. 2.2)**. We also demonstrated the use of a rapid 3D printer in Chapters 3 and 4 in order to generate a casting mold for fabricating an extruded layer of PDMS **(Fig. 5.7)**. These fabrication approaches can significantly reduce the difficulty of generating surface topography and make it easier to prototype new designs.

An alternative strategy for droplet immobilization is to use substrates with differential wetting properties in place of topographical barriers as exemplified in the SET technology [18] **(Fig. 5.6B)**. Instead of confining aqueous droplets using structural barriers, hydrophilic spots are used to define regions where the droplets can wet selectively. One key advantage of this approach over the topographical features is the ability to aliquot reagents, since liquid is retained in the hydrophilic spot once wet. This feature is particularly useful in several applications, including spatial multiplexing of reactions and generating dilution series. Moreover, because the processing steps in which patterning takes place is generally subtractive rather than additive, this approach is particularly attractive for fabrication in large batches. In an approach described by Inagaki *et al* and utilized by Lehmann *et al* [9, 37], coating of hydrophilic substrate with hydrophobic film is followed by selective oxygen plasma etching to generate hydrophilic spots. More recently, Zhang and Wang developed an improved version of this technique by using lithographically defined SU-8 membrane as a shadow mask [18]. Since droplet immobilization is independent of physical features, cartridge design can be substantially miniaturized for the benefit of reduced thermal mass and reagent consumption.

5.3.3 Packaging and storage

It should be noted that previous investigators in open-surface droplet magnetofluidics, including our own, limited the scope of our investigation to a laboratory proof-of-concept. In the process, consideration for packaging has been abstracted or overlooked altogether. Considering that packaging is critically linked to various design constraints, it is appropriate that we discuss this topic in some detail. While the patterned surface features are theoretically well-suited to thermal control due to the superior thermal conductivity of thin glass slides, it also exhibits poor handling capacity with limited stability in presence of mechanical perturbation. Making this feature accessible in a POC platform requires design modification and packaging. To this end, we developed an enclosure for patterned glass substrates using a combination of oxygen plasma-

based surface patterning and a thermoplastic shell to enclose the features **(Fig. 5.8A)**. Ports were added to facilitate reagent and sample loading as shown in **Figure 5.8B**. Surface patterns were designed such that buffers remain wetted on the hydrophilic patterns with a low profile, which has the dual purpose of minimizing the distance required for particle extraction **(Fig. 5.9)** and flattening droplet profile to enhance particle mixing via raster motion.

While the approach in **Figure 5.9** is substantially more robust than open-top cartridges, it was observed that the SET strategy in general provided insufficient droplet stability under moderate perturbations expected during transportation in an automobile. Two strategies were devised and investigated to circumvent this challenge. First, the use of an immiscible fluid with densities matched to the droplet reagents during packaging provided a way to enhance droplet stability in transport conditions. While this approach was found to be tractable, we still observed high rates of device failure due to the material fragility of glass substrate. As such, an entirely new strategy for cartridge fabrication was devised. In this fabrication workflow **(Fig. 5.10)**, the entire cartridge material was replaced with poly-methylmethacrylate (PMMA) to address device fragility. In transitioning to the new material, an alternative method for hydrophobic surface generation had to be developed. Our solution is a patterning strategy based on lamination of surface with Teflon tape, followed by tracing and peeling away of patterned areas via CO_2 laser cutting. As the transition between the Teflon tape and hydrophilic PMMA substrate were no longer on the same plane, particle translocation had to take place on another substrate. To accommodate this requirement, we introduced a second layer of Teflon tape-laminated substrate on the opposite side to the patterned layer, resulting in an enclosed droplet 'sandwich'. This design has the benefit of having two planar surfaces accessible to instrumentation, making it possible to accommodate particle actuation and thermal incubation simultaneously. In addition, the two planes enable magnetic actuation on both surfaces, enabling the strategy for particle mixing based solely on permanent magnets.

5.4 ASSAY DESIGN

5.4.1 Design considerations

Single-stream assays have one underlying principle, which is that the analyte of interest must be retained on the surface of the moving solid-phase substrate from the initial sample to the readout reagent. This is a tractable requirement for the most common biochemical assays using nucleic acids as the analyte. Nucleic acid extraction chemistry facilitates adsorption of nucleic acids on the particle surface, whether the process is driven by electrostatic attraction (e.g. ChargeSwitch chemistry) or chaotrope-driven precipitation (e.g. guanidine thiocyanate chemistry). Nucleic acids remain bound during rinsing steps where buffers conditions favor precipitation, and are eluted once the conditions are reversed. Fortunately, buffer compositions for amplification reactions such as PCR tend to possess low ionic strength and basic pH, allowing nucleic acids to be eluted for either methods of extraction. In this section, we will discuss various strategies for analyte transport using magnetic particles, followed by an overview of amplification assays and indicator reagents with their implication in overall system design.

5.4.2 Analyte capture and transport

The backbone of a single-stream assay is the mobile substrate for analyte capture, transport and elution. While the synthesis of magnetizable particles is a diverse and interesting topic of research, our discussion will focus on its utility as a carrier of biomolecules, specifically nucleic acids. Surface-modified magnetic particles have become a widely used platform technology that is now accessible to investigators without extensive knowledge in particle synthesis.

Surface capture of nucleic acid targets can be achieved in several ways **(Fig. 5.12)**. Perhaps by far the most common approach involves silica-coated magnetic particles in a process known as nucleic acid extraction by silica adsorption [82]. In the presence of a chaotropic (water-binding) buffer such as guanidine thiocyanate, the highly-charged phosphate backbone of nucleic acid

precipitates from solution and forms a cationic salt bridge on the silica surface. Once bound, the nucleic acid remains precipitated in water-poor medium such as ethanol and becomes eluted when introduced to a low ionic strength aqueous environment that characterizes many nucleic acid amplification reagents. A potential drawback of this approach is the use of guanidine thiocyanate, which is a hazardous chemical that is also degradable in light, presenting a potential bottleneck due to its limited storage capacity. Furthermore, the presence of high ethanol content in washing buffers present a unique challenge to droplet magnetofluidic cartridge design, where designs must account for the reduced surface tension and boiling point of buffers due to ethanol. As ethanol is a known inhibitor of PCR, process control for particle washing may become more stringent [83].

Another method involves the use of nonspecific electrostatic interaction. Magnetic particles functionalized with zwitterionic molecules such as histidine residues have been demonstrated to capture and release negatively-charged molecules such as nucleic acids based on the acidity of solution [84]. In the presence of an acidic buffer (around pH 4) the protonated histidine residues assume a positive charge on the bead surface, whereupon the negatively-charged phosphate backbone of nucleic acids may bind via electrostatic attraction. Only when the beads are introduced in a basic environment, the histidine residues are deprotonated and nucleic acid dissociated from the beads via electrostatic repulsion. While there are some variations among preparations of amplification reagents regarding their pH, many formulations are available in the moderately basic pH ranges of 8.3 and above [85]. Using this approach, all solutions can be fully aqueous, mitigating the implications of reduced surface tension associated with ethanol-based buffers. However, a potential concern for this approach include whether its operation will be impeded in presence of proteases in solution that may be detrimental to the integrity of the polyhistidine residues.

The last method involves the use of specific molecular binding interaction. Magnetic particles may be functionalized with complementary nucleic acid strands [86] or analogues such as peptide nucleic acids [87] or locked nucleic acids [88] using a wide range of linker chemistries. Alternatively, magnetic particles may be functionalized with other macromolecules having moieties with binding affinity towards specific nucleic acid moieties, such as methyl-binding domain (MBD) [89] and JBP1 [90] among others. These approaches are particularly useful for target enrichment and concentration, where nonspecific purification of all nucleic acids may contribute to poor background during downstream processing. This may not be a concern when target molecules are abundant in a sample, as enzymatic amplifications are generally specific to target sequence. Furthermore, protein-coated particles have a unique conundrum with regards to storage. While desiccation is a common approach for storage of functional proteins, the same process is generally detrimental to the integrity of colloidal particles.

5.4.3 Amplification assay

A key consideration involves the selection of amplification strategy for signal development. Since the formulation of the polymerase chain reaction (PCR) by Kary Mullis and colleagues [91], nucleic acid amplification strategies have evolved to encompass a wide range of techniques and reagents. In the context of droplet magnetofluidics, we will classify these assays under two categories: variable thermal reaction and isothermal reaction.

In the first instance, conventional PCR and its variants such as the nested PCR [92], methylation-specific PCR [93] and multiplex PCR [94] all constitute reactions which require active control of the incubation temperature in order for the reaction to proceed in the required direction. Aside from practical concerns, thermal cycling is challenging because it requires a precise control of incubation temperatures. Rapid transition between each temperature zones is essential to generating specific and efficient amplification products, in addition its importance to the rapidity

at which the result can be obtained. Instrumentation and reaction cartridges utilizing large surface-to-volume ratios may assist in enhancing the rapidity of this process, although this often comes at the expense of increased device complexity and a concomitant increase in cost and risk of process failure. Thin microfluidic cells utilized by platforms such as the Cepheid GeneXpert adopt this approach, a feature which may contribute to the device's failure rate of 7.94% [95]. Furthermore, it should be understood that the performances of PCR assays depend critically on the integrity of sample preparation process. Carryover of inhibitory substances such as proteins and other small molecules may substantially disrupt the reaction and lead to false negatives [83]. Some formulations of the PCR reaction are being designed to provide robust amplification performance of crude biological samples without purification [96], although countervailing factors in signal acquisition such as turbidity may challenge direct use of crude samples in field applications.

In the second instance, isothermal reactions do not require continuous cycling between various incubation temperatures. For a comprehensive overview of these assays and their mechanisms, the readers are encouraged to refer to a recent review article [97]. From a system design perspective, single-temperature incubation is advantageous since the cartridge and instrumentation requirement for isothermal incubation is substantially simpler than that for rapid thermal cycling. From an assay development perspective, isothermal amplification may carry additional challenges that are less pervasive in PCR-based reactions. Due to the lack of control over primer annealing and denaturation, isothermal amplification is susceptible to varying degrees of nonspecific background amplification [98]. As such, care must be taken during primer design process in order to develop an assay with high sensitivity and specificity. While the ability to identify target-specific amplification is possible with the appropriate choice of indicator dyes, it remains to be seen whether quantitative analysis via techniques such as melting curve analysis can be achieved from clinical samples.

5.4.4 Indicator selection

Indicators are chemicals which couple to the reaction taking place, generating a detectable signal as a result. The choice of indicator is intimately linked to signal acquisition strategy as discussed in the preceding section, which in turn affects cartridge and instrument design. In this section, our discussion will focus specifically on optical indicators for nucleic acid detection due to their predominance in current practices of assay development.

Perhaps the oldest class of nucleic acid indicators are nucleic acid stains [99]. These stains are typically fluorescent dyes that remain quenched in solution, undergoing a dramatic increase in quantum yield only when complexed to nucleic acids via interaction with stacked bases along the side grooves. From a design standpoint, nucleic acid stains are useful indicators for melting curve analysis which can generate qualitative information from an assay without additional sample processing. Furthermore, a wide range of dyes have been developed for real-time PCR to enable a single-pot reaction that does not require a separate addition of the indicator into the amplification reaction. However, because signal generation is not specific to the target sequence being amplified, assays may be susceptible to false positive signals. To address this limitation, hybridization probes such as molecular beacons have been used [100]. These indicators typically consist of a strand-specific moiety functionalized to an indicator molecule such as a fluorophore, with a quenching mechanism that is reversed upon hybridization of the probe to target. While these probes may be more target-specific, it should be noted that these probes are generally more expensive and will contribute to the overall cost of a single test. Affordability is one of the key criteria for POC platform development [65], and other strategies to improve target specificity such as primer design optimization should be considered.

An emerging class of indicators for point of care applications are dyes capable of generating signal changes that can be visualized by naked eye. With regards to nucleic acid amplification,

metal ion indicators such as hydroxynaphthol blue (HNB) and calcein has been successfully demonstrated [101]. When coupled to reactions that generate a high abundance of amplicons such as loop-mediated isothermal amplification (LAMP) assay, fluorescent dyes may also exhibit colorimetric changes that can be detected visually [102]. In another instance, gold nanoparticle-based indicator capable of colorimetric change upon target hybridization has been studied [103]. The ability to visually identify reaction status without the need for instrumentation is advantageous with regards to platform cost and simplicity. However, rigorous classification of colorimetric changes is a challenging task that may introduce ambiguity when left solely at the user's discretion. When robustness is considered, quantitative measurements such as fluorescence or absorbance analyzed by standardized methods such as a sensory instrument may be the prudent direction for platform development.

5.5 CONCLUSION

Platform design is a multifactorial task consisting of various interdependent considerations for the cartridge, instrument and the assay. A key concept that should be understood in this chapter is that each component of the system has a range of options varying in both complexity and capabilities. While it may be an ideal goal for a diagnostic platform developer to optimize the system towards the fastest, smallest and the most specific and sensitive assay possible, practical considerations as discussed in this chapter suggest that some system parameters may need to be sacrificed in favor of others. A device that is capable of performing the most sophisticated PCR assay may require a highly sophisticated instrument and an expensive cartridge, while a simper system capable of isothermal assay could deliver a comparable level of sensitivity at a small fraction of the cost. In the context of POC diagnostics, factors such as accessibility in terms of cost and user friendliness may take a higher priority than marginal advantages in analytical sensitivity or specificity, and systems will need to be designed with such priorities in mind.

(A)

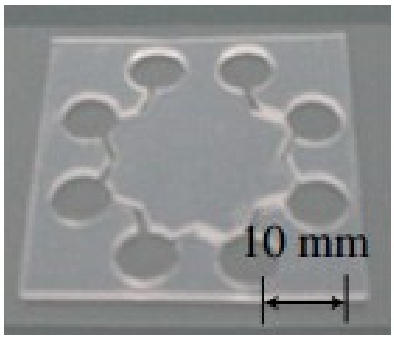
10 mm

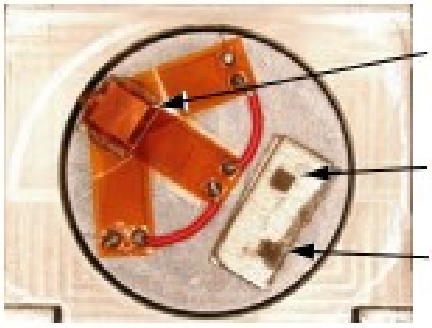
Flat coil and magnet (A)
Magnet (T1)
Magnet (T2)

(B)

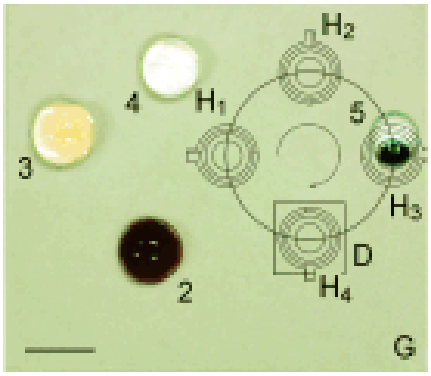
H2
4
H1
5
3
H3
D
2
H4
G

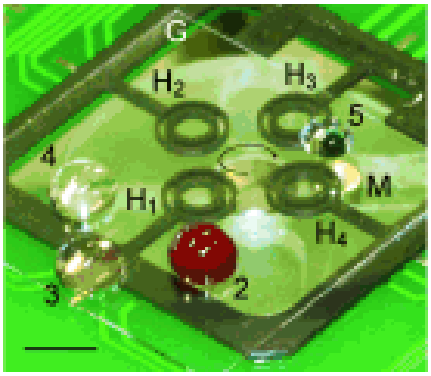
G
H2
H3
5
4
H1
M
H4
3
2

(C)

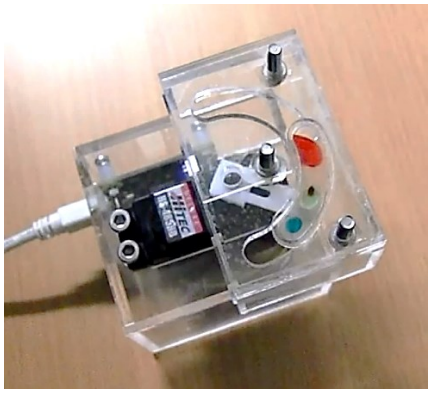

Figure 5.1: Rotary actuation of magnetic particles using a stepper motor.

A) Device proposed by Shikida *et al* incorporates permanent magnets alongside a coil electromagnet to enable particle agitation via magnetic repulsion. **B**) Device proposed by Pipper *et al* utilizes rotary actuation for thermal cycling between temperature zones on a micro PCR platform. [from refs. 12 and 13]; **C**) Our proposed device based on servomotor-driven rotary actuation.

(A)

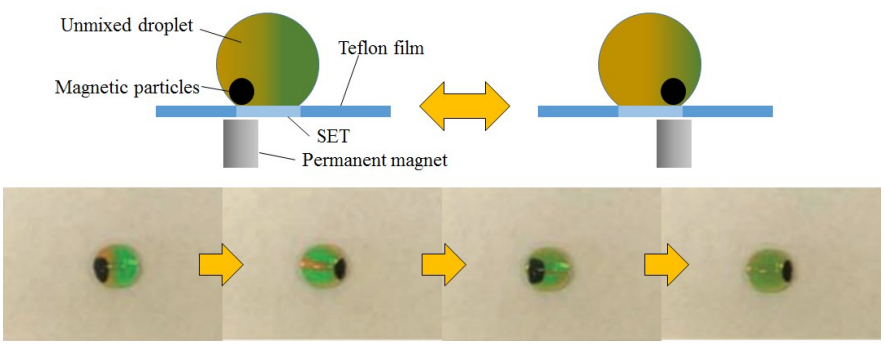
Unmixed droplet
Teflon film
Magnetic particles
SET
Permanent magnet

(B)

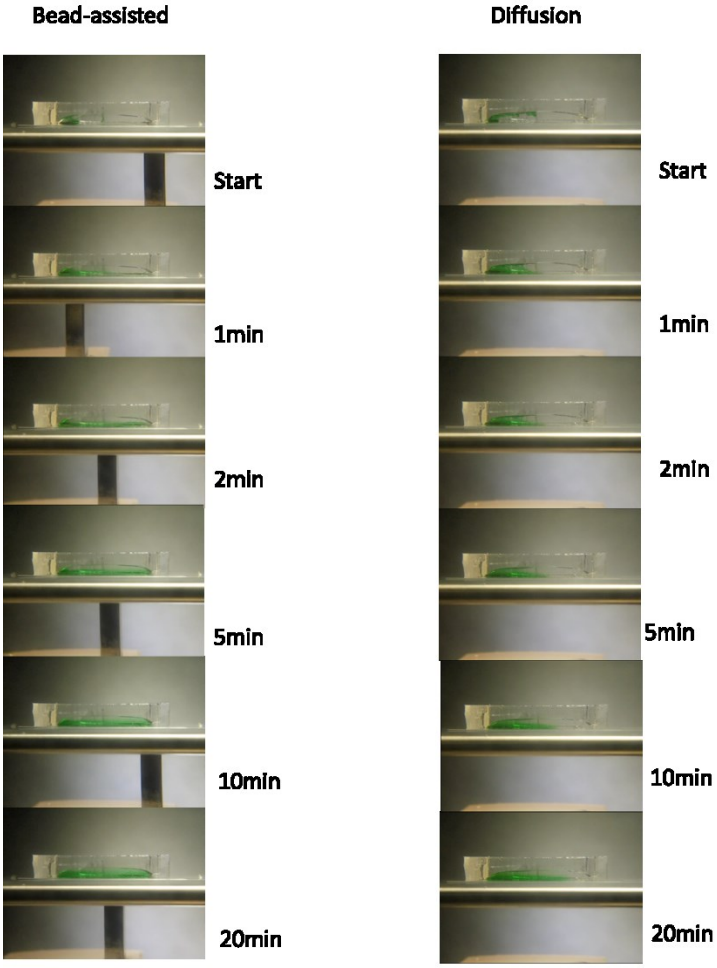
Bead-assisted
Diffusion
Start
1min
2min
5min
10min
20min
Start
1min
2min
5min
10min
20min

Figure 5.2: Particle mixing on a permanent magnet-based actuator via raster motion.

A) In the example demonstrated by Zhang *et al*, a particle plug is oscillated back and forth in order to generate internal flow. However, the particle is confined to the volume proximal to the substrate and thorough sampling of the reagent by the particles may not be achieved. **B**) Comparison of raster mixing to regular diffusion in a larger volume (200uL). In the example of bead-assisted dye mixing, it is apparent that dye diffusion takes place only in the vicinity of particle motion while leaving the unsampled areas intact, as evident by the slow diffusion of dye towards the top of the droplet in both conditions.

(A)

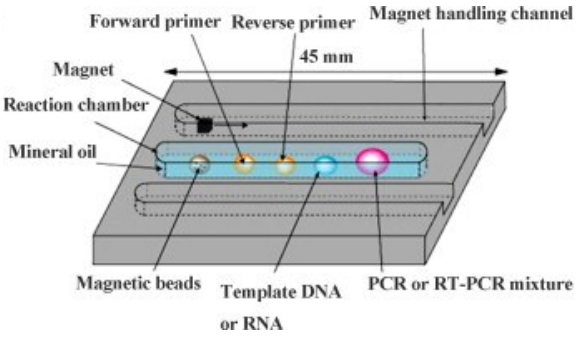
Forward primer
Reverse primer
Magnet handling channel
45 mm
Magnet
Reaction chamber
Mineral oil
Magnetic beads
Template DNA
or RNA
PCR or RT-PCR mixture

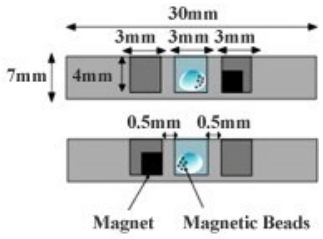
30mm
3mm 3mm 3mm
7mm
4mm
0.5mm 0.5mm
Magnet
Magnetic Beads

(B)

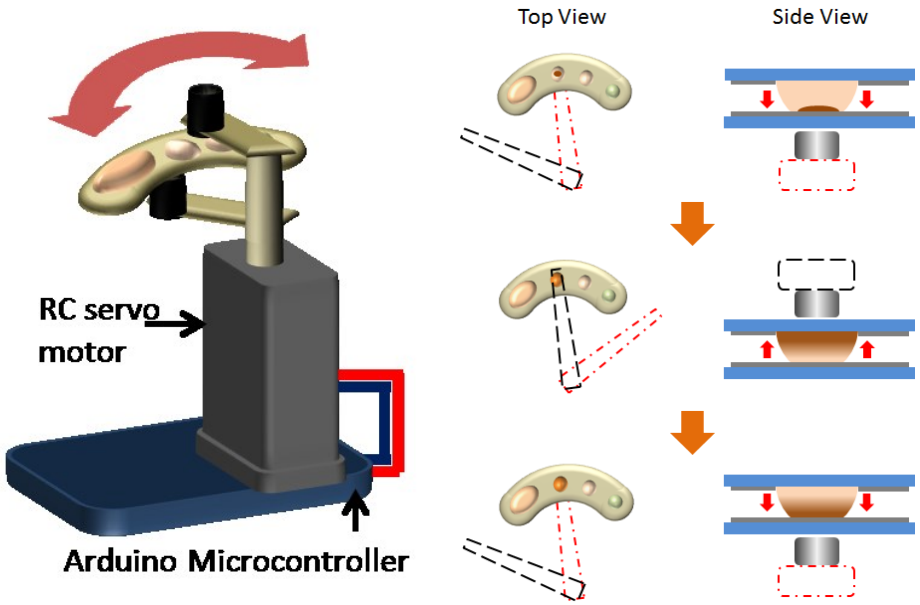
Top View
Side View
RC servo
motor
Arduino Microcontroller

Figure 5.3: Particle mixing on a permanent magnet-based actuator via alternation of field.

A) Particle mixing in an open-top chamber. In the droplet PCR system described by Tsuchiya *et al*, two magnets are used to sample the entire volume of the droplet more efficiently from both sides of the fluidic chamber. [adopted from ref. 11] **B**) Diagram describing washing mechanism on a thermoplastic cartridge using a rotary actuator. In order to facilitate efficient rinsing of magnetic beads and reduce the amount of buffer carried over with the bead plug at each step of the assay, the instrument utilized two magnetic spokes for mixing. Top (black dashed line) and bottom (red dashed line) spokes alternate in order to facilitate transversal motion of the magnetic beads. Magnetic field pulls beads across from one surface to the opposite surface (red block arrows), facilitating disintegration of bead plug into a plume as magnets alternate position.

(A)

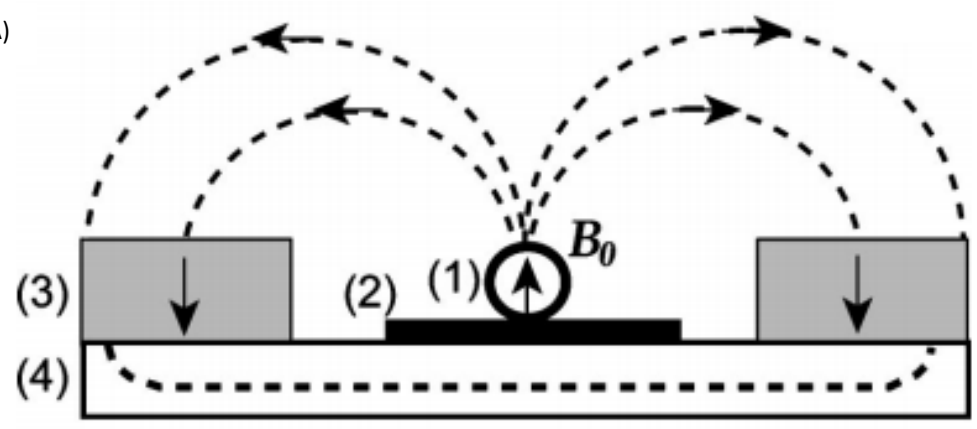

(B)

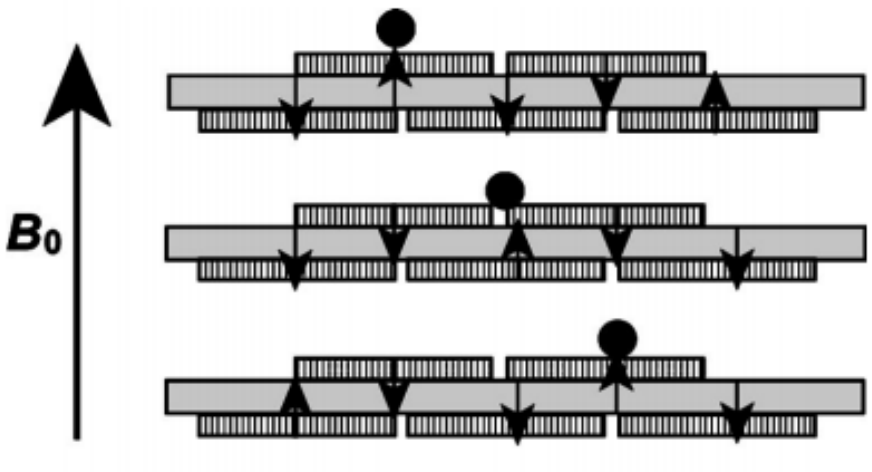

Figure 5.4: Electromagnetic manipulation for droplets containing magnetic particles.

A) Uniform magnetic field B generated by placing permanent magnets (3) on a highly field-permeable soft iron plate (4) strongly polarizes magnetic particle (1) perpendicular to the device plane (2). **B**) Two layers of overlapping electromagnetic coil array generates magnetic field in the component perpendicular to the device, such that magnetic particle can be actuated along the field gradient. [from ref. 8]

(A)

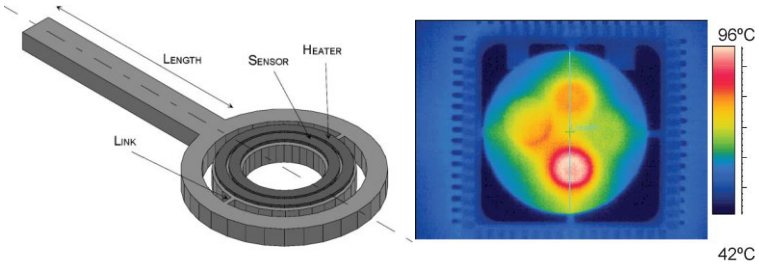
Length
Sensor
Heater
Link
96°C
42°C

(B)

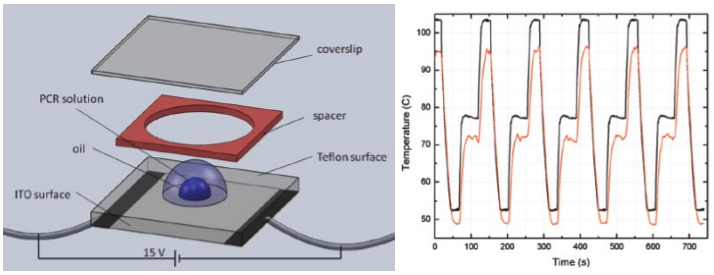
coverslip
PCR solution
spacer
oil
Teflon surface
ITO surface
15 V
Temperature (C)
Time (s)

(C)

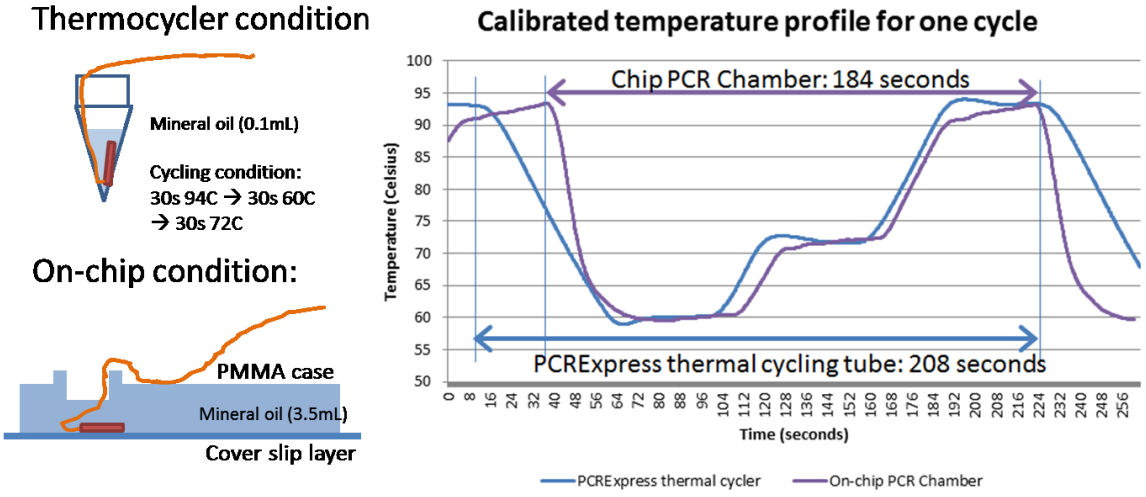
Thermocycler condition
Mineral oil (0.1mL)
Cycling condition:
30s 94C → 30s 60C
→ 30s 72C
On-chip condition:
PMMA case
Mineral oil (3.5mL)
Cover slip layer
Calibrated temperature profile for one cycle
Chip PCR Chamber: 184 seconds
PCRExpress thermal cycling tube: 208 seconds
Temperature (Celsius)
Time (seconds)
PCRExpress thermal cycler
On-chip PCR Chamber

Figure 5.5: Thermal control on droplet platforms.

A) A micro-PCR device proposed by Neuzil *et al* utilizes three microheaters which maintain steady-state temperature at annealing, denaturing and extension temperatures. **B**) A static micro-PCR device proposed by Angione *et al* utilizes a single heating element underneath the reagent which cycles through three temperature zones over time [from refs. 6 and 69]. **C**) Example of thermal calibration in a static micro-PCR device without embedded temperature sensing element. Thermal calibration in this example involves monitoring of reaction temperature using an external thermistor.

(A)

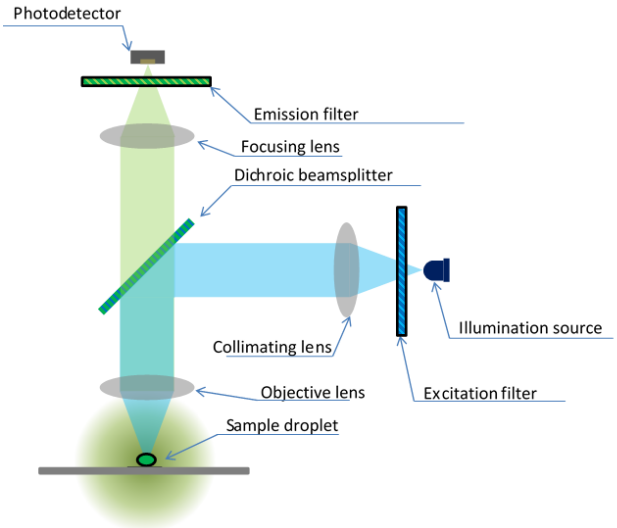
Photodetector
Emission filter
Focusing lens
Dichroic beamsplitter
Illumination source
Collimating lens
Objective lens
Excitation filter
Sample droplet

(B)

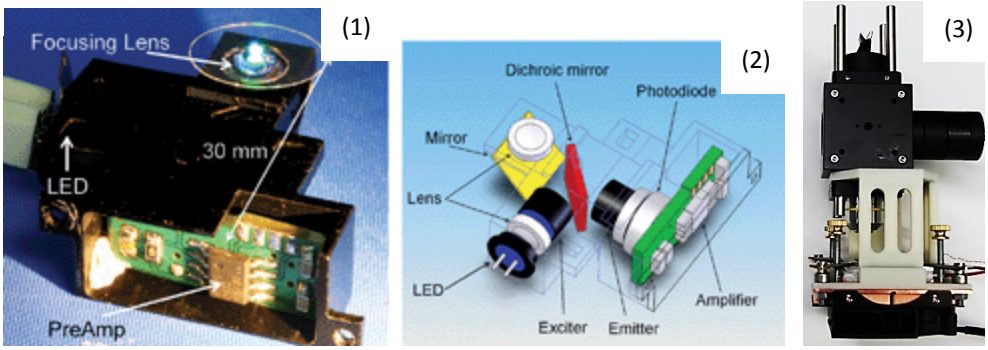
Focusing Lens
(1)
30 mm
LED
PreAmp
Dichroic mirror
Photodiode
Mirror
Lens
LED
Exciter
Emitter
Amplifier
(2)
(3)

(C)

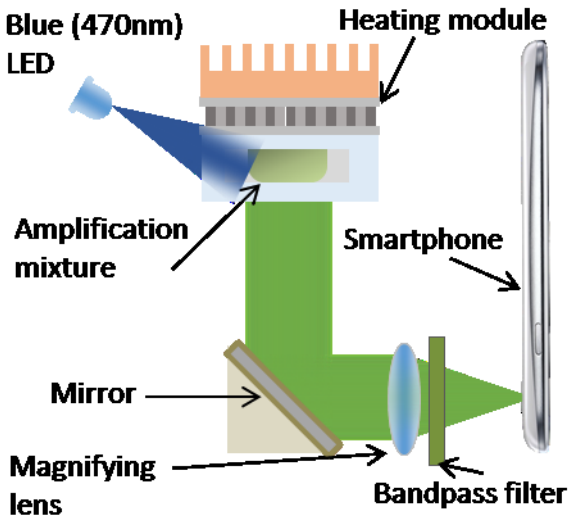
Blue (470nm)
LED
Heating module
Amplification
mixture
Smartphone
Mirror
Magnifying
lens
Bandpass filter

Figure 5.6: Instrumentation for optical signal acquisition.

A) epifluorescence microscope configuration. A collimated illumination source is reflected at a right angle by a dichroic beamsplitter and directed towards the objective lens, which focuses directly on the sample droplet. The fluorescence emitted by the droplet is collected by the objective lens and directed through the dichroic beamsplitter, which allows the emitted light to pass into the focusing lens and to be collected at the photodetector and converted into electrical signal. **B**) (1) Photograph and (2) schematic of a miniaturized fluorescence detector in epifluorescence microscope configuration as proposed by Novak *et al*. [adopted from ref. 79]; (3) adaptation of the miniaturized epifluorescence detector coupled to a PID-controlled thermoelectric unit, developed for our own investigation. **C**) an example of a cellphone-based signal acquisition, utilizing direct excitation at a direction orthogonal to signal path via LED source rather than the epifluorescence arrangement described in **Fig. 5.6A**. Data may be extracted as a fluorescent signal as in the example shown, or a colorimetric data using bright field illumination and removal of the color filter.

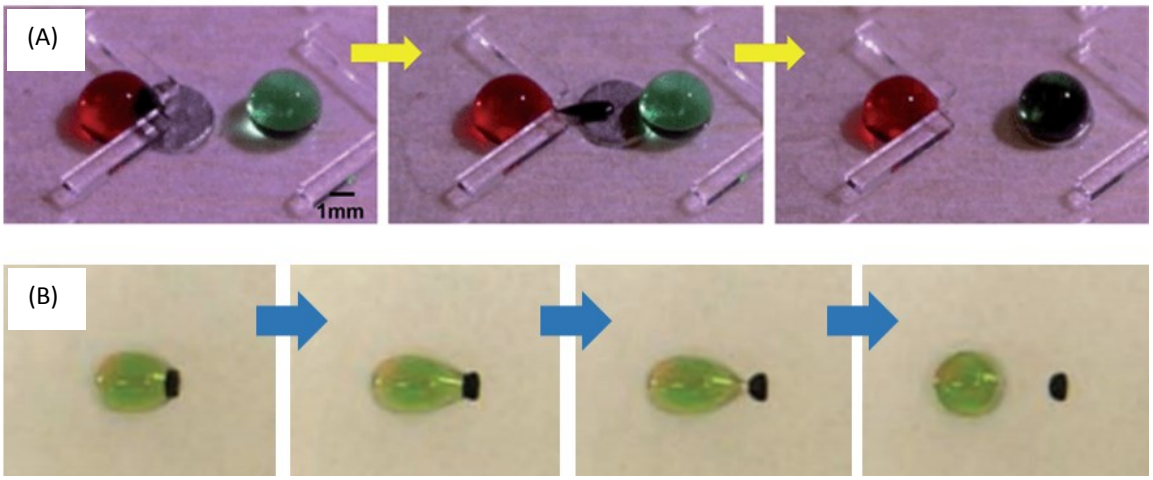
(A)
1mm
(B)

Figure 5.7: Magnetofluidic particle extraction via passive elements.

A) topography assisted particle extraction and **B**) surface energy trap-assisted particle extraction. [adopted from refs. 14 and 18]

(A)

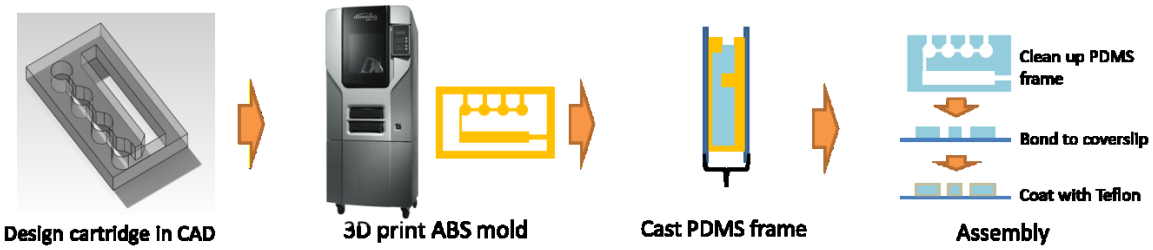

Design cartridge in CAD | 3D print ABS mold | Cast PDMS frame | Assembly

(B)

Figure 5.8: 3D rapid prototyper-based mold generation.

A) Fabrication workflow for a topography-based droplet magnetofluidic cartridge using 3D-printed mold. Design is first generated using a computer-assisted drawing tool and converted into a mold with appropriate bridges in place to secure all features together. The mold is used in combination with a smooth hydrophobic substrate in order to cast PDMS blocks with smooth surfaces for bonding to glass. **B)** Photograph of assembled cartridge loaded with reagents.

(A) (1) Hydrophilic pattern generation (2) Lamination-based thermoplastic packaging

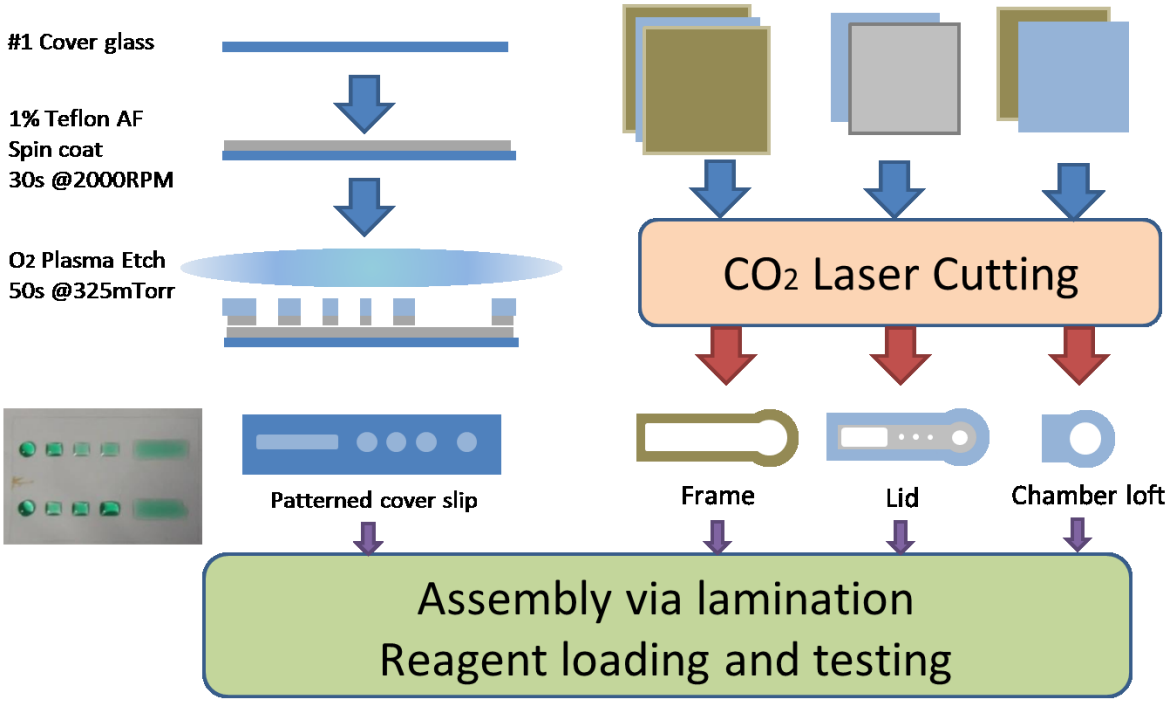

(B)

Figure 5.9: Packaging strategy for patterned glass substrates.

A) Packaging strategy for patterned glass substrates using a combination of thermoplastic lamination and oxygen plasma etching. This manufacturing strategy requires two parallel processes: (1) hydrophilic pattern generation on hydrophobically coated glass substrates using shadow mask etching strategy as described by Zhang and Wang [18]; (2) lamination-based packaging fabrication by assembling PMMA sheets patterned with CO_2 laser cutter. **B)** Photograph of assembled cartridges loaded with reagents.

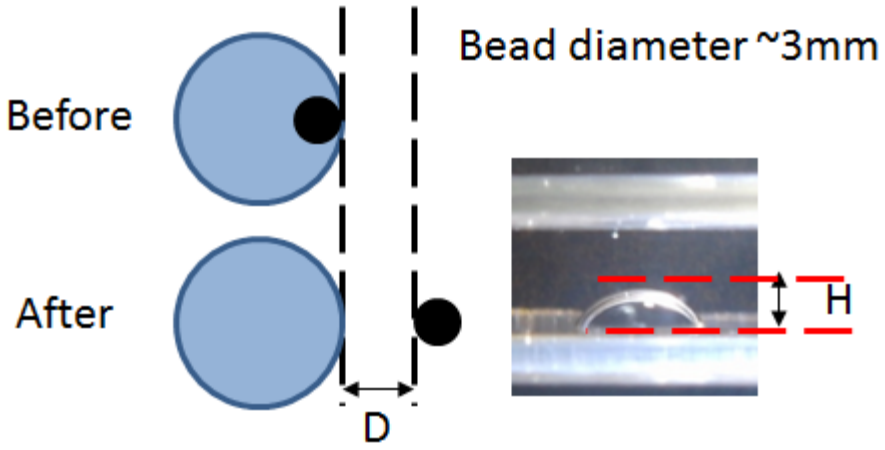
Bead diameter ~3mm
Before
After
D
H

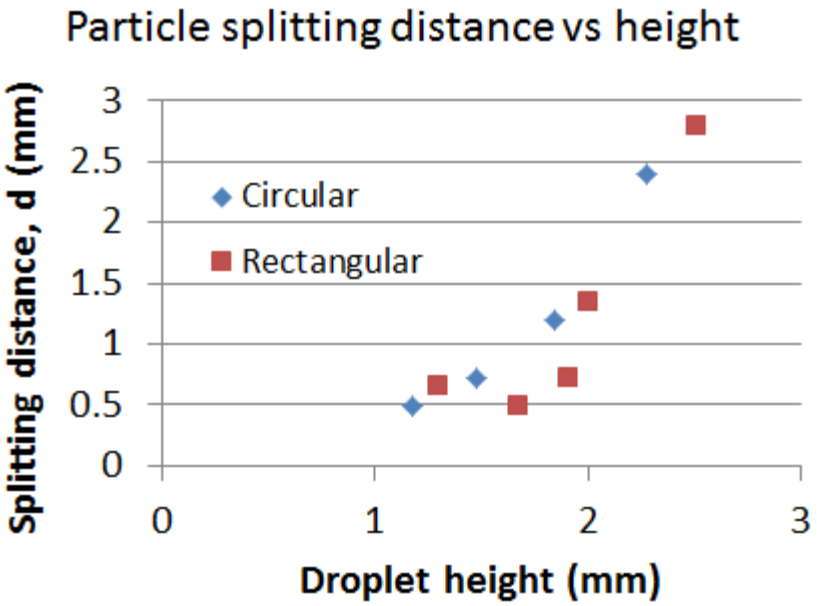
Particle splitting distance vs height
Splitting distance, d (mm)
3
2.5
2
1.5
1
0.5
0
Circular
Rectangular
0
1
2
3
Droplet height (mm)

Figure 5.10: Characterization of particle extraction distance.

Characterization of particle extraction distance using packaged hydrophilic patterns on a hydrophobic substrate. Low droplet profile (and droplet stability on substrate) can be achieved using larger hydrophilic patterns, which also results in shorter distance for particle extraction.

(A)

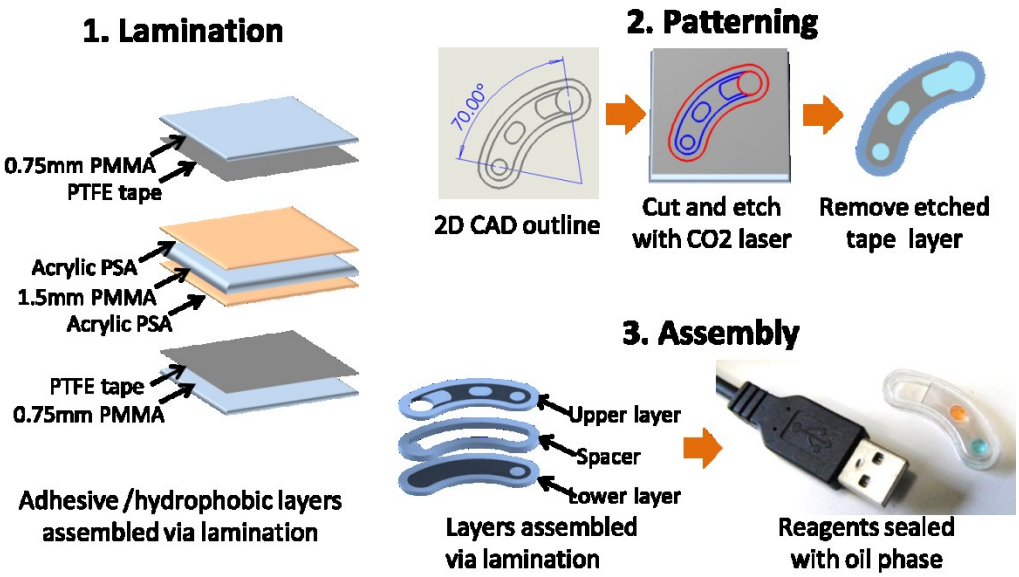
1. Lamination
0.75mm PMMA
PTFE tape
Acrylic PSA
1.5mm PMMA
Acrylic PSA
PTFE tape
0.75mm PMMA
Adhesive /hydrophobic layers assembled via lamination
2. Patterning
70.00°
2D CAD outline
Cut and etch with CO2 laser
Remove etched tape layer
3. Assembly
Upper layer
Spacer
Lower layer
Layers assembled via lamination
Reagents sealed with oil phase

(B)

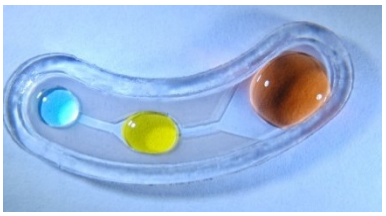

Figure 5.11: Packaged thermoplastic cartridge.

A) Packaged SET cartridge assembly strategy using thermoplastic lamination only. (1) Device is prepared on a layer-by-layer basis. Upper and lower layers are generated by coating the surface of a 0.75mm PMMA sheet with PTFE tape. The spacer frame between two layers is generated by coating a 1.5mm PMMA sheet on both surfaces with acrylic pressure-sensitive adhesive (PSA). The well layer is similarly generated using a 0.75mm PMMA sheet. (2) CAD software was used to generate laser paths for the CO_2 laser cutter, operating in both cutting and engraving modes. The engraving mode allowed cutting of the PTFE film only, which could be selectively peeled away in order to reveal hydrophilic surface that could be used to anchor aqueous reagents or provide bonding surface for acrylic PSA. (3) Layer assembly results in a sealed droplet cartridge. Reagents are primed on an upside-down upper layer, followed by assembly of the spacer and lower layer via compression. Flipping the entire cartridge right side up and filling with fluorinated oil results in an assay-ready cartridge. **B)** Photograph of assembled cartridges loaded with reagents.

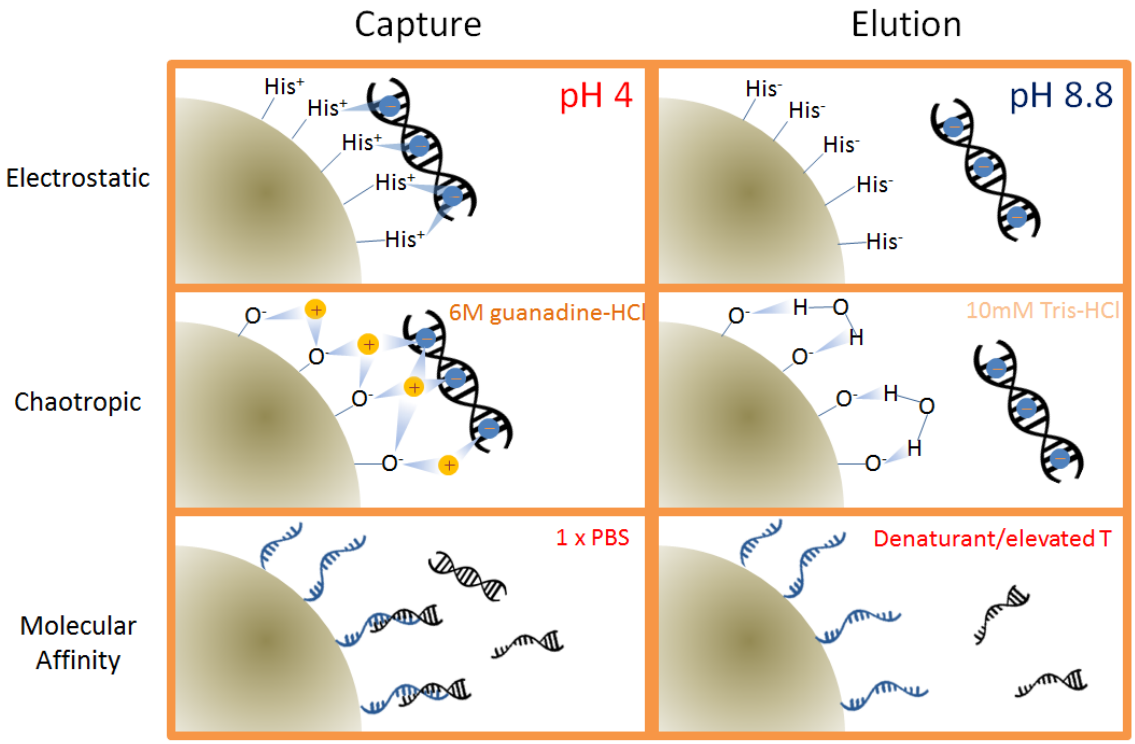
Capture
Elution
Electrostatic
Chaotropic
Molecular Affinity
pH 4
pH 8.8
6M guanadine-HCl
10mM Tris-HCl
1 x PBS
Denaturant/elevated T

Figure 5.12: Magnetofluidic strategies for nucleic acid capture and release.

Chapter 6

6. Mobile molecular diagnostic suite: design and evaluation of a clinical problem

6.1 BACKGROUND

In this chapter, we revisit the topic of point-of-care diagnostics from an enhanced vantage point drawn from the discussion on platform design in Chapter 5. As we have seen, the multifactorial nature of platform development process encourages us to focus on a specific set of needs. To facilitate this process, it is essential to first identify the clinical need for a more sensitive POC test.

During our search for an appropriate clinical problem, we identified chlamydia surveillance as a model problem that conveys many of the key rationale for a more sensitive and accessible diagnostic platform. Chlamydia trachomatis is one of the most common notifiable infectious diseases in the United States, with 2.86 million diagnosed cases and direct medical cost estimated at $516.7 million in 2008 [104]. While chlamydia infection is treatable with antibiotics, the prevalence of asymptomatic cases estimated at levels as high as 70% of all infection has given rise to its moniker ‘the silent epidemic’ [105]. When left undiagnosed and untreated, its long-term sequelae entail serious complications such as pelvic inflammatory disease (PID), chronic pelvic pain, infertility and ectopic pregnancy [106]. As such, routine screening of all sexually active women under the age 26 years has become the approach for chlamydia surveillance recommended by the Center for Disease Control and Prevention (CDC) [107], and methods for rapid detection of chlamydia is in great demand.

A closer look at chlamydia screening technologies reveal a gap that has yet to be addressed. Nucleic acid amplification tests (NAAT) are the current de facto gold standards recommended by the CDC, with >90% sensitivity and 99% specificity [108, 109]. However, the technology remains bound to the clinical laboratory workflow with consequent increase in delay between testing and diagnosis. While immunoaffinity-based rapid POC tests for chlamydia have been available as early as 1998, they suffer from poor sensitivity at 41-87% [110-113]. The demand for a sensitive chlamydia POC test exceeds that of any other sexually-transmitted infections among clinical staff and directors, as well as industry professionals [114, 115] Competitive effectiveness studies also suggest that POC tests that are both sensitive and affordable could be expected to substantially reduce the cost and prevalence of chlamydia infection [109, 116].

To address this need, we developed a platform (named mobiNAAT) that combines the mobility and accessibility of a smartphone with the scale and robustness of fluidic processing offered by droplet magnetofluidics. Our design rationale focuses on the accessibility of the platform with regards to user interface, mobility and cost, while delivering the high sensitivity afforded by nucleic acid amplification-based assay. In our platform, all steps of a conventional benchtop nucleic acid amplification tests are redesigned in a format that is accessible to a first-time user. The proposed platform demonstrates high analytical sensitivity and specificity for urogenital chlamydia, as well as clinical sensitivity tested using vaginal swab samples. To our knowledge, this demonstration presents the first mobile integrated platform for NAAT-based detection of chlamydia from clinical samples.

6.2 EXPERIMENTAL DETAILS

6.2.1. Cartridge design and fabrication

The droplet cartridge was fabricated by assembling four layers of polymethylmethacrylate (PMMA) sheets (McMaster-Carr, Elmhurst, IL, USA) as outlined in **Figure 6.1**. The chamber

layer was laminated with polytetrafluoroethylene (PTFE) tape (McMaster-Carr, Elmhurst, IL, USA) on one side in order to render the surface hydrophobic. The sheet was subsequently cut and laminated with the upper layer to generate hydrophilic PMMA chambers. The lower layer was laminated with PTFE film and engraved in order to expose the PMMA surface along the perimeter for bonding. A spacer frame was laminated on both sides with acrylic pressure-sensitive adhesive film (3M Company, St. Paul, MN, USA) and was used to provide a watertight seal and spacing between the upper and lower layers.

Cartridge assembly was achieved as follows. The top layer was pre-assembled with chamber and spacer layers to form a single component. The pre-assembled component was laid upside down and two 25µL aliquots of wash buffer and one 25µL aliquot of amplification mixture were dispensed sequentially on the hydrophilic patches. The lower layer of the cartridge was aligned to the pre-assembled component and bonded via compression. The cartridge was then flipped right side up and filled with approximately 100 µL FC-40 fluorinated oil in order to seal the reagents. Afterwards, a mixture of 30 µL binding buffer and 4 µL magnetic beads was loaded into the sample chamber and sealed at the inlet port with plastic tape. Prior to each assay, sample lysate was loaded into the sample chamber of the cartridge using a disposable pipette.

6.2.2. Single-stream Chlamydia trachomatis LAMP assay design

Valid target sequences for primer design were first identified using NCBI database and checked for cross-reactivity with other organisms prior to primer design. Using PrimerExplorer V4 (Fujitsu Ltd., Japan), several primer sets were designed against various targets in Ct genome and tested for threshold time and absolute signal difference from baseline **(Figure 6.2)**. Based on the results, a primer set designed to target a 321-bp region located in Ct OmpA gene was selected for subsequent experiments. All primers used for this experiment are presented in **Table 6.1**.

LAMP reaction mixture consisted of the following: primer set (0.2 µM F3/B3, 0.2 µM FIP/BIP, 0.8 µM LF/LB), 0.8M betaine (Sigma-Aldrich, USA), 1× Isothermal Amplification Reagent, 6 mM $MgSO_4$, 8 U Bst 2.0 WarmStart DNA Polymerase (New England Biolabs, USA), 1× LoopAmp Fluorescent Reagent (EIKEN Corp., Japan) and 1.4 mM dNTP set (Life Technologies, USA). During assay sensitivity characterization, we were able to observe identical results from two sets of complexometric indicator dyes calcein and HNB. While HNB can potentially reduce instrument cost by obviating the need for optical filters required for fluorescent indicators such as calcein, we observed that the limited stability of HNB in solution affected the consistency of signal across experiments. Calcein generated consistent results over time and was selected as the indicator for the assay in subsequent experiments. In quantitative LAMP characterization experiments, the indicator dye was replaced with 1x EvaGreen DNA binding dye (Biotium, Inc., Hayward, CA, USA). Primers and synthetic targets were synthesized by Integrated DNA Technologies (Coralville, IA, USA).

LAMP reaction was then characterized for temperature sensitivity **(Fig. 6.3)** and the effect of reagents on amplification **(Fig. 6.4)**. We subsequently tested the assay on cartridge in order to check whether the presence of magnetic particles during LAMP reaction affected the assay **(Fig. 6.5)**. For each reaction, 10µL plasmid target solution was mixed with input buffer composed of 50µL lysis buffer, 10µL resuspension buffer, 4µL magnetic beads and 30µL binding buffer. Each washing steps used 25µL wash buffer, followed by incubation in a 25µL amplification mixture.

We tested the sensitivity of our amplification mixture with spiked plasmid DNA targets over 6 orders of magnitude using standard qPCR instrument and found it capable of detecting 10^2-10^3 copies of the target sequence **(Fig. 6.6A)**. Afterwards, we assessed the efficiency of bead capture and elution process by capturing plasmid DNA targets using magnetic beads on a benchtop environment, eluting into the amplification mixture and amplifying the targets. We were able to capture and amplify 10^3 copies of gene targets **(Fig. 6.6B)**. Once the bead-based assay workflow

was verified, we added an indicator dye into the amplification mixture in preparation for colorimetric or fluorescent assessment of amplification using a smartphone. The dyes were complexometric indicators which developed positive signature from pyrophosphate, a metal-ion chelating agent and a byproduct of DNA polymerization [101, 126]. Sensitivity of the indicator dye was tested and verified to generate observable signal up to 10^2-10^3 copies per reaction, consistent with the initial assessment **(Fig. 6.7A)**. Specificity of the assay for Chlamydia trachomatis was tested using a panel of genomic DNA isolated from various bacterial species as well as human genomic DNA, and the absence of crosstalk with genomic DNA obtained from vaginal flora was verified **(Fig. 6.7B)**.

6.2.3. Design and fabrication of instrument and software

Following droplet cartridge design, computer-assisted drawing (CAD) software (Solidworks 2013, Dassault Systemes SOLIDWORKS, Waltham, MA, USA) was used to construct a prototype enclosure which incorporates Arduino Uno R3 microcontroller and motor shield, rotary actuator (Hitec RCD, Porway, CA, USA), thermal incubators (Custom Thermoelectric, Bishopville, MD, USA) and optical components (Thorlabs, Inc., Newton, NJ, USA). All components were designed and assembled using PMMA sheets and acrylic adhesive solvent (WeldOn Adhesives, Inc., Compton, CA, USA) where necessary. Pair of cylindrical NdFeB magnets (6 mm diameter) was affixed on each of the spoke tips to provide permanent magnetic fields for bead manipulation.

The software for smartphone application was developed using Android Studio (Google, Inc., Mountain View, CA, USA). In relation to the instrument, the application operates as a serial communicator which initiates various pre-programmed routines on the microcontroller via Bluetooth communication **(Fig. 6.8)**. The smartphone user interface **(Fig. 6.9)** was designed to provide 3 functions: 1) playback of training videos for the first-time users operating the device; 2) main routine which operates the instrument and performs data acquisition; 3) data viewer with

signal processing algorithm to differentiate positive from negative samples. Samsung Galaxy S3 (Samsung Electronics, Suwon, South Korea) was used as the smartphone for this study.

The software code for microcontroller application was written for the Arduino microcontroller. The overall program utilized a finite state machine architecture with each steps of the assay managed as separate states within the code. PID control for thermal incubation modules was programmed and calibrated using an embedded thermistor inside the heating block, and the temperature offset was measured by monitoring liquid temperature directly using an external thermistor **(Fig. 6.10)**.

6.2.4. Droplet cartridge processing routine

Magnetic bead motion was programmed using the Arduino library for RC servo. Briefly, each routine was programmed as a sequence of rotor angle and travel speed. Mixing of particles inside each aqueous droplet was achieved by rapidly switching the position of lower and upper spokes of the manipulator, which prevents bead extraction from buffer and instead generates a transversal motion of beads across the cartridge surface **(Fig. 6.11A)**. Afterwards, washing efficiency of the droplet manipulation module was characterized by spiking fluorescein in the sample inlet and measuring the amount of fluorescence carried over after each washing step under various conditions **(Fig. 6.11B)**.

6.2.5. Image processing

Data acquisition routine was performed by the smartphone application and camera as described in the Results section. In the real-time monitoring experiments, photographs were taken at a resolution of 3264x2448 over a 60-minutes incubation period and normalized by subtracting the first image of the sequence. For each image acquired, a single vector of green component in RGB space along the center line of the image was extracted. After baseline subtraction, area under the curve (AUC) was calculated by integrating all elements of the vector in the region of interest

corresponding to the reaction chamber. For the analysis of blinded samples using end-point measurement, photographs were taken at the beginning and the end of a 30-minute incubation period. Threshold AUC fluorescence for sample classification was established using a training set of 20 positive and negative samples. Positive controls were prepared by spiking 10^4 copies of plasmid target into sample mixture, while the plasmid targets were replaced with PCR-grade distilled water in negative controls. Threshold was established at 5 standard deviations above negative control AUC fluorescence **(Fig. 6.12)**.

For the samples processed using the portable prototype at the emergency room, positivity algorithm was modified to assess the time integral of signal in a 10-minute window rather than the endpoint fluorescence. Using this approach, rapid signal development due to amplification event could be distinguished clearly from low levels of signal developed in negative samples **(Fig. 6.13)**. Raw signal was processed in a similar manner as described previously, except the analysis region was extended to the entire 2-dimensional field rather than a single vector. Threshold AUC fluorescence for sample classification was established at 5 standard deviations above negative control AUC fluorescence using a training set of 15 cartridges with negative control as input.

6.2.6. Clinical sample testing conditions

Vaginal swab samples were collected from the mail-in program and stored in -80˚C before use. The swab was expressed by dabbing against a 600 µL microcentrifuge tube containing ~200 µL lysis solution composed of 50:20:1 lysis buffer, resuspension buffer and proteinase K solution by volume (ChargeSwitch gDNA mini bacteria kit, Life Technologies). Afterwards, the tube was inserted into an on-board lysis chamber and incubated for 30 minutes at 65˚C followed by 15 minutes at 95˚C for proteinase inactivation. For the clinical samples tested at the emergency room, the swab was similarly expressed in lysis buffer without proteinase K and lysed using a portable microbead-beating unit (OmniLyse Kit, Claremont BioSciences). 70 µL of the lysate was

added to 34 μL binding solution composed of a 15:2 mixture of binding buffer and magnetic bead by volume, and the mixture was subsequently transferred to the sample inlet of the pendant droplet cartridge.

6.3 PLATFORM DESIGN PRINCIPLES

Integration of sample processing and detection is an essential feature in the delivery of molecular assays under POC settings. However, an often overlooked pitfall of integration is that it increases the complexity of the instrument and disposable components, which gives rise to sophisticated but expensive devices or instruments whose portability and affordability are compromised. We sought to address this challenge by finding a simple and scalable engineering solution to both the disposable component and the instrument.

6.3.1 Smartphone-based system design

The smartphone is an integrated multifunctional platform equipped with touch screens, optical sensors, communicative and data processing capacities, with both researchers and developers exploring its potential application in medicine. Academic and commercial efforts are exploring its capacity as a low-cost sensor, utilizing on-board CMOS sensors to recreate the functions of various medical and laboratory instruments such as the light microscope [117], a colorimetric or fluorescent reader [118, 119] or a pulse oximeter [120] in a highly portable format. On another level, the on-board display and communicative functions of smartphones are being explored to facilitate hospital-wide communication [121], medical reference [122] and remote diagnostics [123]. Recent application has also demonstrated the use of mobile phones as a power source for a microfluidic immunoassay cartridge [124]. However, current applications of mobile phones have yet to explore its multifactorial capacity as a multimedia training tool and a portable workstation for handling various peripheral electromechanical devices in addition to their sensory function **(Fig. 6.14)**.

The mobile diagnostic platform consists of three discrete units: a droplet magnetofluidic cartridge, a rechargeable lithium polymer battery-powered instrument for cartridge processing, and a smartphone for user interface, data acquisition and processing. The magnetofluidic cartridge enables bioassays requiring multiple buffer exchanges using geometric features that do not require precise microfabrication or pneumatic controls such as pumps and valves. We developed a novel design and fabrication process for a sealed magnetofluidic cartridge using poly-methylmethacrylate (PMMA) as the base material and polytetrafluoroethylene (PTFE) film for hydrophobic surface generation. The cartridge utilizes the adhesive force of aqueous buffers on hydrophilic surfaces in order to form 25 μL columns of reagents that are required for DNA extraction and amplification, which is traversed by magnetic particles on the smooth PTFE surface at each buffer exchange step of the assay. Each cartridge costs less than $2 using off-the-shelf reagents and materials, which compares favorably with the current cost of NAAT (US$33.48) [116].

The smartphone app consists of user interface which facilitates wireless communication with peripheral devices via microcontroller. The entire assay is segmented into four sequential phases consisting of cartridge loading, nucleic acid purification, real-time signal amplification and data analysis. After the sample is loaded into the droplet cartridge and the assay routine initiated on the smartphone app, there is no additional user interaction required until the assay is completed.

6.3.2 Instrument design

The portable instrument is an integrated electromechanical device that performs three major operations. The first component is the rotary bead manipulator, which facilitates transport of magnetic particles across multiple aqueous buffer systems. An RC servo motor coupled to a permanent magnet provides a highly cost-effective mechanism for rotary actuation of permanent magnets. Microcontroller-mediated pulse-width modulation (PWM) enables manipulation of the

rotary arm along a pre-programmed routine for bead washing and transport. Bead washing is facilitated using two spokes attached to a central rotor, each mounted with a permanent magnet in contact with the top and bottom surfaces of the assay cartridge **(Fig. 6.11)**. Routine for each assay is programmed as a series of rotor angle positions and angular speeds and executed in series via microcontroller. The second component is thermal incubation facilitated by a PID-controlled thermoelectric element, driven using a microcontroller-mediated output from an H-bridge amplifier circuit. The last component is a Bluetooth transceiver which facilitates wireless control of the peripheral device using the smartphone user interface. The microcontroller itself utilizes finite state machine (FSM) architecture to enable flexible transition between each phase of the assay. An external lithium-polymer battery can provide the user with the ability to perform assays in the absence of a power outlet, while a standalone USB charger can power the instrument in presence of a power outlet. The instrument has an optical module and a docking station for the smartphone which enables phone camera-based data acquisition from the reaction chamber during the amplification **(Fig. 6.14C)**.

6.3.3 Assay design

We utilized loop-mediated isothermal amplification technique (LAMP) for nucleic acid target amplification [125]. This approach is highly amenable to the assay platform for several important reasons. First, isothermal amplification assay greatly relaxes thermal conductivity constraints of the cartridge, allowing flexibility in cartridge material selection and fabrication strategy. Secondly, the capacity of LAMP assay to generate superabundance of pyrophosphate enabled us to couple these reactions to colorimetric or fluorescent indicators [101, 126]. These images were captured and processed on mobile phones using a custom application built using the Android platform. Lastly, the pH of LAMP reaction condition was readily compatible with the elution conditions for nucleic acid purification chemistry, allowing seamless transition from nucleic acid

extraction to target amplification using the same solid phase transport. **Figure 6.15A** outlines the single-stream assay design as implemented in this chapter.

6.4 ASSAY IMPLEMENTATION ON PLATFORM

We first assessed the level of signal that could be detected using the smartphone camera using data processing algorithm as described in **Figure 6.15C**. Briefly, image of the reaction chamber was captured using the smartphone at the start of the incubation period and at user-specified intervals thereafter. Once an image is acquired, a single vertical line of pixels was sampled from the green component of RGB values for each image at the center of the reaction chamber at a preset image coordinate. Vectors representing each time point were subtracted with baseline vector acquired at the start of the incubation and integrated in order to obtain the area under the curve (AUC) fluorescence corresponding to each time point. A representative image of fluorescence signal that develops over the course of a positive reaction is presented in **Figure 6.15B**. Afterwards, we tested our platform using a set of de-blinded clinical samples in order to establish the signal difference between positive and negative samples. Further analysis of the samples using real-time trace **(Fig. 6.16A)** showed that positive signal began to develop consistently after 20 minutes of incubation, which was subsequently used as the time threshold in the image analysis algorithm. Prior to testing blinded clinical samples, a training set of 10 positive and negative samples were tested in order to generate a threshold AUC florescence value **(Fig. 6.12)**.

We subsequently evaluated the performance of the cartridge by analyzing 20 vaginal swab samples using an experimental prototype instrument. One set of swabs was analyzed using the Gen-Probe Aptima Combo 2 CT assay, currently considered as the gold standard in Chlamydia trachomatis detection. The second set of swabs was tested on the droplet cartridge using the

prototype. The two results were in agreement for 20 out of 20 samples, demonstrating that the droplet assay performance is comparable to NAAT assays for the samples tested **(Fig. 6.16B)**.

6.5 EVALUATION IN EMERGENCY CARE SETTING

In order to evaluate the performance of the mobiNAAT platform in clinical setting, we delivered the smartphone pre-loaded with the app software, the processing module and assembled cartridges to the Emergency Department at Johns Hopkins Hospital (Baltimore, MD, USA). The entire mobiNAAT workflow was designed to take up to 72 minutes from start to finish for a first-time user, including 6 minutes of user training, 60 minutes of incubation and minimal hands-on time **(Fig. 6.16C)**. Volunteers for the study were recruited from a set of patients visiting for pelvic examination in the emergency room. An on-site research coordinator using the platform for the first time was trained using the tutorial resource accessed via the smartphone app. Samples from each patient were tested in parallel by the mobiNAAT platform and the Gen-Probe Aptima Combo 2 CT assay for verification **(Fig. 6.17A)**. The platform correctly identified 2 positives among 30 patients, demonstrating that the droplet assay performance is comparable to the gold standard for the samples tested **(Fig. 6.17C)**. Comparison of results obtained from the app-trained naïve operator and platform developers showed full correspondence for the samples tested, demonstrating the ease of access facilitated by the smartphone interface and training module **(Fig. 6.17D)**.

6.6 CONCLUSION

Accurate and inexpensive POC tests are urgently needed to control STI epidemics, so that patients can receive immediate diagnoses and treatment. STIs represent a significant public health burden in the U.S, both from the high morbidity and mortality and the associated costs. Numerous factors contribute to the persistent STI public health burden, but of particular importance is delay in treatment resulting from lengthy diagnostic protocols. Comparative effectiveness studies attest

to the importance of cost and sensitivity as decisive parameters for patients to seek POC over standard NAAT [116]. In particular, POC tests offer important strategies to address the Chlamydia epidemic, since diagnosis and immediate treatment can prevent transmission to sexual partners.

POC tests based on immunoassay have gathered criticism from various studies due to poor clinical sensitivity [110-113]. Among other studies, a direct comparison of clinical sensitivity for various CT assays using endocervical swab specimen showed <40% sensitivity for immunoassay compared to near-100% for NAAT [127]. These studies reinforced our interest in designing an engineering solution to implementing NAAT in a format that is more amenable to POC. The relevant range of Chlamydia load from vaginal swabs is 5,167-21,163 copies (EB) per swab with 95% confidence interval [128], which is in greater abundance than the analytical sensitivity range of 10^2-10^3/sample described in this platform.

Cost reduction is a major aspect of platform design and an important consideration for the end user. The use of a smartphone as a user interface and an imaging sensor modularizes the instrument as an add-on to the smartphone, such that a more affordable instrument could be made available. Due to the risk of contamination in an amplification reaction, it is important for a cartridge to be robust yet also expendable. To that end, the use of droplet magnetofluidic cartridge reduces reagent and fabrication cost through its simple fabrication process and miniaturization. Moreover, the single-stream assay design also simplifies and reduces the cost of cartridge and instrumentation for automation. This in turn reduces cost of manufacturing and improves affordability and delivery, which would allow more patients to be tested using the platform [129].

The single-stream assay workflow also highlights an important consideration for sample preparation in POC testing. Benchtop assays typically utilize only a fraction of the extracted

target in each reaction due to the diluting nature of combining aqueous reagents. While this allows duplicate testing of identical samples and confers an advantage in a reference laboratory setting, it also dilutes the target concentration and necessitates assays with the highest possible sensitivity. By contrast, the single-stream assay elutes captured nucleic acid targets into a single reaction mixture, which has a sample concentrating effect compared to benchtop assays where nucleic acid extraction and amplification are decoupled. This approach is well-suited to POC screening, where the capacity of each individual test in achieving the highest sensitivity may take precedence over the ability to archive samples or perform technical replicates.

A long-term goal envisioned by this research is to develop a versatile and affordable NAAT platform that can be operated by an untrained person in the absence of laboratory infrastructure. The ASSURED guideline for POC tests set by the World Health Organization (WHO) includes affordability, operability by untrained person, and delivery to end users as its criteria [65]. In addition to the overall cost-economizing platform design, we sought to address the user interaction by using the smartphone as a platform facilitating both training and user interface. It seemed apparent to the authors that some level of complexity is inherent in the design of many useful assays such as NAAT, and harnessing the multimedia capability of a mobile phone could help to bridge the gap between a research concept and a field-tested device.

The real-time amplification data processing capability also highlights a possible application of the mobiNAAT platform in quantitative nucleic acid-based testing. LAMP assay is amenable to quantitative measurement based on amplification time until saturation [130]. This is especially pertinent in HIV monitoring, where the serum titer of the pathogen carries essential diagnostic information [131]. Furthermore, the platform's compatibility with real-time measurement renders it flexible to strategies for multiplexing via broad-based pathogen identification techniques based on molecular beacons and melting curve analysis [132, 133]. In addition, real-time amplification

confers additional level of stringency for differentiating between positive and negative samples via time-based thresholding, thus enhancing the robustness of the platform.

Overall, the mobiNAAT platform proposes a NAAT-based solution that is fully mobile, simple to operate and affordable at the same time, suggesting a direction for designing effective diagnostic tools accessible to individuals outside centralized laboratories.

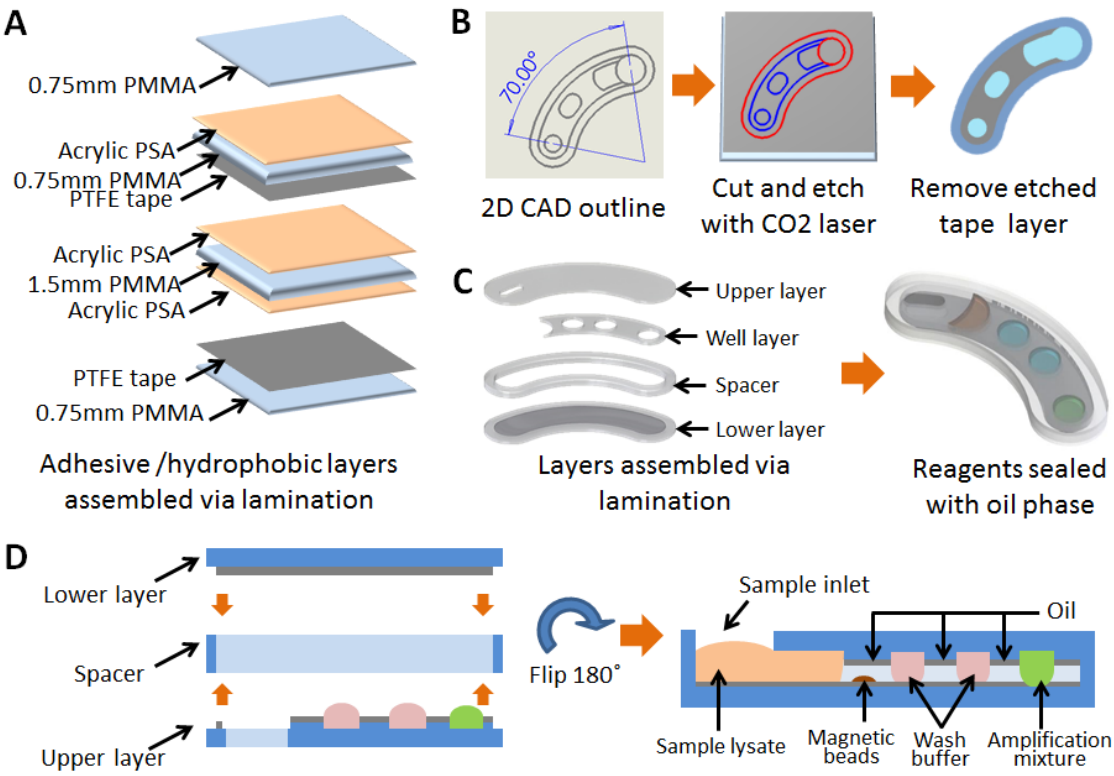
A
0.75mm PMMA
Acrylic PSA
0.75mm PMMA
PTFE tape
Acrylic PSA
1.5mm PMMA
Acrylic PSA
PTFE tape
0.75mm PMMA
Adhesive /hydrophobic layers assembled via lamination
B
70.00°
2D CAD outline
Cut and etch with CO2 laser
Remove etched tape layer
C
Upper layer
Well layer
Spacer
Lower layer
Layers assembled via lamination
Reagents sealed with oil phase
D
Lower layer
Spacer
Upper layer
Flip 180°
Sample inlet
Oil
Sample lysate
Magnetic beads
Wash buffer
Amplification mixture

Figure 6.1: Pendant droplet cartridge fabrication workflow.

A) Device is prepared on a layer-by-layer basis. Upper and lower layers are generated by coating the surface of a 0.75mm PMMA sheet with PTFE tape. The spacer frame between two layers is generated by coating a 1.5mm PMMA sheet on both surfaces with acrylic pressure-sensitive adhesive (PSA). The well layer is similarly generated using a 0.75mm PMMA sheet. **B**) CAD software was used to generate laser paths for the CO_2 laser cutter, operating in both cutting and engraving modes. The engraving mode allowed cutting of the PTFE film only, which could be selectively peeled away in order to reveal hydrophilic surface that could be used to anchor aqueous reagents or provide bonding surface for acrylic PSA. **C**) Layer assembly results in a sealed droplet cartridge. **D**) Detailed description of layer assembly. Reagents were primed on an upside-down upper layer, followed by assembly of the spacer and lower layer via compression. Flipping the entire cartridge right side up and filling with fluorinated oil results in an assay-ready cartridge.

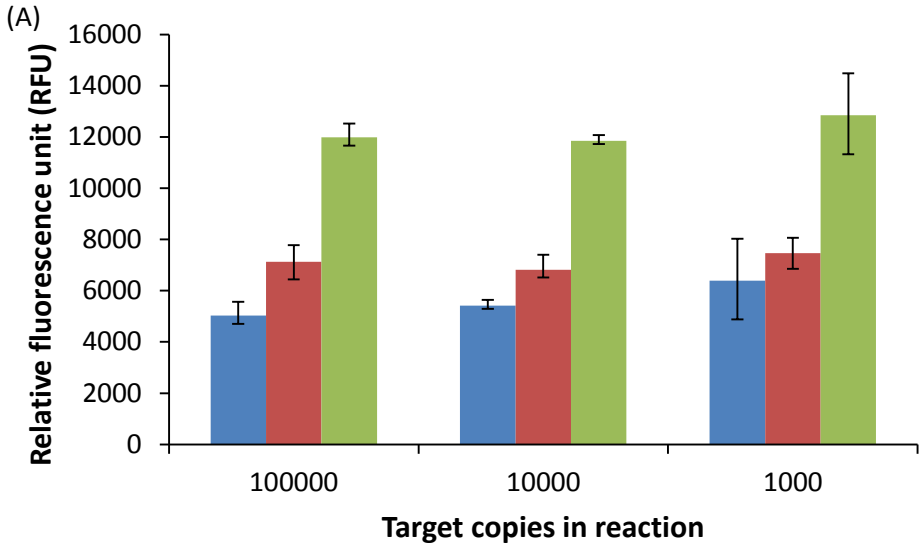
(A)
Relative fluorescence unit (RFU)
16000
14000
12000
10000
8000
6000
4000
2000
0
100000
10000
1000
Target copies in reaction

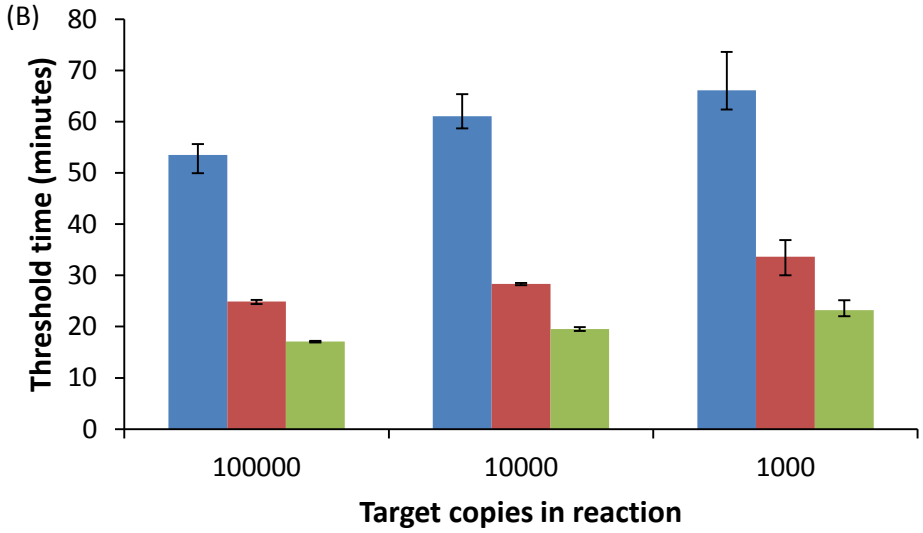
(B)
Threshold time (minutes)
80
70
60
50
40
30
20
10
0
100000
10000
1000
Target copies in reaction

Figure 6.2: Primer design and verification.

A) Absolute baseline-subtracted signal obtained by 3 different LAMP primer sets with targets in 3 orders of magnitude dilution, in relative fluorescence unit (RFU). Primer set 3 (green) demonstrates approximately twofold higher signal than either primer sets 1 (blue) or 2 (red). **B**) Threshold time obtained by the same primer sets. Primer set 3 (green) demonstrates earlier amplification of signal above threshold than either primer sets 1 (blue) or 2 (red).

Primer set 1: targeting OmpA gene in Ct genome

Primer	Sequence
F3	GTTCTGCTTCCTCCTTGC
B3	TGGAATTCTTTATTCACATCTGT
LIP	GATCTCCGCCGAAACCTTCCGGAATCCTGCTGAACCAA
BIP	TTGCGATCCTTGCACCACTTCGGTCGAAAACAAAGTCAC
LF	CAGAATTCCGTCGATCATAAGGC
LB	TGACGCTATCAGCATGCGTATG

Primer set 2: targeting 16S rRNA gene in Ct genome

Primer	Sequence
F3	CGTTAGTTGCCAGCACTTA
B3	ACACGCCATTACTAGCAATT
LIP	CATAAGGGCCATGCTGACTTGAAACTCTAACGAGACTGCCT
BIP	TACAGAAGGTGGCAAGATCGCCAGACTACAATCCGAACTGG
LF	TCGCCTTCCTCCTGGTTA
LB	GATGGAGCAAATCCTCAAAGC

Primer set 3: targeting 16S rRNA gene in Ct genome

Primer	Sequence
F3	GATGCAACGCGAAGGACC
B3	TGGTTAACCCAGGCAGTCT
LIP	GACAGCCATGCAGCACCTGTTGTATATGACCGCGGCAGAA
BIP	GTGCCGTGAGGTGTTGGGTTAACACCCTAAGTGCTGGCAAC
LF	GTCCTTGCGGAAAACGACA
LB	ACGAGCGCAACCCTTATCG

Table 6.1: Primer sequences designed for amplification mixture

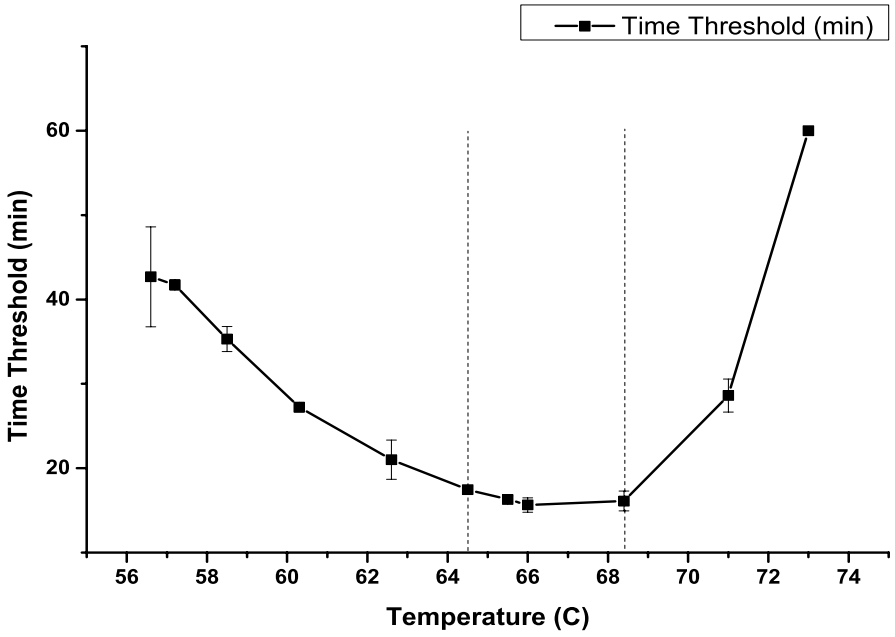
Time Threshold (min)
Time Threshold (min)
60
40
20
56
58
60
62
64
66
68
70
72
74
Temperature (C)

Figure 6.3: LAMP operating temperature characterization.

In order to assess the level of stringency required to maintain adequate isothermal amplification conditions, temperature was varied between 56˚C and 74˚C and its effect on time threshold was observed. Based on real-time signals, we identified an optimal window of approximately 4˚C between 64.5˚C and 68.5˚C. Input DNA was set at 1000 copies of target per reaction. This window was subsequently used as the basis for thermal control on the mNAAT platform.

(A)

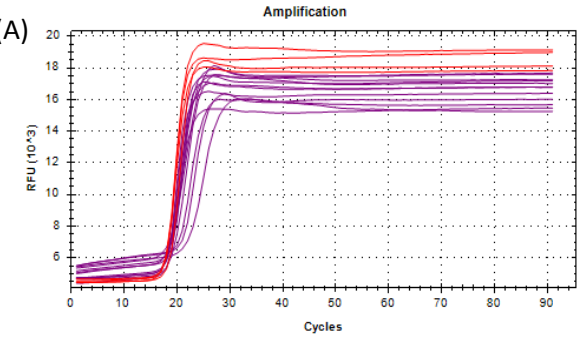
Amplification
RFU (10^3)
Cycles

(B)

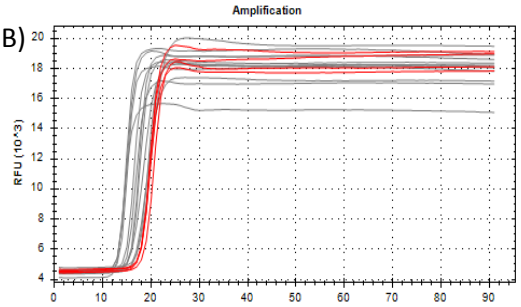
Amplification
RFU (10^3)

(C)

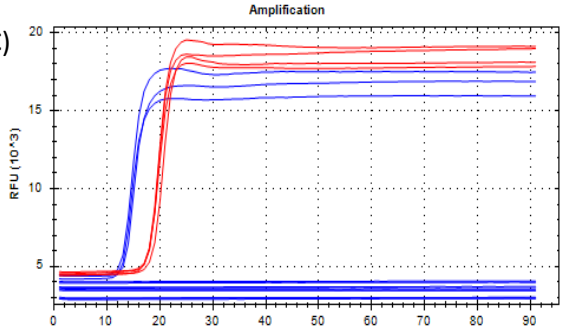
Amplification
RFU (10^3)

(D)

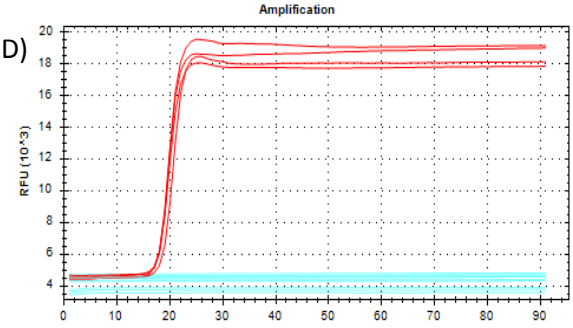
Amplification
RFU (10^3)

(E)

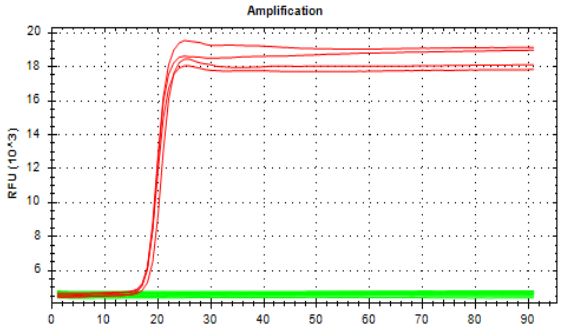
Amplification
RFU (10^3)

Figure 6.4: Inhibitor characterization.

For each of the buffers and components utilized in DNA purification, a small amount of buffer was spiked into amplification mixture containing 10^3 targets and incubated. In all traces, red line indicates positive control reaction. **A)** cell culture (positive control); **B**) lysis buffer. Amplification was not significantly affected. **C**) Binding buffer. This buffer has substantially acidic pH, which may account for most reactions failing. **D**) Proteinase K. All reactions containing proteinase K failed to amplify. **E**) A mixture containing lysis buffer, proteinase K and binding buffer. The results indicated that thorough bead washing and thermal deactivation of proteinase K are important parameters for the single-stream assay to perform optimally.

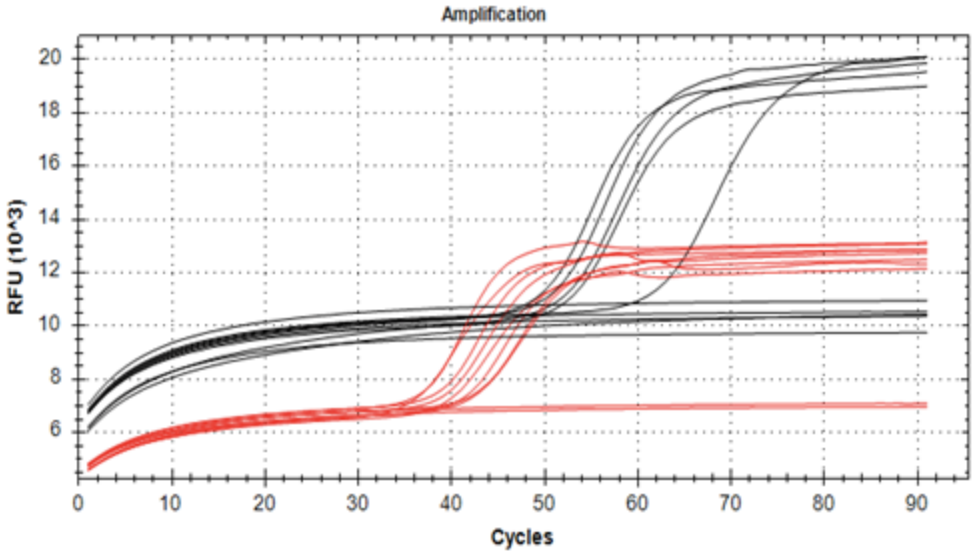
Amplification
RFU (10^3)
Cycles
20
18
16
14
12
10
8
6
0
10
20
30
40
50
60
70
80
90

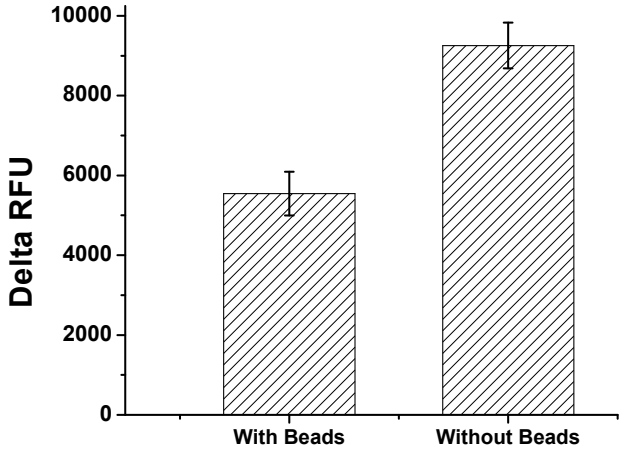
Delta RFU
10000
8000
6000
4000
2000
0
With Beads
Without Beads

Figure 6.5: Bead incubation characterization.

A) Real-time LAMP trace obtained for amplification reagents containing magnetic beads (red trace) and those without beads (red trace). Interestingly, the presence of magnetic particles resulted in an earlier amplification of target above background signal. **B**) Comparison of background-subtracted RFU for LAMP reactions incubated with or without beads. Reactions incubated with beads were identified by a reduction in background-subtracted signal by nearly a factor of two. Based on this result, subsequent processes on chip involved removal of beads after elution of nucleic acid target prior to amplification.

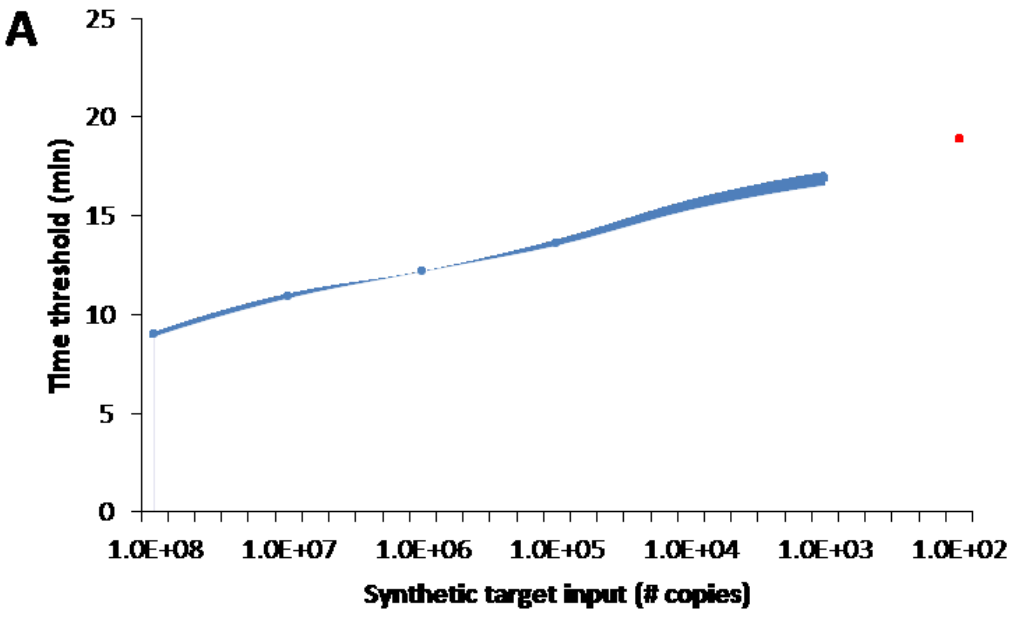
A
25
20
15
10
5
0
Time threshold (mln)
1.0E+08
1.0E+07
1.0E+06
1.0E+05
1.0E+04
1.0E+03
1.0E+02
Synthetic target input (# copies)

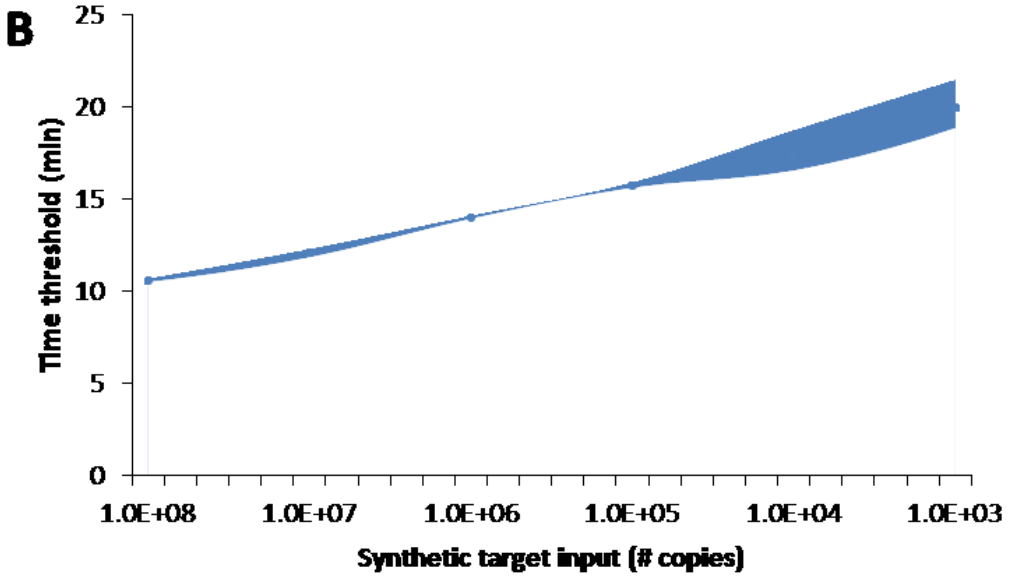
B
25
20
15
10
5
0
Time threshold (mln)
1.0E+08
1.0E+07
1.0E+06
1.0E+05
1.0E+04
1.0E+03
Synthetic target input (# copies)

Figure 6.6: Analytical sensitivity of single-stream LAMP assay.

A) Comparison between amplification of dilutions of synthetic DNA spiked into reaction mixture. A fraction of replicate reactions were amplified for 10^2 copies of input (red marker), indicating analytical sensitivity of 10^2-10^3 copies of target. Shaded areas represent upper and lower bounds of time threshold (n=3). **B**) Real-time signal comparing process efficiency of bead-based target purification and subsequent amplification, demonstrating sensitivity comparable to the standard LAMP process without bead coupling. Shaded areas represent upper and lower bounds of time threshold (n=3).


(A)
10^5 copies
10^4 copies
10^3 copies
10^2 copies
10^1 copies
10^0 copies
Water
(B)
A. vaginae
G. vaginalis
M. mullineris
L. brevi
E. coli
S. epidermidis
B. Fragilis
N. gonhoroeae
T. vaginalis
S. pneumoniae
F. nucleatum
F. necrophorum
Herpes Simplex Virus 1
Herpes Simplex Virus 2
U. ureliticum
C. suis
C. abortus
C. muriderum
C. trachomatis serovar C
C. trachomatis serovar D
C. trachomatis serovar E
C. trachomatis serovar F
C. trachomatis serovar G
C. trachomatis serovar J
C. trachomatis serovar B
C. trachomatis serovar L2
No-template control

Figure 6.7: Sensitivity and specificity panels for LAMP reagent.

A) Sensitivity of the LAMP assay tested using calcein indicator dye at various concentrations of synthetic target. Up to 10^3 copies of target could be consistently amplified with observable difference. **B**) Specificity of the LAMP assay tested using calcein indicator dye using genomic DNA extracts from endogenous and pathogenic vaginal flora. All vaginal C. trachomatis serovars amplified correctly; serovars B and C are associated with ocular infection. All genomic DNA samples tested were prepared at concentrations exceeding or equal to 10^5 copies/mL.

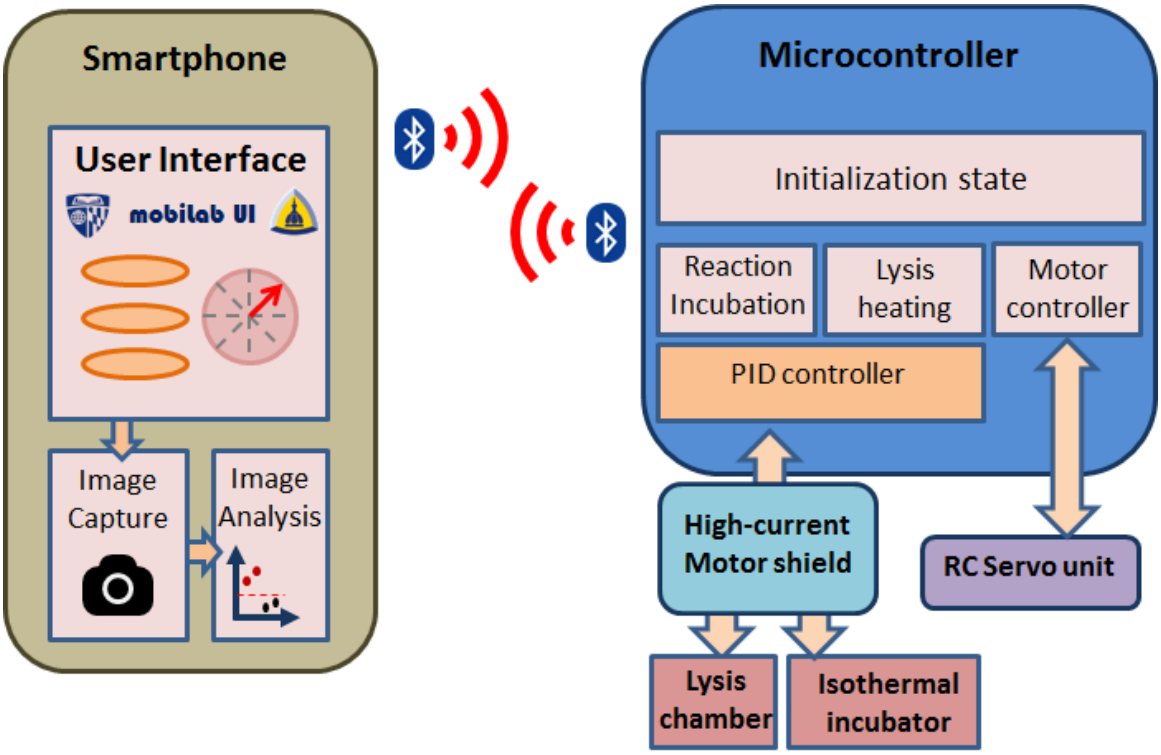
Smartphone
User Interface
mobilab UI
Image Capture
Image Analysis
Microcontroller
Initialization state
Reaction Incubation
Lysis heating
Motor controller
PID controller
High-current Motor shield
RC Servo unit
Lysis chamber
Isothermal incubator

Figure 6.8: Schematic of smartphone-microcontroller control software.

The control software is divided between two physical modules, represented by the smartphone and the microcontroller-embedded instrument. The smartphone application contains the user interface for controlling all stages of the assay. Peripheral devices such as the incubation heater and rotary manipulator are directly controlled by the microcontroller, which initiates routines for each device when prompted by the smartphone via Bluetooth-enabled serial communication. Meanwhile, the smartphone directly manages the image capture/analysis routine facilitated by its on-board CMOS sensor. The microcontroller is arranged as a finite state machine that switches between initialization state, lysis state, motor control state and amplification state. Motor control directly modulates RC servo unit via on-board analog output pins, while thermal control is achieved using a PID control subroutine and facilitated by a peripheral motor shield unit that allows delivery of up to 2A current to the thermoelectric elements.

(A)

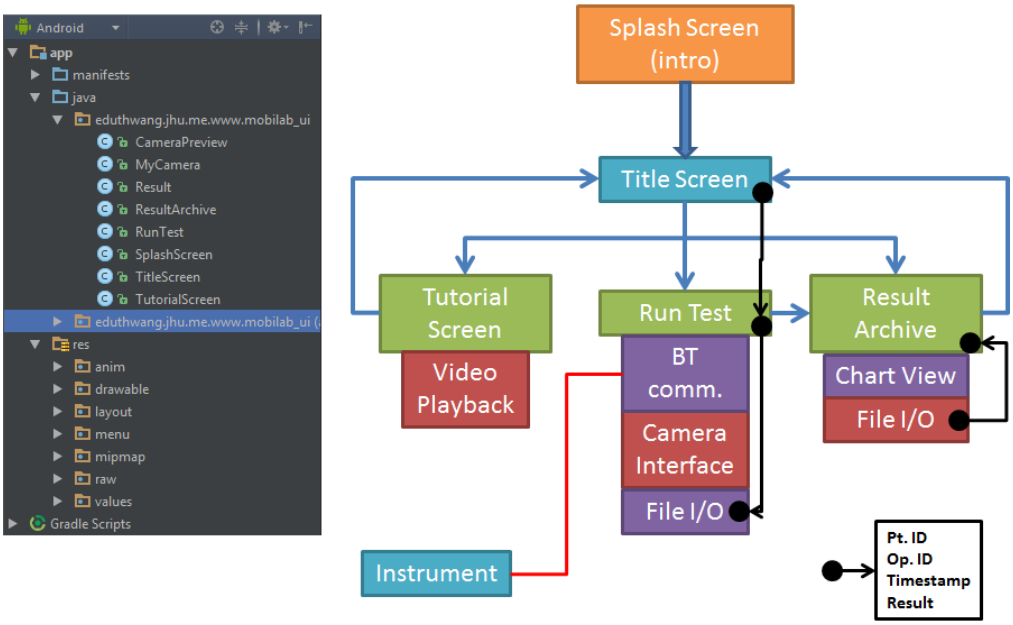
Android
app
manifests
java
eduthwang.jhu.me.www.mobilab_ui
CameraPreview
MyCamera
Result
ResultArchive
RunTest
SplashScreen
TitleScreen
TutorialScreen
eduthwang.jhu.me.www.mobilab_ui
res
anim
drawable
layout
menu
mipmap
raw
values
Gradle Scripts
Splash Screen (intro)
Title Screen
Tutorial Screen
Video Playback
Run Test
BT comm.
Camera Interface
File I/O
Result Archive
Chart View
File I/O
Instrument
Pt. ID
Op. ID
Timestamp
Result

(B)

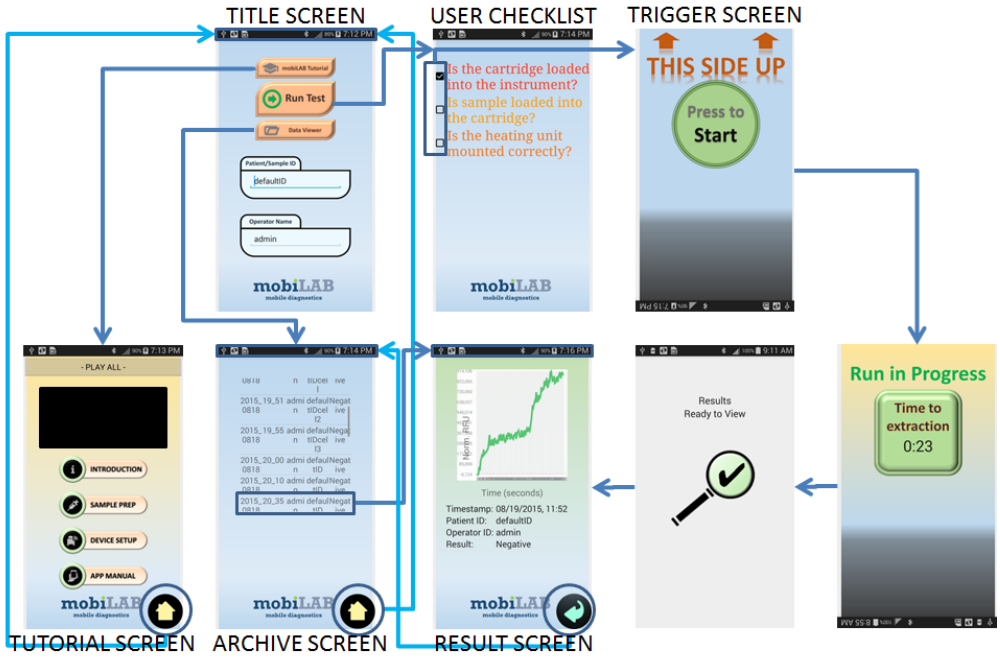
TITLE SCREEN
USER CHECKLIST
TRIGGER SCREEN
Run Test
Is the cartridge loaded into the instrument?
Is sample loaded into the cartridge?
Is the heating unit mounted correctly?
THIS SIDE UP
Press to Start
Run in Progress
Time to extraction
0:23
Results
Ready to View
- PLAY ALL -
INTRODUCTION
SAMPLE PREP
DEVICE SETUP
APP MANUAL
Time (seconds)
Timestamp: 08/19/2015, 11:52
Patient ID: defaultID
Operator ID: admin
Result: Negative
TUTORIAL SCREEN
ARCHIVE SCREEN
RESULT SCREEN

Figure 6.9: Smartphone user interface.

A) UI architecture. The UI consists of a central title screen, which allows the user to access 3 modes of operation: 1) tutorial screen, which facilitates playback of training videos; 2) run screen, which runs the assay; 3) result archive, which provides access to results obtained from previous runs; **B**) Screenshot of the smartphone user interface at various stages of assay progression.

(A)

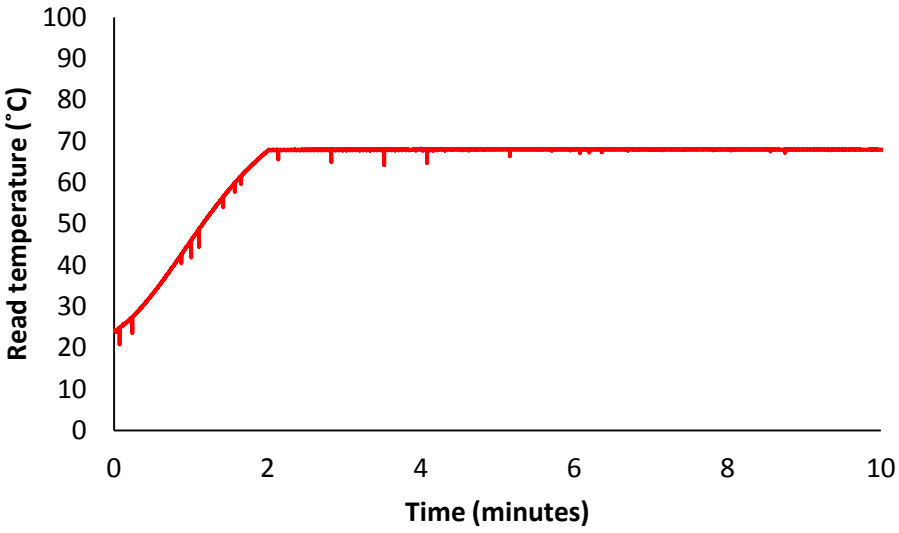
Read temperature (°C)
100
90
80
70
60
50
40
30
20
10
0
0
2
4
6
8
10
Time (minutes)

(B)

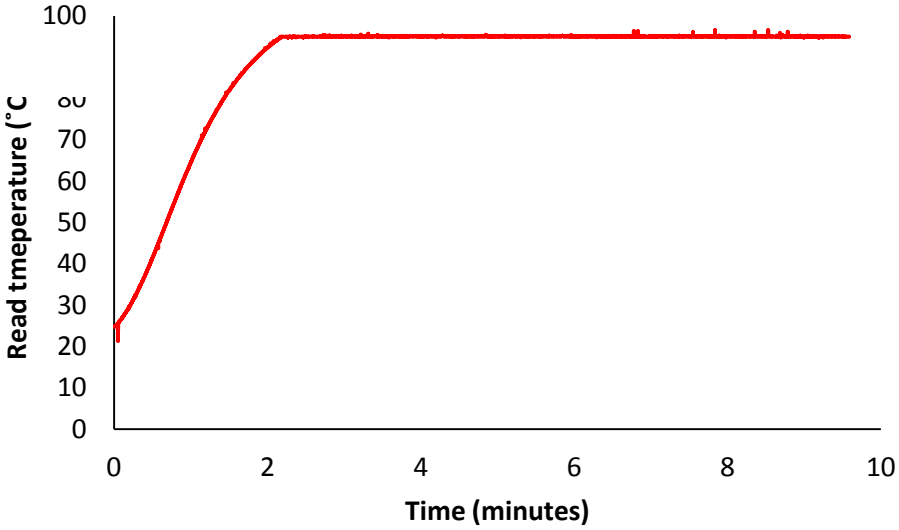
Read tmeperature (°C
100
80
70
60
50
40
30
20
10
0
0
2
4
6
8
10
Time (minutes)

Figure 6.10: Thermal incubator calibration.

Each temperature was calibrated using the following method. First, PID parameters (Kp, Kd and Ki) were modified until overshoot and oscillation were no longer observed with a rise time of about 2 minutes. Afterwards, a test device with thermistor in contact with the heated liquid was placed in contact with the incubator. Target temperature was modified until steady state targe temperature could be achieved by the heated liquid. **A**) Temperature profile for 65˚C incubation. With target temperature at 66 ˚C, the PID controller yielded a steady-state temperature reading at 68˚C, which corresponded to liquid temperature of 65~67˚C. **B**) Temperature profile for 95˚C incubation. With target temperature at 93 ˚C, the PID controller yielded a steady-state temperature reading at 95˚C, which corresponded to liquid temperature of 95~98˚C.

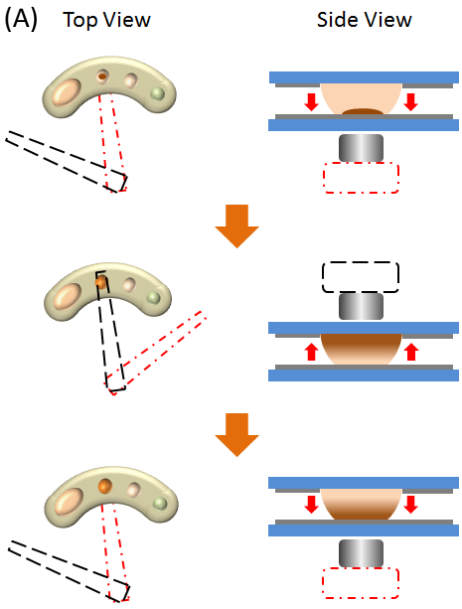
(A)
Top View
Side View

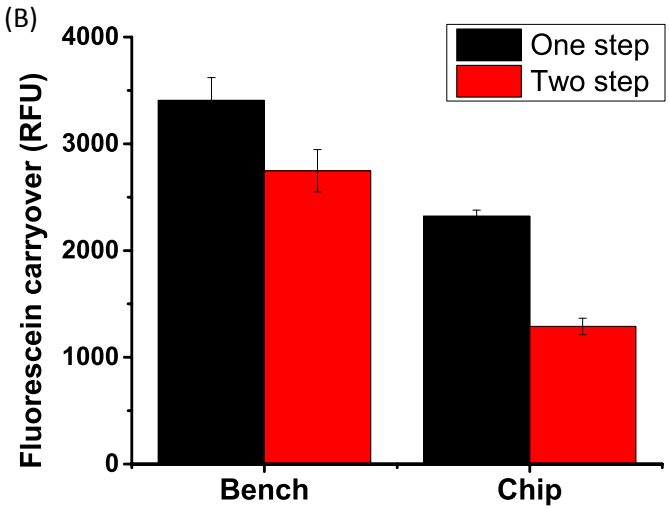
(B)
One step
Two step
Fluorescein carryover (RFU)
4000
3000
2000
1000
0
Bench
Chip

Figure 6.11: Bead washing mechanism and characterization.

A) Diagram describing washing mechanism. In order to facilitate efficient rinsing of magnetic beads and reduce the amount of buffer carried over with the bead plug at each step of the assay, the processing module utilized two magnetic spokes for mixing. Top (black dashed line) and bottom (red dashed line) spokes alternate in order to facilitate transversal motion of the magnetic beads. Magnetic field pulls beads across from one surface to the opposite surface (red block arrows), facilitating disintegration of bead plug into a plume as magnets alternate position. **B**) Characterization of bead rinsing on bench and droplet cartridge. Bead washing was characterized by introducing the organic dye fluorescein into the sample inlet and quantifying the presence of fluorescein at the reaction chamber. Each washing step added an aliquot of 25 μL wash buffer between the sample inlet and the reaction chamber. Reduced fluorescence intensity implies enhanced removal of excess fluid at each bead removal step. Increasing the number of wash steps enhanced carryover removal as expected. The cartridge displays enhanced performance over bench process, likely due to the benefit of minimizing surface area of residual buffer carried with bead plug when it is extracted into the oil phase. The bench process solely relies on aspiration via manual removal of previous buffer, which may result in considerable residual buffer remaining on the tube surface due to the wetting of the tube interior and the limited capacity of conventional pipettors for fluid removal.

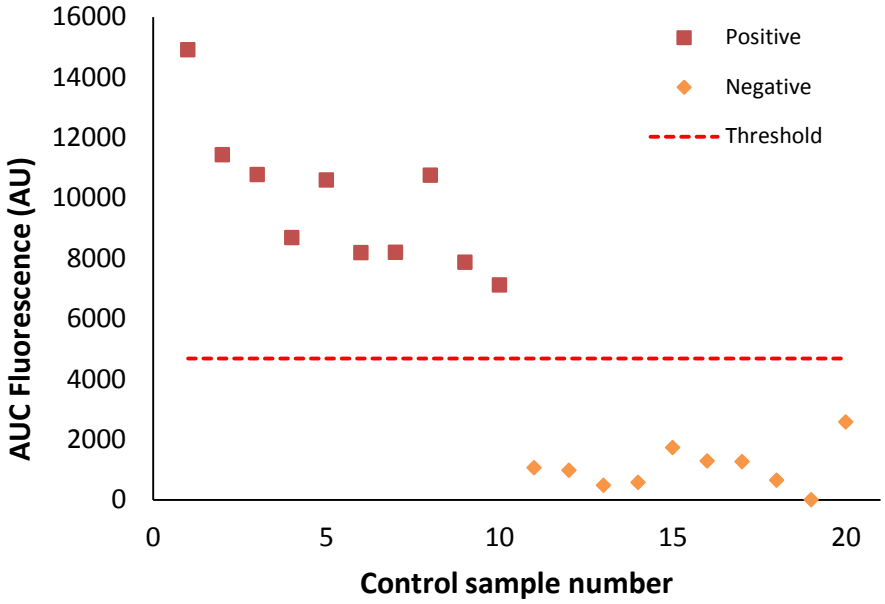
16000
14000
12000
10000
8000
6000
4000
2000
0
AUC Fluorescence (AU)
0
5
10
15
20
Control sample number
Positive
Negative
Threshold

Figure 6.12: Validation set using synthetic targets for clinical testing.

10 positive and 10 negative samples were used as a training set to establish threshold AUC fluorescence for classification. Threshold was initially defined as the average fluorescence level from negative samples + 5σ and verified to be sufficiently stringent to differentiate between positive and negative samples in the testing set.

(A)

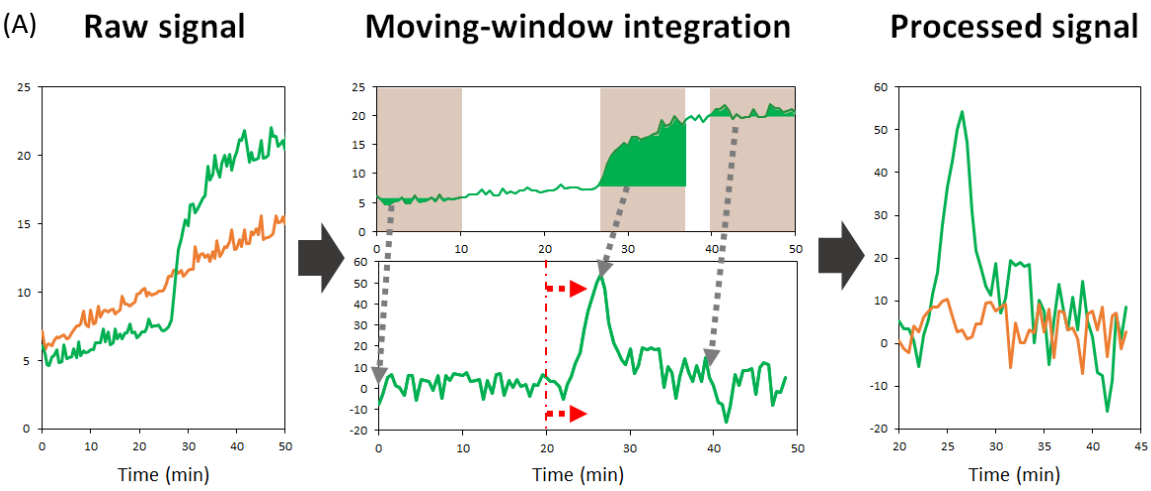
Raw signal
Moving-window integration
Processed signal
Time (min)
Time (min)
Time (min)

(B)

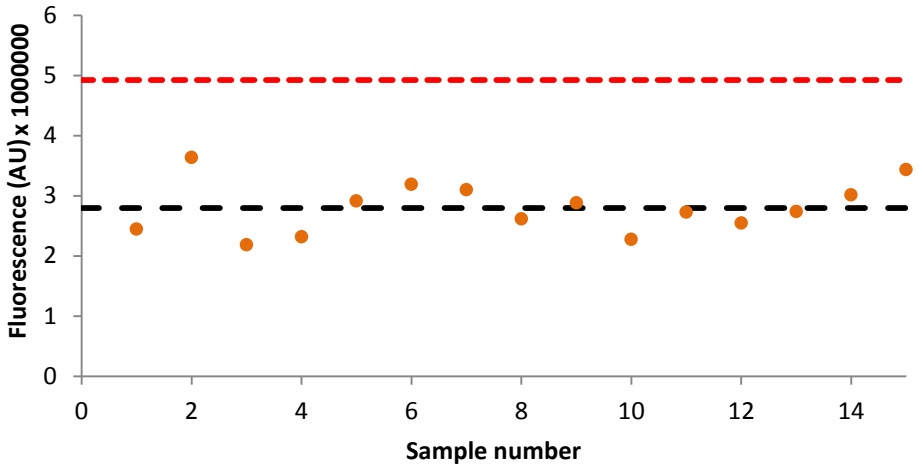
Fluorescence (AU) x 1000000
Sample number

Figure 6.13: Positivity algorithm based on time derivative signal.

A) Positivity algorithm on the field-tested prototype utilizes moving-window integration in order to detect sharp transitions in fluorescence observed during amplification. While endpoint detection based on raw signal can suffice in controlled environment, the differences between positive and negative samples may become obscured due to factors including ambient lighting condition and low levels of background fluorescence development during thermal incubation. In order to discard aberrant signal development at early stages of amplification, a time threshold was applied to process data following 20 minutes of incubation. **B**) Negative controls for field test. Threshold (red dashed) was set 5 standard deviations above average (black dashed).

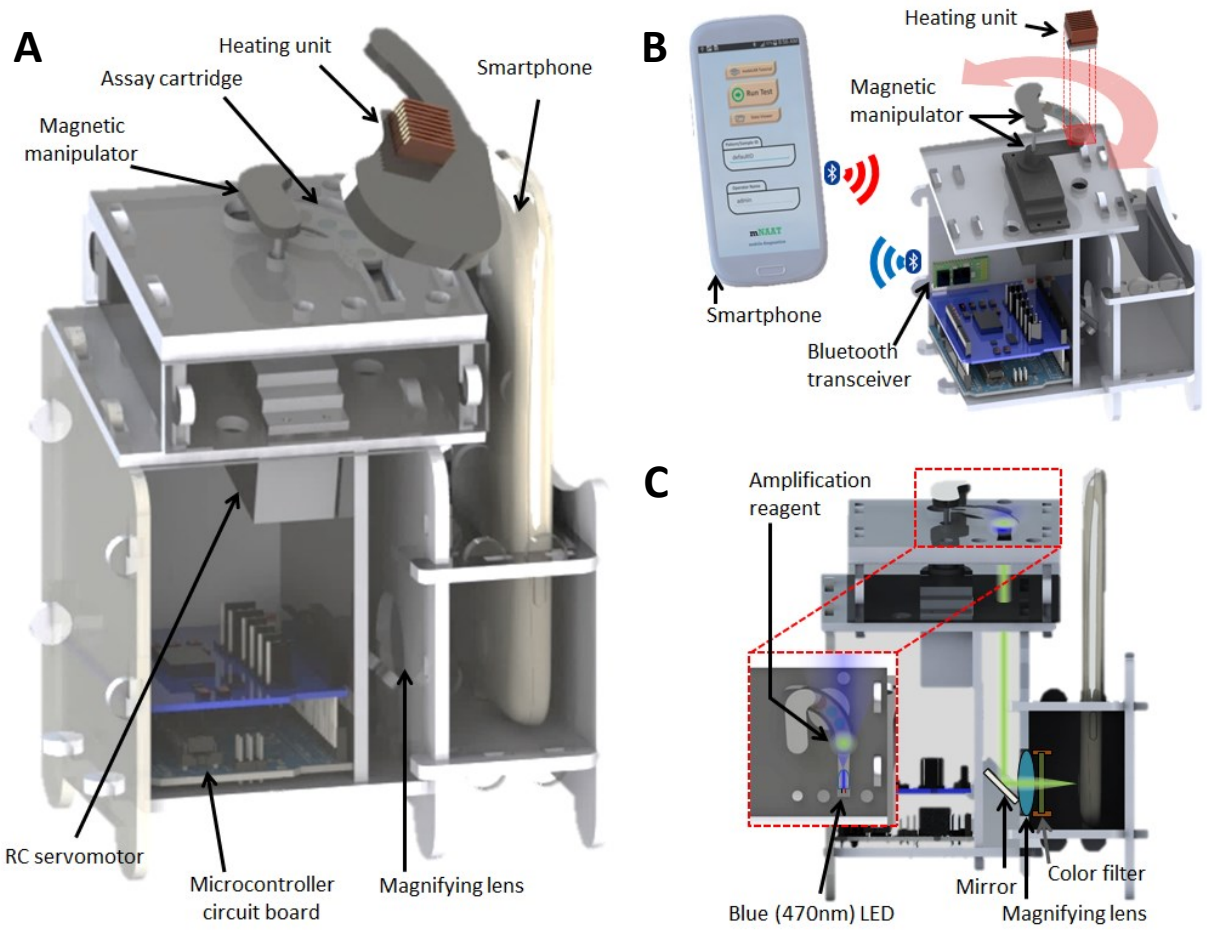
A
Heating unit
Assay cartridge
Magnetic manipulator
Smartphone
RC servomotor
Microcontroller circuit board
Magnifying lens
B
Heating unit
Magnetic manipulator
Smartphone
Bluetooth transceiver
C
Amplification reagent
Blue (470nm) LED
Mirror
Color filter
Magnifying lens

Figure 6.14: Cartridge processing instrument.

A) Overview of the cartridge processing module. The module consists of a microcontroller which controls rotary bead actuator and thermal incubation unit, overlaid with an optical component that relays the image from the reaction chamber to the smartphone camera. The smartphone operates in tandem with the module during optical data collection. **B**) Overview of the functional units in the processing module. An RC servomotor with two magnet-mounted spokes separated by 67˚ facilitates rotary actuation of magnetic particles on both surfaces of the cartridge, in addition to transverse motion for particle mixing in buffer. Thermal incubation is provided by a thermoelectric unit mounted directly in contact with the amplification chamber on the cartridge. An Arduino-based Bluetooth transceiver facilitates communication between the module and the smartphone user interface. **C**) Overview of the optical subsystem. LED is used as illumination source to excite the fluorescent indicator dye in the amplification reagent. Emission is filtered using a color filter, relayed via optical components and collected onto the smartphone camera docked to the side of the processing module.

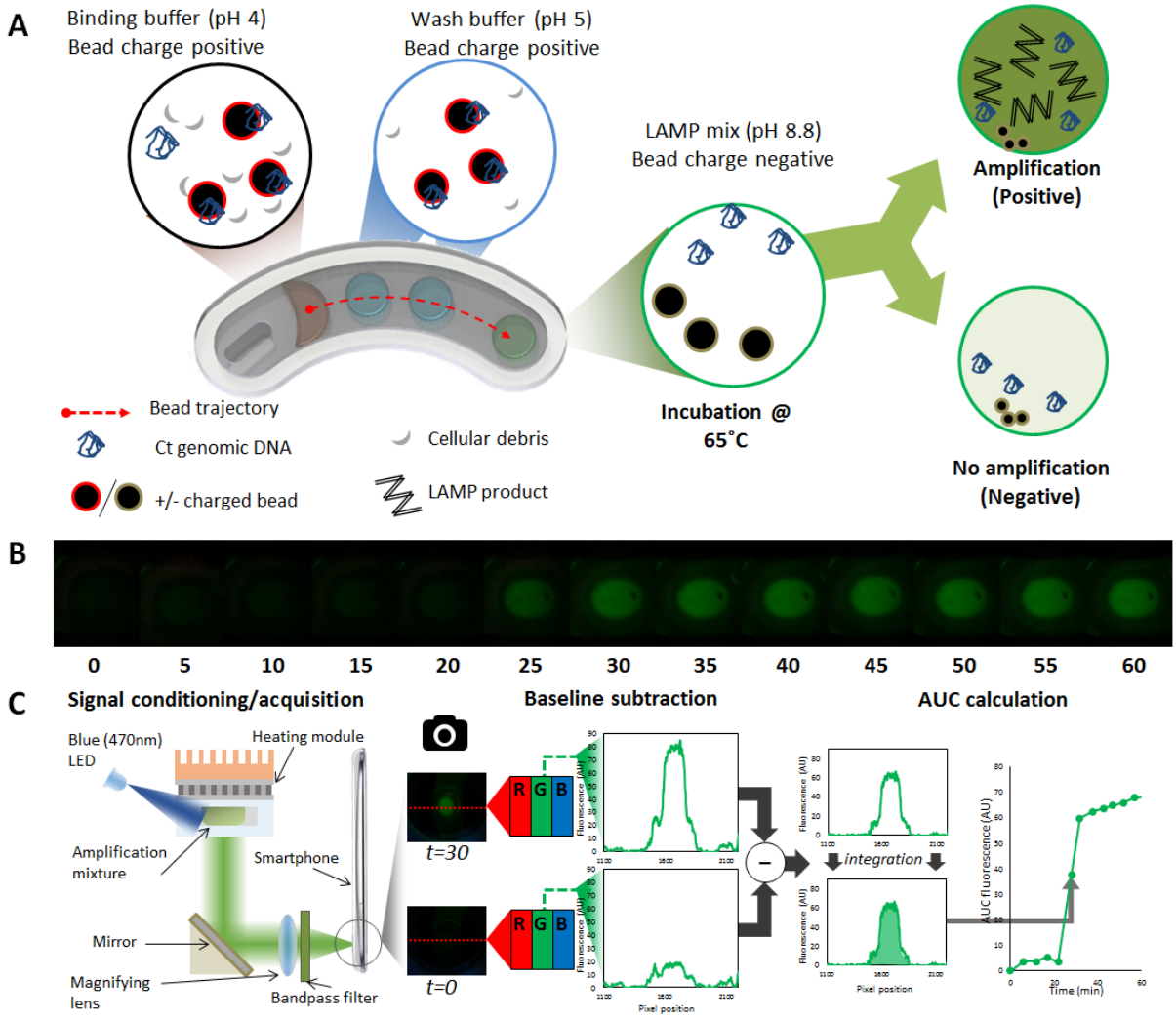
A
Binding buffer (pH 4)
Bead charge positive
Wash buffer (pH 5)
Bead charge positive
LAMP mix (pH 8.8)
Bead charge negative
Amplification
(Positive)
Incubation @
65˚C
No amplification
(Negative)
Bead trajectory
Ct genomic DNA
+/- charged bead
Cellular debris
LAMP product
B
0
5
10
15
20
25
30
35
40
45
50
55
60
C
Signal conditioning/acquisition
Baseline subtraction
AUC calculation
Blue (470nm)
LED
Heating module
Amplification
mixture
Smartphone
Mirror
Magnifying
lens
Bandpass filter
t=30
t=0
R
G
B
integration
Pixel position
Time (min)
AUC fluorescence (AU)

Figure 6.15: Assay design and data acquisition.

A) Schematic of single-stream LAMP assay as implemented on the mobiNAAT platform. Magnetic particles capture nucleic acid targets from sample lysate via electrostatic interaction. The affinity between particles and nucleic acids is maintained at acidic pH, which is reversed upon entry in LAMP amplification mixture facilitating elution. **B**) Image of fluorescence developing over time in a positive control reaction in droplet cartridge. **C**) Image processing algorithm on the smartphone. Initially, image is acquired at the start of the incubation (time = 0). Subsequent images are captured and segmented to extract information from a single row of pixels across the incubation chamber. Only the green value of the RGB data is used. Data acquired at each time point is normalized by subtracting segmented data from time = 0. Afterwards, the area under the resultant vector is integrated in order to yield a single value, which is either used for end-point analysis or plotted sequentially over time for real-time monitoring.

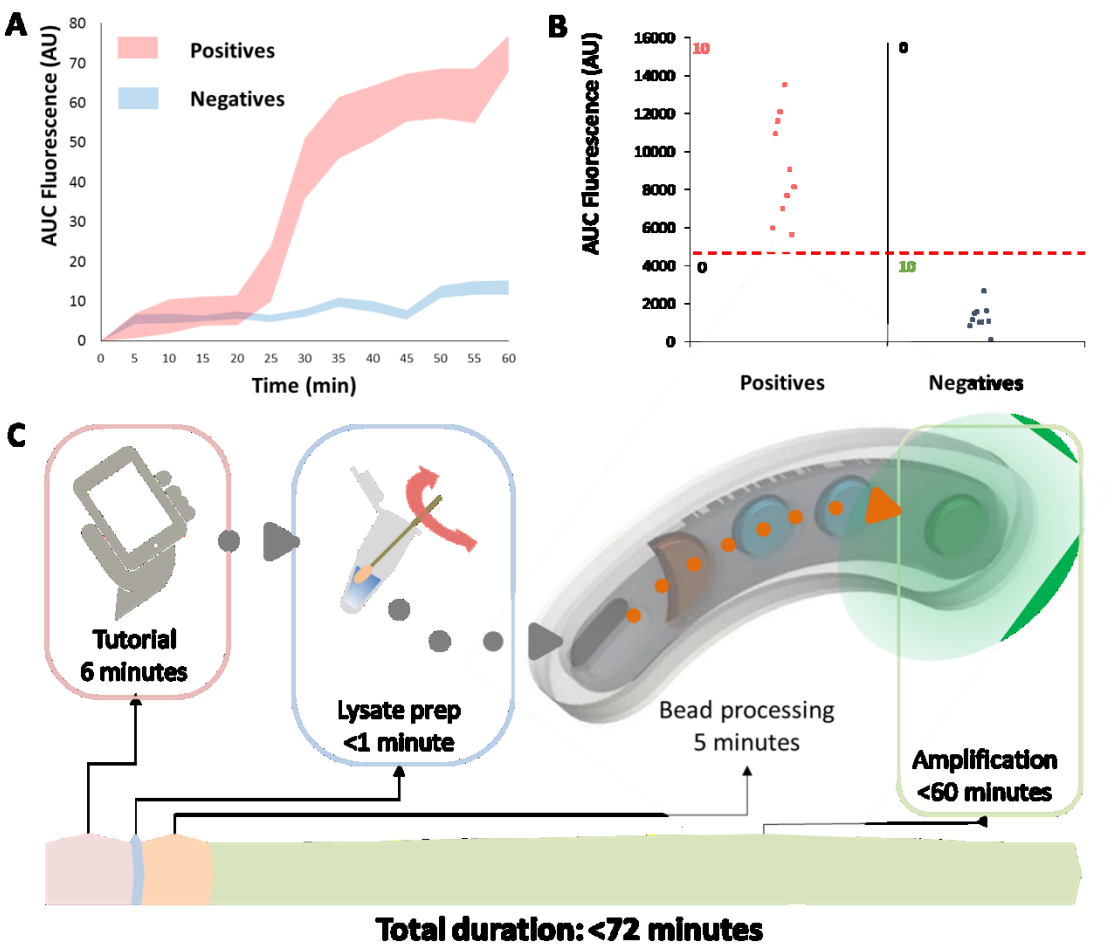
A
AUC Fluorescence (AU)
Positives
Negatives
Time (min)
B
AUC Fluorescence (AU)
Positives
Negatives
C
Tutorial
6 minutes
Lysate prep
<1 minute
Bead processing
5 minutes
Amplification
<60 minutes
Total duration: <72 minutes

Figure 6.16: Platform validation study.

A) Real-time monitoring of select deblinded clinical samples using time-lapse image acquisition. Positive samples show development of signal, and are clearly differentiated from signal developed by negative samples. Shaded areas represent upper and lower bounds of AUC fluorescence (n=3). **B**) Validation of mobiNAAT platform using blinded vaginal swab samples obtained from an equal number of chlamydia positive and negative individuals (n=20). AUC fluorescence levels of swab samples that are positive (blue) or negative (orange) are shown. Student's t-test performed with two-sample unequal variance and two-tailed distribution yields $p<0.00001$. Classification threshold (red dotted line) is established using signals obtained from a set of control samples (n=20) **(Fig. 6.12)**. **C**) Overview of the system workflow for a naïve operator. The training module (6 minutes total) included in the smartphone app trains a first-time user prior to operating the device. Following expression of swab in lysis medium, sample is loaded into the cartridge. The cartridge is loaded into the processing module, and the assay is initiated by the smartphone app. Following incubation for up to1 hour, signal is processed to determine whether the tested sample is positive or negative.

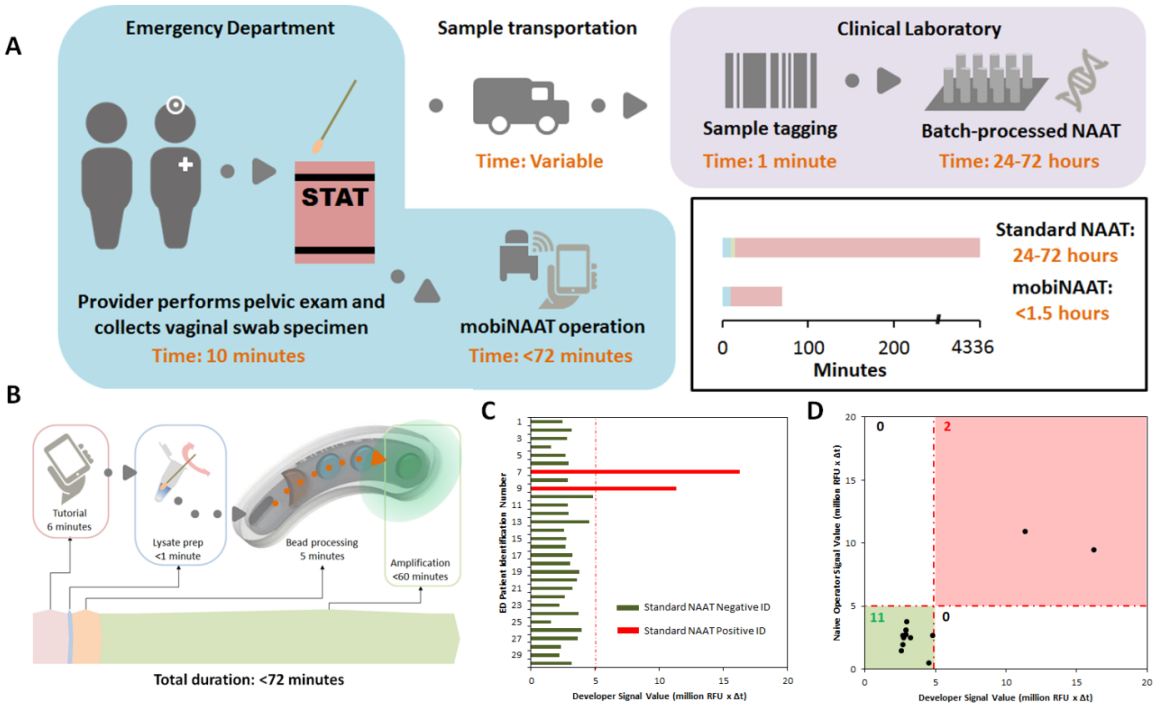
A
Emergency Department
STAT
Provider performs pelvic exam and collects vaginal swab specimen
Time: 10 minutes
Sample transportation
Time: Variable
mobiNAAT operation
Time: <72 minutes
Clinical Laboratory
Sample tagging
Time: 1 minute
Batch-processed NAAT
Time: 24-72 hours
Standard NAAT:
24-72 hours
mobiNAAT:
<1.5 hours
0
100
200
4336
Minutes
B
Tutorial
6 minutes
Lysate prep
<1 minute
Bead processing
5 minutes
Amplification
<60 minutes
Total duration: <72 minutes
C
ID Patient Identification Number
Standard NAAT Negative ID
Standard NAAT Positive ID
Developer Signal Value (million RFU x Δt)
D
Naïve Operator Signal Value (million RFU x Δt)
0
2
11
0
Developer Signal Value (million RFU x Δt)

Figure 6.17: Clinical validation of platform.

A) Comparison of standard and mobiNAAT workflow in the emergency room. In a standard workflow, vaginal swab acquired during a pelvic exam by the provider is collected by a study coordinator, who transports the sample to the microbiology laboratory. The sample is then batch processed, taking approximately 24 to 72 hours until the test result is made available on the electronic medical record accessible by the provider. In the mobiNAAT workflow, the test is performed directly in the emergency room, yielding result that can be reported in less than 1.5 hours following the pelvic exam. **B)** Overview of mobiNAAT workflow. The training module (6 minutes total) included in the smartphone app trains a first-time user prior to operating the device. Following expression of swab in lysis medium, sample is loaded into the cartridge. The cartridge is loaded into the processing module, and the assay is initiated by the smartphone app. Following incubation for up to1 hour, a report is generated based on the signal acquired during this period. **C)** Comparison of results obtained using the mobile diagnostic platform using clinical samples collected at the ED (n=30). Samples were tested in parallel using the Gen-Probe Aptima Combo 2 CT assay for verification (positives marked by red bars, negatives marked by green). Among all patient samples tested, two patients (ID 7 and 9) reported positive in the verification assay, in agreement with the result obtained using the mobiNAAT platform. **D**) Comparison of results obtained using mobiNAAT platform by the developers and a naïve operator trained using the smartphone app (n=13). Patients 5~17 were tested in parallel by a clinical staff member at the ED (green markers) and showed full correspondence with the results obtained by the developers (11 negative, 2 positive).

Conclusion

7.1 SUMMARY OF CONTRIBUTIONS

Our contribution to the field of droplet magnetofluidics based on the contents of this document is threefold. First, we successfully established the utility of droplet magnetofluidics by consolidating the idea of a single-stream assay, demonstrating its use in genetic and epigenetic applications. Next, we expanded our perspective to consider the requirements of the entire system for true point of care diagnostics, resulting in several key innovations in instrument and cartridge design. Lastly, we integrated droplet magnetofluidics with a smartphone interface in order make the transition from a research concept into an easy-to-use platform that could be deployed in a clinically relevant scenario.

7.2 FUTURE DIRECTIONS

The main hurdles in bringing open-surface droplet platforms to commercialization are twofold. The first is reagent storage and transport, which is a challenge shared by many other technologies developed for point-of-care diagnostics. Although many of the buffers containing salts and other soluble, inorganic substances may be kept at room temperature without degradation, fragile organic components such as enzymes may expire when stored outside a freezer. Enzymatic processes are indispensable as they are involved in both the sample preparation stage as well as signal amplification and detection stage. To overcome this challenge, various preservation strategies have been investigated to enhance the shelf life of enzymes [60]. An issue that remains at large is the modification of cartridge design to render it compatible with dry storage. As the magnetofluidic cartridge is operational only when its reagents are fully assembled in liquid droplets, it will likely require additional

cartridge components to isolate liquid components from dry reagents prior to reconstitution. Among the techniques described in literature, blister packs may be a possible strategy for liquid storage on cartridge [134].

The second challenge is miniaturization and power management of supporting instrumentation. While microfluidic cartridges themselves are generally small by design, the supporting instrumentation for operating the device is often overlooked in a laboratory testing environment. To this end, miniaturized components for various aspects of device operation have been reported. A miniaturized optical detector for fluorescence detection with sensitivity of 10^{-9} M fluorescein has been proposed by Novak *et al* [79] using light-emitting diodes as an illumination source and silicon photodiode as a detector. Similarly, miniaturization of actuation instruments has also been demonstrated by Shikida et al [12], utilizing a stepper motor to design a magnetic actuator in a palmtop-sized format. Planar electromagnetic coil actuation also lends itself to small form factor, although power requirements remain to be resolved.

A key strength of magnetic droplet-based techniques comes from the ability to translate workflow developed for tube-based benchtop assays in a miniaturized format without significant alterations to the assay mechanism. As the technology reaches maturity, magnetic droplet platforms may function as a portable replica of the benchtop environment that can dramatically shorten the development time required to translate a benchtop assay into a point-of-care format. As such, the utility of this technology is expected to expand in parallel with the growing repository of benchtop molecular diagnostic assays.

References

[1] Zeka, A. N.; Tasbakan, S.; Cavusoglu, C. *J. Clin. Microbiol.* 2011. 49(12): 4138-4141.

[2] Babady, N. E. *Expert Rev Mol Diagn.* 2013. 13(8): 779-88.

[3] Yetisen, A. K.; Akram, M. S.; Lowe, C. R. *Lab Chip* 2013. 13: 2210-2251.

[4] Gervais, L.; Hitzbleck, M.; Delamarche, E. *Biosens Bioelectron.* 2011. 27(1): 64-70.

[5] Hosokawa, K.; Omata, M.; Sato, K.; Maeda, M. *Lab Chip* 2006. 6: 236-241.

[6] Neuzil, P.; Pipper, J.; Hsieh, T. M. *Mol Biosyst.* 2006. 2(6-7):292-8.

[7] Shikida, M.; Takayanagi, K.; Inouchi, K.; Honda, H.; Sato, K. *Sens. Actuators B Chem.* 2006. 113(1): 563-569.

[8] Rida, A.; Fernandez, V.; Gijs, M. A. M. *Appl. Phys. Lett.* 2003. 83(12): 2396.

[9] Lehmann, U.; Vandevyver, C.; Parashar, V. K.; Gijs, M. A. M. *Angew. Chem. Int. Ed.* 2006. 45(19): 3062-3067.

[10] Pipper, J.; Inoue, M.; Ng, L. F-P.; Neuzil, P.; Zhang, Y.; Novak, L. *Nat. Med.* 2007. 13(10): 1259-1263.

[11] Tsuchiya, H.; Okochi, M; Nagao, N.; Shikida, M.; Honda, H. Sens. Actuators B Chem. 2008. 130(2): 583-588.

[12] Shikida, M.; Nagao, N.; Imai, R.; Honda, H.; Okochi, M.; Ito, H.; Sato, K. *J Micromech Microeng.* 2008. 18: 35034-35041.

[13] Pipper, J.; Zhang, Y.; Neuzil, P.; Hsieh, T. M. *Angew. Chem. Int. Ed.* 2008. 47(21): 3900-3904.

[14] Zhang, Y.; Park, S.; Liu, K.; Tsuan, J.; Yang, S.; Wang, T. H. *Lab Chip* 2011. 11(3): 398-406.

[15] Berry, S. M.; Alarid, E. T.; Beebe, D. J. *Lab Chip*. 2011. 11(10):1747-53.

[16] Ali-Cherif, A.; Begolo, S.; Descroix, S.; Viovy, J-L.; Malaquin, L. *Angew. Chem. Int. Ed.* 2012. 51(43): 10765-10769.

[17] Chiou, C. H.; Shin, D. J.; Zhang, Y.; Wang, T. H. *Biosens Bioelectron.* 2013. 50: 91-99.

[18] Zhang, Y.; Wang, T. H. *Adv Mater.* 2013. 25: 2903-2908.

[19] Zhang, Y.; Shin, D. J.; Wang, T. H. *Lab Chip* 2013. 13: 4827-4831.

[20] Long, Z. C.; Shetty, A. M.; Solomon, M. J.; Larson, R. G. *Lab Chip* 2009. 9(11): 1567-1575.

[21] Ohashi, T.; Kuyama, H.; Hanafusa, N.; Togawa, Y. *Biomed Microdevices* 2007. 9: 695-702.

[22] Zhang, Y.; Park, S.; Yang, S.; Wang, T. H. *Biomed Microdevices* 2010. 12(6): 1043-1049.

[23] Velev, O. D.; Prevo, B.G.; Bhatt, K.H. *Nature* 2003. 426(6966): 515-6.

[24] Hunt, T. P.; Issadore, D.; Westervelt, R. M. *Lab Chip* 2008. 8(1): 81-7.

[25] Fan, S. K.; Hsieh, T. H.; Lin, D. Y. *Lab Chip* 2009. 9(9): 1236-42.

[26] Boles, D. J.; Benton, J. L.; Siew, G. J.; Levy, M. H.; Thwar, P. K.; Sandahl, M. A.; Rouse, J. L.; Perkins, L. C.; Sudarsan, A. P.; Jalili, R.; Pamula, V. K.; Srinivasan, V.; Fair, R. B.; Griffin, P. G.; Eckhardt, A. E.; Pollack, M. G. *Anal Chem.* 2011. 83(22): 8439-47.

[27] Pollack, M. G.; Pamula, V. K.; Srinivasan, V.; Eckhardt, A. E. *Expert Rev Mol Diagn.* 2011. 11(4): 393-407.

[28] Sista, R.; Hua, Z.; Sudarsan, A.; Srinivasan, V.; Eckhardt, A.; Pollack, M. G.; Pamula, V. K. *Lab Chip* 2008. 8(12): 2091-104.

[29] Srinivasan, V.; Pamula, V. K.; Fair, R.B. *Lab Chip* 2004. 4(4): 310-5.

[30] Welch, E. R.; Lin, Y. Y.; Madison, A.; Fair, R.B. *Biotechnol J.* 2011. 6(2): 165-76.

[31] Lu, H. W.; Bottausci ,F.; Fowler, J. D.; Bertozzi, A. L.; Meinhart, C.; Kim, C. J. *Lab Chip* 2008. 8: 456-461.

[32] Hua, Z. S.; Rouse, J. L.; Eckhardt, A. E.; Srinivasan, V.; Pamula, V. K.; Schell, W. A.; Benton, J. L.; Mitchell, T. G.; Pollack, M. G. *Anal. Chem.* 2010. 82: 2310-2316.

[33] Thery, J.; Borella, M.; Le Vot, S.; Jary, D.; Rivera, F.; Castellan, G.; Brachet, A.G.; Plissonnier, M.; Fouillet, Y. Proceedings of μTas 2007 conference, vol. 1, pp. 349–351

[34] Dhindsa, M.; Kuiper, S.; Heikenfeld. J. *Thin Solid Films* 2011. 519: 3346-3351.

[35] Chiou, P. Y.; Moon, H.; Toshiyoshi, H.; Kim, C. J.; Wu, M. C. *Sens. Actuators A Phys.* 2003. 104(3): 222-28.

[36] Park, S. Y.; Kalim, S.; Callahan, C.; Teitell, M. A.; Chiou, P. Y. *Lab Chip.* 2009. 9(22): 3228-35.

[37] Inagaki, N.; Narushim, K.; Tuchida, N.; Miyazaki, K.; *J. Polym. Sci. Part B* 2004. 42: 3727

[38] Shevkoplyas, S. S.; Siegel, A. C.; Westervelt, R. M.; Prentiss, M. G.; Whitesides, G. M. *Lab Chip* 2007. 7(10): 1294-1302.

[39] Tsiatis AC, Norris-Kirby A, Rich RG, Hafez MJ, Gocke Cd, Eshleman JR, Murphy KM (2010) J Mol Diagn 12(4): 425-432.

[40] Wittwer CT (2009) Hum Mutat 30(6): 857-9.

[41] Wittwer CT, Reed GH, Gundry CN, Vanderstenn JG, Pryor RJ (2003) Clin Chem 49(6): 853-860.

[42] Wu DY, Ugozzoli L, Pal BK, Wallace RB (1989) Proc Natl Acad Sci USA 86(8): 2757-2760.

[43] Saiki RK, Chang CA, Levenson CH, Warren TC, Boehm CD, Kazazian HH, Erlich HA (1988) N Engl J Med 319: 537-541.

[46] Palais R, Wittwer CT (2009) Chapter 13 Mathematical Algorithms for High-Resolution DNA Melting Analysis. In: Johnson ML, Brand L, (ed), Methods in Enzymology, vol 454. Academic Press 323-343.

[47] Melzak KA, Sherwood CS, Turner RFB, Haynes CA (1996) J Colloid Interface Sci 181: 635-644.

[48] Griffiths-Chu S, Patterson JA, Berger CL, Edelson RL, Chu AC (1984) Blood 64(1): 296-300.

[49] Ho CL, Kurman RJ, Dehari R, Wang T, Shih IM (2004) Cancer Res 64(19): 6915-6918.

[50] Wittwer CT, Reed GH, Gundry CN, Vandersteen JG, Pryor RJ (2003) Clin Chem 49(6 Pt 1): 853-860.

[51] Ohlander A, Zillo C, Hammerle T, Zelenin S, Klink G, Chiari M, Bock K, Russom A (2013) Lab Chip 13: 2075-2082.

[52] A. P. Bird, Nature 321, 209 (1985).

[53] J. G. Herman, F. Latif, Y. Weng, M. I. Lerman, B. Zbar, S. Liu, D. Samid, D. S. Duan, J. R. Gnarra, and W. M. Linehan, Proc. Natl. Acad. Sci. U. S. A. 91, 9700 (1994).

[54] J. G. Herman and S. B. Baylin, N. Engl. J. Med. 349, 2042 (2003).

[55] A. Merlo, J. G. Herman, L. Mao, D. J. Lee, E. Gabrielson, P. C. Burger, S. B. Baylin, and D. Sidransky, Nat. Med. 1, 686 (1995).

[56] M. Frommer, L. E. McDonald, D. S. Millar, C. M. Collis, F. Watt, G. W. Grigg, P. L. Molloy, and C. L. Paul, Proc. Natl. Acad. Sci. U. S. A. 89, 1827 (1992).

[57] B. Keeley, A. Stark, T. R. Pisanic, R. Kwak, Y. Zhang, J. Wrangle, S. B. Baylin, J. G. Herman, N. Ahuja, M. V. Brock, and T.-H. Wang, Clin. Chim. Acta 425, 169 (2013).

[58] C. A. Eads, K. D. Danenberg, K. Kawakami, L. B. Saltz, C. Blake, D. Shibata, P. V Danenberg, and P. W. Laird, Nucleic Acids Res. 28, e32 (2000).

[59] V. J. Bailey, Y. Zhang, B. P. Keeley, C. Yin, K. L. Pelosky, M. V. Brock, S. B. Baylin, J. G. Herman, and T.-H. Wang, Clin. Chem. 56, 1022 (2010).

[60] R. Mori, Q. Wang, D. Kd, P. Jk, and D. Pv, Prostate 380, 1 (2008).

[61] S. A. Bustin, V. Benes, J. a Garson, J. Hellemans, J. Huggett, M. Kubista, R. Mueller, T. Nolan, M. W. Pfaffl, Clin Chem. 2009 Apr;55(4):611-22.

[62] D. Svec, A. Tichopad, V. Novosadova, M. W. Pfaffl, and M. Kubista, Biomol. Detect. Quantif. 3, 9 (2015).

[63] J. M. Yi, A. a. Guzzetta, V. J. Bailey, S. R. Downing, L. Van Neste, K. B. Chiappinelli, B. P. Keeley, A. Stark, A. Herrera, C. Wolfgang, E. P. Pappou, C. a. Iacobuzio-Donahue, M. G. Goggins, J. G. Herman, T.-H. Wang, S.

[64] C. Spits, C. Le Caignec, M. De Rycke, L. Van Haute, A. Van Steirteghem, I. Liebaers, and K. Sermon, Nat. Protoc. 1, 1965 (2006).

[65] Peeling R. W. et al. Rapid tests for sexually transmitted infections (STIs): the way forward, Sex Transm Infect. 2006;82(suppl 5):v1Yv6. Sex Transm Infect 2006;82:v1-v6.2005).

[66] Beyzavi, A.; Nguyen, N. T. *J. Phys. D: Appl. Phys.* 2009. 42(1): 015004.

[67] Chau, A.; Rignier, S.; Delchambre, A.; Lambert, P. *Modelling Simul. Mater. Sci. Eng.* 2007. 15(3): 305-317.

[68] Wilson, I. G. *Appl. Environ. Micobiol.* 1997. 63(10): 3741-3751.

[69] Angione, S. L.; Chauhan, A.; Tripathi, *Anal Chem.* 2012. 84(6): 2654-61.

[70] Xiang, Q.; Xu, B.; Fu, R.; Li, D. Biomed. Microdevices 2005. 7(4): 273-279.

[71] Kopp, M. U.; de Mello, A. J.; Manz, A. Science 1998. 280(5366): 1046-1048.

[72] Hashimoto, M.; Chen, P. C.; Mitchell, M. W.; Nikitopoulos, D. E.; Soper, S. A.; Murphy, M. C. Lab Chip. 2004. 4: 638-645.

[73] Liu, J.; Enzelberger, M.; Quake, S. Electrophoresis 2002. 23: 1531-1536.

[74] Burns, M. A.; Johnson, B. N.; Brahmasandra, S. N.; Handique, K.; Webster, J. R.; Krishnan, M.; Sammarco, T. S.; Man, P. M.; Jones, D.; Heldsinger, D.; Mastrangelo, C. H.; Burke, D. T. Science 1998. 282(5388): 484-487.

[75] Legendre, L. A.; Bienvenue, J. M.; Roper, M. G.; Ferrance, J. P.; Landers, J. P. *Anal. Chem.* 2006. 78(5): 1444-1451.

[76] Huhmer, A. F. R.; Landers, J. P. *Anal Chem.* 2000. 72: 5507–12.

[77] Issadore, D.; Humphry, K. J., Brown, K. A.; Sandberg, L.; Weitz, D. A.; Westervelt, R. M. *Lab Chip* 2009. 9: 1701–6.

[78] Athamanolap, P.; Shin, D. J.; Wang, T. H. *J Lab Autom.* 2013. Oct 10. 2211068213507923

[79] Novak, L.; Neuzil, P.; Pipper, J.; Zhang, Y.; Lee, S. Lab Chip 2007. 7: 27-29.

[80] S.K. Vashik et al., A smartphone-based colorimetric reader for bioanalytical applications using the screen-based bottom illumination provided by gadgets. Biosens Bioelectron. 2015 May 15; 67:248-55.

[81] D. A. Selck et al., Increased robustness of single-molecule counting with microfluidics, digital isothermal amplification, and a mobile phone versus real-time kinetic measurements. Anal Chem. 2013 Nov 19;85(22):11129-36.

[82] Vogelstein, B.; Gillespie, D. Proc Natl Acad Sci USA. 1979. 76: 615–619.

[83] C. Schrader et al., J Appl Microbiol. 2012 Nov; 113(5):1014-26.

[84] M. J. Baker, inventor; Invitrogen Corporation, assignee. Isolation of nucleic acids. US Patent App. 12/137,125, 2008.

[85] T. Moretti et al., Enhancement of PCR amplification yield and specificity using AmpliTaq Gold DNA polymerase. Biotechniques. 1998 Oct; 25(4):716-22.

[86] N. J. Parham et al., Specific magnetic bead-based capture of genomic DNA from clinical samples: application to the detection of group B streptococci in vaginal/anal swabs. Clin Chem. 2007. 53(9): 1570-1576.

[87] J. Chen et al., Design of embedded chimeric peptide nucleic acids that efficiently enter and accurately reactivate gene expression in vivo. Proc. Natl. Acad. Sci. U. S. A. 2010. 107 (39): 16846-16851.

[88] N. Jacobsen et al., Direct isolation of poly(A)+ RNA from 4 M guanidine thiocyanate-lysed cell extracts using locked nucleic acid-oligo(T) capture. Nucleic Acids Res. 2004 Apr 19;32(7):e64.

[89] M. Wielscher et al., Methyl-biding domain protein-based DNA isolation from human blood serum combines DNA anylses and serum-autoantibody testing. BMC Clin Pathol. 2011; 11:11

[90] A. B. Robertson et al., Nature Protocols. 2012, 7, 340-350

[91] Saiki, R.; Gelfand, D.; Stoffel, S.; Scharf, S.; Higuchi, R.; Horn, G.; Mullis, K.; Erlich, H. (1988). "Primer-directed enzymatic amplification of DNA with a thermostable DNA polymerase". Science 239 (4839): 487–491.

[92] J. A. Garson et al., Lancet. 1990. 335 (8703): 1419-1422.

[93] J. G. Herman, J. R. Graff, S. Myöhänen, B. D. Nelkin, and S. B. Baylin, Proc. Natl. Acad. Sci. U. S. A. 93, 9821 (1996).

[94] J. S. Chamberlain et al., Nucleic Acids Res. 1988 Dec 9; 16(23): 11141–11156.

[95] World Health Organization. WHO monitoring of Xpert MTB/RIF roll-out. Accessed November 29, 2013 http://who.int/tb/laboratory/mtbrifrollout/en/

[96] Z Zhang et al., Direct DNA Amplification from Crude Clinical Samples Using a PCR Enhancer Cocktail and Novel Mutants of Taq. J Mol Diagn. 2010 Mar; 12(2): 152–161.

[97] L. Yan et al., Isothermal amplified detection of DNA and RNA. Mol. BioSyst., 2014, 10, 970-1003.

[98] E. Tan et al., Specific versus nonspecific isothermal DNA amplification through thermophilic polymerase and nicking enzyme activities. Biochemistry. 2008 Sep 23;47(38):9987-99.

[99] H. Gudnason et al., Comparison of multiple DNA dyes for real-time PCR: effects of dye concentration and sequence composition on DNA amplification and melting temperature. Nucleic Acids Res. 2007 Oct; 35(19): e127.

[100] E. Navarro et al., Real-time PCR detection chemistry. Clin Chim Acta. 2015 Jan 15;439:231-50.

[101] Goto, M. et al. Colorimetric detection of loop-mediated isothermal amplification reaction by using hydroxyl naphthol blue, Biotechniques. 46 (3): 167-172 (2009).

[102] M. A. Almasi et al., Visual detection of Potato Leafroll virus by loop-mediated isothermal amplification of DNA with the GeneFinder™ dye. J Virol Methods. 2013 Sep;192(1-2):51-4.

[103] Q. Wang et al., An enzyme-free colorimetric assay using hybridization chain reaction amplification and split aptamers. Analyst, 2015,140, 7657-7662.

[104] Owusu-Edusei Jr, K. et al. The estimated direct medical cost of selected sexually transmitted infections in the United States, 2008, Sex Transm Dis. 40 (13), (2013).

[105] Walsh, C. et al. Observations from the CDC: The Silent Epidemic of Chlamydia trachomatis: The Urgent Need for Detection and Treatment in Women, Journal of Women's Health & Gender-Based Medicine. May 2000, 9(4): 339-343.

[106] Cunningham, S. D. et al, Relationships between perceived STD-related stigma, STD-related shame and STD screening among a household sample of adolescents, Perspect Sex Reprod Health. 41(4): 225-230 (2009).

[107] Centers for Disease Control and Prevention. Sexually transmitted diseases treatment guidelines, 2010 MMWR Morb Mortal Wkly Rep. 2010; No.59(RR-12):1-110. Erratum in: MMWR Recomm Rep. 2011;60(1):18.

[108] Howick, J. et al. Current and future use of point-of-care tests in primary care: an international survey in Australia, Belgium, the Netherlands, the UK and the USA, BMJ Open 4, e005611 (2014).

[109] Hui, B. B. et al. The potential impact of new generation molecular point-of-care tests on gonorrhea and chlamydia in a setting of high endemic prevalence, Sex Health. 10 (4): 348-356 (2013).

[110] Van Dommelen, L. et al. Alarmingly poor performance in Chlamydia trachomatis point-of-care testing, Sex Transm Infect. 86 (5): 355-359 (2010).

[111] Van der Helm, J. J. et al. Point-of-care test for detection of urogenital chlamydia in women shows low sensitivity. A performance evaluation study in two clinics in Suriname, PLoS One. 7 (2): e32122 (2012).

[112] Michel, C. E. et al. Pitfalls of internet-accessible diagnostic tests: inadequate performance of a CE-marked Chlamydia test for home use, Sex Transm Infect. 85 (3): 187-189 (2009).

[113] Brook G. The performance of non-NAAT point-of-care (POC) tests and rapid NAAT tests for chlamydia and gonorrhoea infections. An assessment of currently available assays, Sex Transm Infect 2015 May 2. pii: sextrans-2014-051997. doi: 10.1136/sextrans-2014-051997.

[114] Hsieh, Y-H. et al. What qualities are most important to making a point of care test desirable or clinicians and others offering sexually transmitted infection testing? PLoS One. 6 (4): e19263 (2011).

[115] Hsieh, Y-H. et al. Perceptions on point-of-care tests for sexually transmitted infections: comparison between frontline clinicians and professionals in industry, Point of Care. 11 (2): 126-129.

[116] Huang, W. et al. Comparative effectiveness of a rapid point-of-care test for detection of Chlamydia trachomatis among women in a clinical setting, Sex Transm Infect. 89 (2): 108-114 (2013).

[117] Mundanyali, O. et al. Compact, light-weight and cost-effective microscope based on lensless incoherent holography for telemedicine applications, Lab Chip. 10(11), 1417-1428 (2010).

[118] Shen, L., Hagen, J. A. & Papautsky, I. Point-of-care colorimetric detection with a smartphone, Lab Chip. 12 (21), 4240-4243 (2012).

[119] Connelly, J. T. et al. “Paper machine” for molecular diagnostics, Anal Chem. 87 (15): 7595-7601 (2015).

[120] Losa-Igelsias, M. E., Becerro-de-Bengoa-Vallejo, R. & Becerro-de-Bengoa-Losa, K. R. Reliability and concurrent validity of a peripheral pulse oximeter and health-app system for the quantification of heart rate in healthy adults, Health Informatics J. July 18. pii: 1460458214540909 (2014).

[121] Wu, R. A smartphone-enabled communication system to improve hospital communication: Usage and perceptions of medical trainees and nurses on general internal medicine wards, J Hosp Med. Oct 29. doi: 10.1002/jhm.2278. (2014).

[122] Payne, K. B., Wharrad, H. & Watts, K. Smartphone and medical related App use among medical students and junior doctors in the United Kingdon (UK): a regional survey, BMC Med Inform Decis Mak. 12:121 (2012)

[123] Bellina, L. & Missoni, E. Mobile cell-phones (M-phones) in telemicroscopy: increasing connectivity of isolated laboratories, Diagn Pathol. 4:19 (2009).

[124] Laksanasopin, T. et al. A smartphone dongle for diagnosis of infectious diseases at the point of care, Sci Transl Med. 7 (273): 273re1 (2015).

[125] Notomi, T. et al. Loop-mediated isothermal amplification of DNA, Nucleic Acids Res. 28 (12): E63 (2000).

[126] Tomita, N. et al. Loop-mediated isothermal amplification (LAMP) of gene sequences and simple visual detection of products, Nat Protoc. 3(5): 877-882 (2008).

[127] Van Dyck, E. et al. Detection of Chlamydia trachomatis and Neisseria gonorrhoeae by Enzyme Immunoassay, Culture, and Three Nucleic Acid Amplification Tests, J. Clin Microbiol. 39 (5): 1751-1756.

[128] Wiggins, R. et al. Real-time quantitative PCR to determine Chlamydial load in men and women in a community setting, J Clin Microbiol. 47 (6): 1824-1829 (2009).

[129] Gift T. L. et al. The rapid test paradox: When fewer cases detected lead to more cases treated, a decision analysis of tests for Chlamydia trachomatis, Sex Transm Dis 1999;26:232-240

[130] Mori, Y. et al. Real-time turbidimetry of LAMP reaction for quantifying template DNA, J Biochem Biophys Methods. 59 (2): 145-157 (2004).

[131] Wei, X. et al. Viral dynamics in human immunodeficiency virus type 1 infection, Nature. 373 (6510): 117-122 (1995).

[132] Zhao, Y. et al. Rapid real-time nucleic acid sequence-based amplification-molecular beacon platform to detect fungal and bacterial bloodstream infections, J Clin Microbiol. 47 (7): 2067-2078 (2009).

[133] Yang, S. et al. Rapid identification of biothreat and other clinically relevant bacterial species by use of universal PCR coupled with high-resolution melting analysis, J Clin Microbiol. 47 (7): 2252-2255 (2009).

[134] A. Disch et al., Low cost production of disposable microfluidics by blister packaging technology. Conf Proc IEEE Eng Med Biol Soc. 2007; 2007:6323-6.

Curriculum Vitae

DONG JIN SHIN

Email: shin.dongjin@gmail.com
Tel: +1(443)845-6909

Education

Johns Hopkins University, Baltimore, MD, United States (January 2016)

Doctorate of Philosophy, Biomedical Engineering

- **Advisor: Jeff Tza-Huei Wang, Ph. D**
- **Thesis:** Design and application of magnetofluidic droplet microfluidic platform for delivery of molecular diagnostics at the point of care

Duke University, Durham, NC, United States (May 2010)

Bachelor of Science and Engineering, *magna cum laude*, Biomedical Engineering, Electrical and Computer Engineering (GPA:3.871/4.00; Graduation with Distinction)

- **Advisor: Dr. Chris Dwyer**, Spring 2009 - Spring 2010
- **Thesis:** Design for FRET-based Pass Gate using DNA Self-Assembly

List of Peer-Reviewed Publications (*first author)

- A. Stark*, D. J. Shin*, T. Pisanic II, K. W. Hsieh and T. H. Wang, *A parallelized microfluidic DNA bisulfite conversion module for streamlined methylation analysis*. Biomedical Microdevices, 2016.
- P. Athamanolap, V. Parekh, S. I. Fraley, V. Agarwal, D. J. Shin, M. A. Jacobs, T. H. Wang and S.Yang, *Trainable high resolution melt curve machine learning classifier for large-scale reliable genotyping of sequence variants.* PloS One, 2014. DOI: 10.1371/journal.pone.0109094
- H. C. Zec, D. J. Shin and T. H. Wang, *Novel droplet microfluidic platforms for the detection of disease biomarkers: implications for molecular diagnostics.* Expert Review of Molecular Diagnostics, 2014. 14(7):787-801.
- D. J. Shin* and T. H. Wang, *Magnetic droplet manipulation platforms for nucleic acid detection at the point of care*. Annals of Biomedical Engineering, 2014. 42(11):2289-302. doi: 10.1007/s10439-014-1060-2.
- D. J. Shin*, Y. Zhang* and T. H. Wang, *A droplet microfluidic approach to single-stream nucleic acid isolation and mutation detection.* Microfluidics and Nanofluidics, 2014. 17(2):425-430.
- Y. Zhang, D. J. Shin and T. H. Wang, *Serial Dilution via Surface Energy Trap-Assisted Magnetic Droplet Manipulation.* Lab on a Chip. 2013. 13(24): 4827–4831.
- P. Athamanolap, D. J. Shin and T. H. Wang, *Droplet Array Platform for High Resolution Melt Analysis of DNA Methylation Density.* Journal of Laboratory Automation. 2013. 19(3):304-312.
- C. H. Chiou*, D. J. Shin*, Y. Zhang and T. H. Wang, *Topography-Assisted Electromagnetic Platform for Blood-to-PCR in a Droplet.* Biosensors and Bioelectronics, 2013. 50:91-9.

List of Patents

- T. H. Wang and D. J. Shin, *Self-contained cartridge and methods for integrated biochemical assay at the point-of-care.* US Patent App. 14/523,412
- T. H. Wang, C. H. Chiou and D. J. Shin, *Electromagnetically actuated droplet microfluidic chip and system*. US Patent App. 13/745,511

List of Presentations

- D. J. Shin, P. Athamanolap, L. Chen J. Hardick, C. A. Gaydos and T. H. Wang, *A low-cost mobile NAAT platform for Chlaymdia Trachomatis.* National Coalition of STD Director's 2015 Annual Meeting
- D. J. Shin, P. Athamanolap, L. Chen J. Hardick, C. A. Gaydos and T. H. Wang, *A low-cost mobile NAAT platform for Chlaymdia Trachomatis.* 2015 World STI/HIV Congress
- D. J. Shin, P. Athamanolap, L. Chen J. Hardick, C. A. Gaydos and T. H. Wang, *Clinical evaluation of MobiLab, a smartphone-enabled microfluidic NAAT platform for Chlaymdia Trachomatis screening.* 2015 AACC Annual Meeting & Clinical Lab Expo (AACC 2015)
- D. J. Shin, P. Athamanolap, L. Chen and T. H. Wang, *An Integrated Droplet Diagnostic Platform For DNA Amplification Testing Of Chlamydia Infection*. ASME 3rd Global Congress on Nanoengineering for Medicine and Biology (NEMB 2014)
- T. D. Rane, H. C. Zec, D. J. Shin and T. H. Wang, *A Multiplexed microfluidic Droplet Platform for Matrix Metalloproteinase Screening.* The 17th International Conference on Miniaturized Systems for Chemistry and Life Sciences (μTAS 2013)
- D. J. Shin, L. Chen, P. Athamanolap and T. H. Wang, *A Simple Integrated Diagnostic Platform for DNA Testing of Chlamydia Trachomatis Infection.* The 17th International Conference on Miniaturized Systems for Chemistry and Life Sciences (μTAS 2013)
- D. J. Shin, A. Stark and T. H. Wang, *Droplet Bisulfite Conversion Platform for Epigenetic Cancer Biomarker Detection.* The 17th International Conference on Solid-State Sensors, Actuators and Microsystems
- D. J. Shin, C. H. Chiou, S. Hosmane, Y. Zhang and T. H. Wang, *Electromagnet-actuated droplet platform for sample-to-answer genetic detection.* IEEE MEMS 2013
- T. H. Wang, *Quantum dots and Microfluidics for Rapid Screening of Cell-Free DNA Biomarkers.* NCI Cancer Detection and Diagnostic Technologies for Global Health (August 22-23, 2011)
- D. J. Shin, Y. Zhang, and T. H. Wang, *Detecting Genetic Variation in a Droplet.* The 16th International Conference on Miniaturaized Systems for Chemistry and Life Sciences (μTAS 2011)

Honors

- Siebel Scholar (2016)
- International Society for STD Research (ISSTDR) Scholarship (July 2015)
- National Academy of Clinical Biochemistry Distinguished Abstract Award (May 2015)
- Cancer Nanotechnology Training Center Predoctoral Fellowship (2013-present)
- NIST/Lab on a Chip Art in Science Award, MicroTAS 2011 Conference, Seattle, Washington, USA (October 2011)
- Tau Beta Pi, NC Gamma Chapter (2008-present)
- Pratt Undergraudate Research Fellowship, Duke University, NC, USA (2009- 2010)